The University of Nottingham

UNITED KINGDOM • CHINA • MALAYSIA

INVESTIGATION OF SMALL PUNCH CREEP TESTING

MIROSLAV STOYANOV

BEng. (Mechanical Engineering)

Thesis submitted to the University of Nottingham

for the degree of Doctor of Philosophy

DECEMBER 2012

ABSTRACT

Creep in metals has been a major engineering problem for many years. Most of the creep failures which occur at high temperature are in welds, due to creep. Assessing the damage level of in-service components and obtaining material properties for welded structures exposed to creep is essential for the safe operating of power generation industry. Standard creep testing techniques require relatively large volumes of material for the machining of testing samples. For that reason they are not usually suitable for obtaining creep properties of in-service structures. It has been found that significant amount of the failures in welds exposed to elevated temperatures occur in an area formed due to the complex thermal and cooling cycles during the welding process. Because of this a different approach is needed for the derivation of creep properties from small amounts of metal. The small punch creep testing method is considered to be a, potentially, powerful technique for obtaining creep and creep rupture properties of in-service welded components. However, relating small punch creep test data to the corresponding uniaxial creep data has not proved to be simple and a straightforward approach is required.

The small punch creep testing method is highly complex and involves interactions between a number of non-linear processes. The deformed shapes that are produced from such tests are related to the punch and specimen dimensions and to the elastic, plastic, and creep behaviour of the test material, under contact and large deformation conditions, at elevated temperature. Owing to its complex nature, it is difficult to interpret small punch creep test

data in relation to the corresponding uniaxial creep behaviour of the material. One of the aims of this research is to identify the important characteristics of the creep deformation results from 'localized' deformations and from the 'overall' deformation of the specimen. For this purpose, the results of approximate analytical methods, experimental tests and detailed finite element analyses, of small punch tests, have been obtained. It is shown that the regions of the uniaxial creep test curves dominated by primary, secondary and tertiary creep are not those that are immediately apparent from the displacement versus time records produced during a small punch test. On the basis of the interpretation of the finite element results presented, a method based on the reference stress approach is proposed for interpreting the result of small punch experimental test data and relating it to the corresponding uniaxial creep data. Another aim of this study is to investigate the effect of friction between the sample and the punch as well as the effects of the basic dimensions, on the small punch creep testing data.

ACKNOWLEDGEMENTS

I would like to take this opportunity to express my sincere appreciation to the following people who have helped me in the preparation of this PhD thesis during the course of this research.

First, I would like to give my deepest thanks and appreciation to Professor T. H. Hyde, my supervisor. He offered me his invaluable guidance, patience and support during the course of this research.

I would also like to acknowledge the support, expertise, encouragement and advice that have been given to me in the project by Associate Professor W. Sun, my second supervisor.

Also, I would like to acknowledge the support of EPSRC through the Supergen programme and the University of Nottingham for providing me with the opportunity to do this work and for financial support for the research work.

I would like to thank my parents for their never ending faith and all of my friends for their support throughout the project, especially Shukri Afazov.

CONTENTS

NOMENCLATURE

Ac_1, Ac_3	temperatures defining the formation of γ phase in steel
B, n	constants in Norton's creep law
BM, HAZ, WM	base material, heat-affected zone, and weld metal respectively
D	reference multiplier
E	Young's modulus
E_0	modulus of elasticity for undamaged material
FE	Finite element
K_S	correction factor for membrane stress
M, ϕ	constants in the Kachanov damage model
P, P_L	load and limit load
Q	the activation energy
q_2	constant in the Liu and Murakami damage model
R	the Boltzmann constant
S_{ij}	deviatoric stress
SCF	stress concentration factor
SPT	small punch test
T	absolute temperature
T_p	peak temperature
t, t_f	time and failure time
a_p, R_s, t_o, D	dimensions of small punch specimens

Δ	displacement
Δ, $\dot{\Delta}_{min}$, $\dot{\Delta}^{c}$	displacement rate and minimum displacement rate, creep strain rat
α	reference stress scaling factor or material constant in Kachanov damage model
β, η	reference conversion parameters
χ	constant in the Kachanov damage model
μ	coefficient of friction
θ	cone ange
ε, ε^{c}, ε_{eng}, ε^{c}_{eq}, ε_{m}	strain, creep strain engineering strain, equivalent creep strain, and mean strain respectively
$\dot{\varepsilon}$, $\dot{\varepsilon}^{c}_{min}$, $\dot{\varepsilon}(\sigma_{ref})$	strain rate, minimum creep strain rate, and strain rate at reference stress respectively
σ, σ_{m}, σ_{y}	stress, meridional membrane stress, and yield stress respectively
σ_{1}, σ_{eq}	maximum principal stress and von-Mises equivalent stress
σ_{nom}, σ_{0}	nominal stress and initial (nominal) stress
σ_{ref}, σ^{R}_{ref}	reference stress and rupture reference stress
ω, $\dot{\omega}$	damage variable and damage rate in Kachanov damage model

CHAPTER 1. INTRODUCTION

The growth of any economy requires an efficient and uninterrupted supply of electricity. Major technological advances and the increasing population, in general, lead to steep rises in the amount of power being consumed. The common types of power stations in UK are nuclear, fossil fired and hydro-electrical. The future of nuclear energy is uncertain because the consequences of accidents (e.g. Chernobyl, Fukushima). Another technological problem is related to the radioactive waste and the cost for storage and recycling it. A lot of effort and resources have been used in the development of renewable and green sources of energy. However, fossil fired power stations are still a main source for the supply of electricity. There are strict environmental requirements applied to those power plants, i.e. they have to produce power with reduced effect on the environment, by controlling the levels of exhaust gases released from the plant. The present power stations therefore need to provide a reliable and constant supply of power, while at the same time maintaining a safe operating environment. These new policies, relating to environmental protection and to the safety at work, together with major advances in analytical techniques for life assessment (which suggest the initial safety factors of these plants were excessively conservative) have made it more profitable to invest in the modernisation of existing plants rather than in building new ones. However, such modernisation only makes economic sense if existing plants have sufficient residual life. Therefore, reducing the uncertainty in evaluating remaining plant life is of primary importance to the power generating industry. This can be achieved by understanding the reasons for failure and preventing

them. The kind of failures which are relevant here are long term failures generally occurring with normal operating conditions, mainly due to the material degradation during service. Fossil fuel power stations have boilers and steam generators. The boiler section consists of many kilometres of tubing. A boiler section in repair is shown in Fig. 1.1. A schematic diagram of coal-fired power plant is illustrated in Fig. 1.2. The working principle of those plants involve water, which is heated up in the boiler into steam usually at temperature between 560 and 600° C and at pressure up to 30MPa. Then the steam drives the turbine which in turn powers the connected generator. The steam is, after it has expended its energy in the turbine, liquefied in the condenser at ambient temperature. In some cases the steam from the boiler can be passed through a re-heater or a super heater, where it is heated up further to produce a higher temperature and pressure. From the above, it is clear that the components of the boiler, re-heater and the turbine are subjected to high operating pressures and temperatures, thereby making them vulnerable to creep failure. In addition to these main components, the plant also contains straight and branched pipes which are susceptible to failure. One of the main reasons for failure of welded constructions in power stations is high temperature creep.

Creep in metals is the deterioration of materials under load and exposed to elevated temperatures for extended periods of time. The phenomenon of creep is most relevant to welded components in the power generating and nuclear industries, where the equipment includes steam pipes, boiler and heat exchanger tubes, which are subjected to high operating temperatures of around 560 and 600° C, for periods of over fifteen to twenty years. Assessment of creep and fatigue interaction is also a major area of concern in other industrial

and aerospace components such as gas turbines. Since many conventional, high temperature plants, in power generating industries, have now been operating for periods in excess of 150,000 hrs, i.e. near the end of their original design life, there is an increasing risk of failure of steam piping components due to creep. As a result of this, interest in innovative and efficient life assessment techniques, which can enhance the safety and help to improve the creep resistance of components, has increased.

Most creep studies use theoretical and analytical techniques as well as actual experimental testing in order to: a) assess the level of material deterioration and the remaining creep life of in-service components; b) improve the design of new components. Life assessment methods form an integral part in the development of design codes and life extension technology for ageing plant. These life assessment techniques involve conducting experimental tests on specimens, at a desired temperature. Material tests are relatively short and require the extrapolation of the results in order to predict the life of the components. Welds and welded components are essential parts of any power station. The development of fusion welding technology had enabled the construction of large plants, which consist of large pipes welded together. Both the parent and weld metals of existing pipes are mostly made from low alloy ferritic steels such as CrMoV. However, a new creep resistant high chromium alloy steel called P91 was developed in the late 1970s in order to extend the operating life and the efficiency of power plants.

P91, which contains 9% chromium, 1% molybdenum with additions of niobium and vanadium, is utilized in conventional power stations for piping systems with operating temperatures of about 600° C and high pressures in the

range of 270 bar. The premature failure of welded and individual components of these materials has been a problem for engineers and researchers for a long time. The higher quality of the weld metal in comparison with the base metal of the welded component cannot guarantee the integrity of the welded construction. A basic weld has a heterogeneous structure which is formed due to the complex heating and cooling cycles taking place during the welding process. Obtaining properties for those various material zones and predicting their behaviour is the key to accurate and reliable creep life assessments. Previous studies of failures in welds **[1-3]** show that the most vulnerable zone for creep micro voids and micro cracks is the so called heat-affected zone (HAZ). The testing of small scale creep specimens is potentially one of the most useful approaches for deriving the creep properties of HAZ's. A variety of creep testing techniques are reviewed in the next chapter. However, standard uniaxial creep tests are not suitable for the purpose of obtaining properties for the various material zones of welds, because they require large volumes of metal, which is not available in those zones. Another conventional creep testing method is the testing of cross-welded specimens. That technique provides useful information for the likely failure location in welds, but it is not appropriate for the derivation of material properties. Many components in conventional and nuclear power plant, chemical plant and aeroengines, for example, operate at temperatures high enough for creep strains, creep damage, microstructure degradation etc. to occur [**4**]. These phenomena may result in the premature failure of components [**5**]. Hence, non - destructive testing is often carried out as part of remaining plant life assessment processes [**6**]. For some components it is possible to extract small samples of material without

significantly reducing the integrity of the structure from which the material is taken [6]. Also, in some regions, such as the heat - affected zones of welds [7], the amount of material which exists may be small. Similarly, when new alloys are being developed, it may only be viable to manufacture small quantities of the material. As a result, a number of attempts have been made to devise small specimen tests for determining mechanical properties from small material samples [8].

The main goal of the present research is to study the small punch creep testing method in detail by means of both analytical and experimental testing approaches. It is also an aim to provide a straightforward technique for relating the small punch creep data to the corresponding uniaxial data.

Chapter 2 consists of a description of the main problems of the power generating industry. A literature survey has been made for the main creep testing techniques and different evaluation methods with their advantages and weaknesses. Chapter 2 also describes damage constitutive equations and creep material constant calculation approaches.

Detailed numerical and finite element analyses of small punch creep tests have been presented in Chapter 3. A technique based on the reference stress method has been suggested for the interpretation of the small punch creep test data to the corresponding uniaxal creep data.

Further finite element results of small punch creep tests using the Liu and Murakami damage model have been described in Chapter 4. The geometries of two small punch test set-ups under different coefficients of friction have been investigated in order to show their effect on the creep data response.

The effect of the geometry of small punch creep testing set-up on the creep data has been analysed in Chapter 5. A set of parametric FE analyses has been run and the results have been investigated.

Chapter 6 is dedicated to the creep testing of actual small punch specimens. The testing rig and experimental procedures have been outlined in this chapter. All of the samples have been manufactured from a P91 (bar 257) steel.

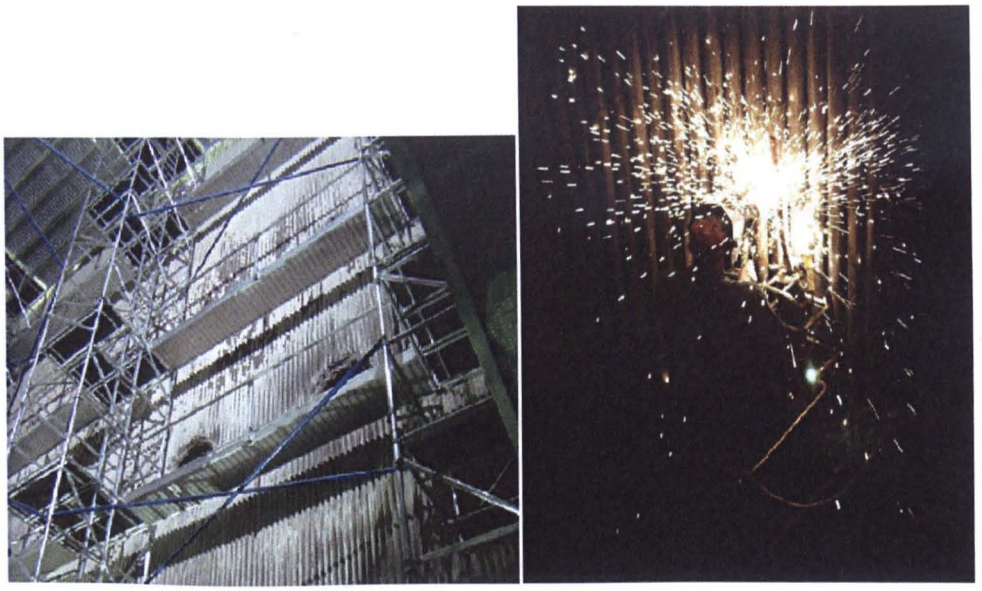

Fig. 1.1 Fossil fuel power plant boiler.

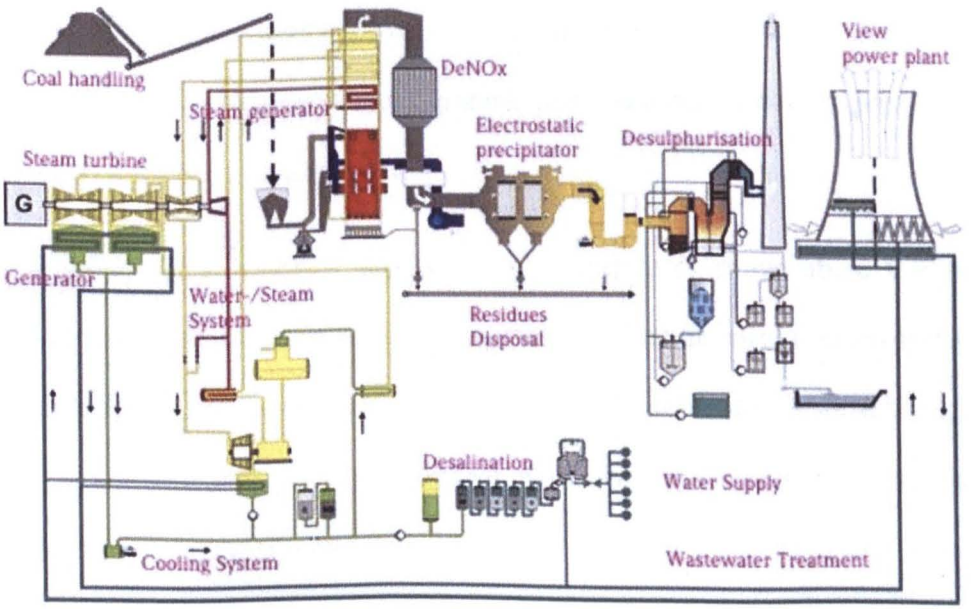

Fig. 1.2 Schematic Diagram of coal-fired power plant.

CHAPTER 2. LITERATURE REVIEW

2.1 Uniaxial Tensile Tests

Creep is the tendency of a solid material to slowly and permanently deform under the influence of stresses. It occurs as a result of long term exposure to high levels of stress that may be below the yield strength of the material. Creep is more severe in materials that are subjected to elevated temperature for long periods. When a material like steel is plastically deformed at ambient temperatures its strength may be increased due to work hardening. This work hardening effectively prevents any further deformation from taking place if the stress remains approximately constant. Annealing the deformed steel at an elevated temperature removes the work hardening. However if the steel is plastically deformed at an elevated temperature, then both work hardening and annealing take place simultaneously. A consequence of this is that steel under a constant stress, at an elevated temperature, will continuously deform with time **[1, 2, 3]**, it is said to 'creep'.

In general, creep becomes significant at temperatures above about $0.4T_m$, where T_m is the absolute melting temperature. Conceptually, a creep test is simple: Apply a force to a test specimen and measure its dimensional change (extension) over time with exposure to a relatively high temperature. A typical extension - time curve is shown in Fig. 2.1.

Three regions can be identified on the curve:

Stage I Primary Creep - creep proceeds at a diminishing rate due to work hardening of the metal.

Stage II Secondary Creep - creep proceeds at a constant rate because a balance is achieved between the work hardening and annealing (thermal softening) processes.

Stage III Tertiary Creep - the creep rate increases due to damage and necking of the specimen and the associated increase in local stress.

In terms of dislocation theory, dislocations are being generated continuously in the primary stage of creep. With increasing time, more and more dislocations are present and they produce an increasing interference with the movement of others, thus causing the creep rate to decrease. In the secondary stage, a situation arises where the number of dislocations being generated is equal to the number of dislocations being annealed out. This dynamic equilibrium causes the metal to creep at a constant rate. Eventually, however, the creep rate increases and the specimen fails due to localized necking, void and micro crack formation at the grain boundaries and the various metallurgical effects such as coarsening of precipitates **[4-7]**.

When in service, it is desirable to ensure that engineering components should not enter into the tertiary stage of creep. It is therefore the secondary creep rate, which is usually of prime importance as a design criterion. Components, which are subject to creep, spend most of their lives in the primary and secondary stages, so it follows that the metals or alloys chosen for such components should have as small a secondary creep rate as possible. In general, it is the secondary creep rate, which determines the life of a given component **[8, 9]**.

The life assessment, and the design of components operating in creep environments is complicated and involves numerical and finite element approaches and analyses as well as experimental testing techniques. Many forms of creep constitutive equations have been developed from fundamental concepts that the creep strain rate at any instant is a function of stress (σ), time (t) and temperature (T). These equations are expressed as combination functions of one or more of the above three parameters. Therefore, any generalized creep law must have the form **[1]**.

$$\dot{\varepsilon}^c = f_1(\sigma) f_2(t) f_3(T) \qquad (2.1)$$

Some of the most common forms for the case of a dependence on the stress function are summarized below:

$f_1(\sigma) = A\sigma^n$ (Norton **[10]**)

$f_1(\sigma) = A\ sinh\ (\sigma/\sigma_0)$ (Mc Vetty **[11]**)

$f_1(\sigma) = C' \exp(\sigma/\sigma_0)$ (Dorn **[12]**)

$f_1(\sigma) = A\{sinh(\sigma/\sigma_0)\}^m$ (Garofalo **[13]**)

where A, n, C' and m are material constants.

The most commonly used of the above is the function developed by Norton **[10]**, which describes the dislocation theory of creep better than any other laws. Some commonly used functions for the dependence on time are as follows:

$f_2(t) = B' t^m$ (Bailey **[14]**)

$f_2(t) = \sum a_i t^{n_i}$ (Graham and Walles **[15]**)

where B', m, a_i and n_i are material constants.

The best available form of the function for temperature dependence is the form suggested by Dorn **[12]**, which includes the combined effect of time and temperature:

$$f_3(T) = t\, exp(-Q/RT)$$

where t is the time, Q is the activation energy, R is the Boltzmann constant and T is the absolute temperature.

Among the definition of creep laws discussed, the combination of Norton **[10]** and Bailey **[14]** equations have been mostly used to represent primary and secondary ($m = 1$) creep behaviour.

$$\varepsilon^c = A\sigma^n t^m \qquad (2.2)$$

However, a simple uniaxial tensile creep testing technique cannot provide creep data for the various material regions in welds of in-service components, operating under creep conditions. Another method for estimation the material deterioration with time of welded components, such as boilers, heat exchangers and steam turbines, operating under elevated temperatures, is the uniaxial creep test of cross-weld specimens.

2.2 Cross-Weld Tests

Grade 91 steel is widely used for the production of components for fossil fuel plants, which operate under severe service conditions for many years. Great attention has been paid to investigating the creep properties of this grade, and a lot of creep data have been collected. Nevertheless experience has shown that

some difficulties persist in production and operating of components made of P91 steel. A number of unexpected in-service failures of grade P91 **[16-22]** components produced with correct tempered martensitic structure demonstrates that study of long-term properties and failure development is still of a great importance. The integrity of the welded structure relies on the performance of the complete welded joint, not just the weld or base metal properties.

In general, a weld consists of three basic material regions: the parent material (PM), weld metal (WM) and the heat-affected zone (HAZ), the last of which may show at least two distinct regions, i.e. the high temperature part of the HAZ and the lower temperature part of the HAZ **[23]**. It has been found that the most premature failures of P91 welds occurred in the lower temperature part of the HAZ, also known as Type IV cracks. Classification of cracking in weldments is shown in Fig. 2.2. A typical Type IV cracking of a power plant pipe weld can be seen in Fig. 2.3. The microstructural regions of a weld are illustrated in Fig. 2.4 and have been categorised by Manahan and Laha as follows: (i) coarse grain region (CGHAZ): Material near the fusion boundary that reaches a temperature well above Ac_3 (temperature defining the formation of γ phase in steel) during welding. Any carbides, which constitute the main obstacle to growth of the austenite grains, dissolve resulting in coarse grains of austenite. In the P91 steels, this austenite transforms into martensite on cooling; (ii) fine grain region (FGHAZ): Away from the fusion boundary where the peak temperature T_P is lower, but still above Ac_3. Austenite grain growth is limited by the complete dissolution of carbides. Fine grain austenite is produced, which subsequently transforms into martensite in the high chromium steels; (iii) intercritical region (ICHAZ): Here $Ac_1 < T_P < Ac_3$,

resulting in partial reversion to austenite on heating. The new austenite nucleates at the prior austenite grain boundaries and martensite lath boundaries, whereas the reminder of the microstructure is simply tempered. The austenite transforms into untempered martensite on cooling; (iv) over tempered region: With T_P below Ac_1 (temperature defining the formation of γ phase in steel) the original microstructure of the plate material undergoes further tempering. The testing of full scale welded components is generally not possible or economically unjustified. However, the accurate estimation of the remaining life of welds requires better understanding of the material behaviour and properties from the various heat affected regions which formed as a result of the complicated cooling and heating processes during welding. A compromising method to assess the high temperature properties of the welds and understand the failure mechanisms and micro structural degradation (Parker **[24]**, Storesund and Tu **[25]**) is to use the uniaxial cross-weld specimens. This type of specimen can be machined parallel with the weld, perpendicular to the weld interface, or, less commonly, at an intermediate angle (Fig. 2.5).

The creep testing of cross-weld specimens, with the stress applied normal to the weld interface, can provide an understanding of the type of failure where the circumferential weld in a pipe is subjected to a significant axial stress component. The weakening effect of the weld is interpreted by comparing these results to the tests on homogeneous weld and parent metals. However, the triaxial-stress state, which is caused by the differences in material properties of the various zones in the weldment, makes it difficult to analytically predict the stress and strain distributions with the knowledge of individual creep properties

and apply them to practical situations. Furthermore, significant scatter of the creep data for the uniaxial cross-weld specimens has been observed **[26-28]**. This is owing to the effect of restraint at the inhomogeneous interface.

Testing of different sizes cross-weld specimens, showed that meaningful prediction of the service capabilities of welds requires testing specimens of the right configuration at the right stress. The lack of exact specified specimen design for cross-weld specimens in any of the existing codes has led to analytical and numerical studies, which have been performed in order to understand the effect of the specimen size and geometry of cross-weld specimens on the creep behaviour (Williams **[29]**. Sun **[30]**, and Hyde and Tang **[31]**). For example, axisymmetric FE analysis of the cross-weld specimen (Storesund and Tu **[32]**) have been used to study the influence of diameter of specimen and fraction of each constituent and has found that there is a significant life enhancement with increasing diameter. Moreover, it has been found that for some weldments, the cross-weld specimen of a large diameter may have a creep strength comparable with that of a pure parent metal or weld metal specimen and that the change in HAZ width also influences the creep life of the specimen. However, it is important to notice that the failure mode which can be obtained from cross-weld tests is similar to the behaviour of welded in-service components. The most comprehensive survey of cross-weld test data has been done by Etienne and Heerings **[33]**, who characterized rupture data using time temperature parameters and defined "weld factors" to evaluate the relevance of experimental tests on cross-weld specimens to the life of real welds.

However, it is important that the mode of failure obtained from cross-weld tests described above is similar to the behaviour of welded components in service. Cross-weld data could only be applied for welds with significant axial or bending loads and not for the case of circumferential welds in pipes loaded with only internal pressure. The most realistic method for understanding weld failure behaviour is full scale component testing. Since such testing could be very expensive and time consuming, other testing techniques using small scale creep test specimens have been developed for better understanding of creep properties from different material regions in the welds.

2.3 Small Scale Specimen Tests

The life assessment and the potential for failure of in-service components has been a critical issue in the safety and reliability of operating power stations which have been approaching the end of their lives. During operation the components of power plant suffer the material deterioration in terms of strength decrease due to the change in microstructure of the metal caused by long-term operation at high temperatures. The typical degradation mechanisms of power plant components materials are the creep deformation, thermal fatigue, high temperature corrosion, etc.

New policies relating to environmental protection and safety work, together with major advances in analytical techniques for life assessment (which suggest the initial safety factors of these plants were unduly high) have made it more profitable to invest in the modernisation of existing plants rather than in building new ones. However, such modernisation only makes economic sense

if existing plants have sufficient residual life, and so reducing the uncertainty in evaluating remaining plant life is of primary importance to the power generating industry. Non - destructive testing is often carried out as part of remaining plant life assessment processes [34]. Therefore, in order to obtain reliable integrity assessment and remaining life estimation, the determination of material properties for in-service components in their current state of damage is required. In order to estimate the mechanical properties the metal sample should be extracted from the actually exposed components. However, traditional tests, such as the uniaxial creep test, are not well suited to this problem. This is because of insufficient material to sample and because the size of the required sample could undermine the structural integrity of the in-service component. For some components it is possible to extract small samples of material without significantly reducing the integrity of the structure from which the material is taken [34]. Also, in some regions, such as the heat - affected zones of welds [35], the amount of material which exists may be small. Similarly, when new alloys are being developed, it may only be viable to manufacture small quantities of the material. As a result, a number of attempts have been made to devise small specimen tests for determining engineering properties from small material samples [36]. Over the past two decades a number of miniaturised specimens testing techniques have been developed such as impression creep testing, small punch creep testing and circular (elliptical) ring creep testing.

2.3.1 Impression Creep Tests

Determining creep properties at positions where variations of creep properties exist, such as in the base metal, heat affected zone and weld metal of a fusion joint has been considered as one of the most reliable practices for predicting the life of components which have operated under high temperatures for many years. Impression creep testing is one of the approaches used for obtaining material properties from small amount of metal removed by a non-destructive sampling technique of in-service power plant parts. The impression creep testing approach involves the application of a steady load to a flat-ended indenter (cylindrical or rectangular) placed on the surface of a material at elevated temperature. A typical set of displacement-time data obtained from such tests is shown in Fig. 2.6. Studies of impression creep tests (Hyde and Sun **[26]**) show that the displacement rate, $\dot{\Delta}^c$, derived from these tests can be converted to the creep strain rate, $\dot{\varepsilon}^c$, obtained from conventional uniaxial creep tests using the reference stress method:

$$\dot{\varepsilon}^c = \dot{\Delta}^c/\beta d \qquad (2.3)$$

and the mean pressure under indenter, p, to the corresponding uniaxial stress, σ, i.e.

$$\sigma = \eta p \qquad (2.4)$$

where η and β are the reference parameters.

It should be noted that secondary creep properties can be obtained from impression creep test data. Tertiary creep and the internal damage which is created in a conventional tensile creep test and detailed multiaxial stress

behaviour cannot be derived from these tests. However, the technique can produce accurate results when the impression creep deformation occurring during the tests is small, compared with the indenter width (diameter) or the specimen thickness. Nevertheless, care must be taken to ensure that the contact area between the indenter and the test material is relatively large, compared with metallurgical features (grain size), to ensure that bulk properties have been obtained. For this reason a long rectangular indenter, rather than a cylindrical indenter, is preferable and has been used extensively in the last decade. Experimental results have shown that reasonably accurate secondary creep properties can be obtained from impression creep tests for a number of metallic materials (Hyde and Sun[27]).

In order to produce minimum creep deformation rate results corresponding to a number of stress and temperatures levels, from a single impression creep test, the single-step impression creep testing method has been extended to stepped-load and stepped-temperature situations. In a stepped-load test, the temperature remains constant, but the indentation loading is increased (or reduced) when a sufficient section of the deformation curve has been obtained from the previous step. In a stepped-temperature test, the indentation loading is held constant, but the temperature is increased (or reduced) at suitable time intervals. Typical deformation curves for stepped-load tests are shown in Fig. 2.7.

2.3.2 Small Punch Tests

Another small specimen creep test technique which has been widely used is the small punch testing method proposed by Manahan in 1981. It was then extensively developed in Japan, particularly at Tohoku University. The first

collaborative efforts in small punch test standardisation were reported by the Japanese Atomic Energy Research Institute in 1988 **[37]**. In the United States, further work by the Electric Power Research Institute and Failure Analysis Associates, since the late 1980s, has led to the introduction of the technique in Europe, from 1992, by Swansea University and Electric Research Association in the UK and Centro Elettroecnico Sperimentale Italiano in Italy. The small punch test is a semi-destructive technique because it uses a very limited amount of material, with the specimens being discs of around 0.5 mm thick and around 8-10 mm in diameter. Such small samples taken from components in service not only leave the structural integrity of thick components intact, or at least repairable, but allow also for the possibility of focusing on the critical locations of the component (those areas that are more highly stressed and damaged).

Despite these advantages, the power generating industry has been slow to accept the use of this technique. This in part reflects concerns about the reproducibility of the results from such a test which is highly dependent upon the geometry of the specimen and on the test apparatus. This concern can only be overcome through the development and imposition of a strong code of practice covering both testing and analysis. Another major concern with the technique is associated with the conversion of the small punch test data into the required uniaxial equivalents. On the experimental front and in Europe, an important push towards such standardisation has come from two main sources. First, between 1994 and 1997 the Copernicus SP project **[38-44]**, developed a creep small punch test configuration but no code of practice was agreed. Second, between 2000 and 2003, and inside the European Pressure Equipment

Research Council, a collaborative project has been set up among a few interested parties (CESI in Italy, Joint Research Centre Institute for Energy of the European Community in the Netherlands and the University of Swansea in the UK) that consisted of a creep round robin exercise. As a result of that exercise a step towards a real code of practice has been made **[45]**. More recently, the CEN (one of the three European Standardisation organisations recognised by EC) has been working to produce a code of practice for the small punch creep test. In 2006 they have published, as a Workshop Agreement, a CEN code of practice **[46]**. With regard to test specimen geometry they have concluded that test specimens should measure 8 mm in diameter with thickness of 0.5 mm and that these should be tested in an inert argon environment.

The SP testing technique is based on the determination of the curve of force versus displacement for a small disk shaped specimen when a central force is applied through indenter (ceramic ball or super-alloy hemi-sphere) **[47-54]**. Small punch tests can be performed at both room temperature and elevated temperature in order to obtain elastic-plastic fracture and creep properties. Usually, a force-displacement curve obtained from a room temperature SP test can be divided into four regions (Fig. 2.8): I elastic bending, II plastic bending, III membrane stretching, IV plastic instability. However, experimental studies of such tests show that the four regimes are difficult to be identified and the yield strength of the materials could not be determined with sufficient accuracy by means of small punch tests.

Fig. 2.9 shows typical displacement versus time curves for SP creep tests which includes an initially high, but rapidly decreasing displacement rate which reduces to a minimum value and persists for a relatively long time, before accelerating towards the end of the test, leading to fracture. Studies of SP tests at elevated temperatures have been carried out in order to derive creep rupture properties of various material zones of welded joints. However, it is difficult to interpret and convert the data of such tests to the data of corresponding standard uniaxial creep tests.

2.4 Basics of Damage Mechanics

Continuum damage mechanics (CDM) is mainly used to represent the creep deformation in the tertiary creep stage (Kachanov **[55]**). Creep damage in metals occurs due to the growth of micro voids (ductile transgranular creep fracture) and also due to the accumulation and growth of micro cracks on intergarnular boundaries (brittle intergranular creep fracture) (Kraus **[56]**). Creep CDM is aimed at predicting an upper bound to lifetime by finding the stress-bearing capability without the presence of any macro-crack in the structure. The earliest form of creep CDM was based on a pragmatic single empirical mathematical parameter referred to as ω, which accounts for the effect of the macroscopic material degradation on the strain accumulation.

Any constitutive equation describing damage is time-dependent and the damage rate, $\dot{\omega}$, increases gradually until the material fails due to rupture and the creep strain reaches infinity. The concept of isotropic damage was first introduced by Kachanov **[55]**.

Consider a section S of the body with the unit normal v, as shown in Fig. (2.10a) Let A_i and A_l be the initial and lost are a due to damage. Therefore the actual area of the section available after damage, ω, is given by A_i - A_l. Isotropic damage or the damage where the voids are distributed equally in all directions, can be described as a scalar, and is represented by:

$$\omega = A_l/A_i \; ; 0 \leq \omega \leq 1 \qquad (2.5)$$

Therefore damage is always a monotonically increasing function, i.e. $\dot{\omega} > 0$.

Continuity, Ψ, is defined as:

$$\Psi = 1 - \omega = (A_i - A_l)/A_i \qquad (2.6)$$

For undamaged material, $\omega = 0$ (or $\Psi = 1$); at fracture $\omega = 1$ (or $\Psi = 0$).

Another important definition involving damage is the concept of effective stress introduced by Rabotnov **[57]**. Consider a volume element shown in Fig. (2.10b) , loaded by force F

Uniaxial stress, $\sigma = F/A_i$

If all of the defects are open in a way that no micro forces are acting on the micro cavities represented by A, we can introduce an effective stress, σ^e that acts on the load bearing area (A_i- A_l).

$$\sigma^e = F/(A_i - A_l) \qquad (2.7)$$

Therefore

$$\bar{\sigma} = \sigma/(1 - \omega) \qquad (2.8)$$

These fundamental concepts of effective stress and damage have been used in the formulation of multiaxial strain rate and damage rate constitutive equations. When studying the deformation state of the material, the total strain at any point is the summation of elastic strain, rate dependent creep strain and a plastic strain.

$$\varepsilon^T = \varepsilon^e + \varepsilon^c + \varepsilon^p \qquad (2.9)$$

When there is no plasticity, total strain consists of only the elastic and creep strains. Most authors e.g. (Rabotnov **[57]**, Hayhurst **[59]**) have proposed that the effective area reduction due, to damage, only effects the creep strain accumulation and the elastic strains are unaffected. Other authors, e.g. Bhattacharya *et al* [1999] and Yatomi *et al* [2004] suggested that since $\omega = 1$ refers to the state of infinite strain, it is essential to take account of this contribution of damage on the elastic strain accumulation. They proposed that the Young's modulus, E, of the material reaches zero as damage approaches unity, as follows:

$$E = E_0(1 - \omega) \qquad (2.10)$$

where E_0 is the modulus of elasticity for an undamaged material. The following definitions of damage constitutive equations use only the isotropic approach.

2.4.1 Kachanov Damage Constitutive Equations

The single parameter damage accumulation approach is essentially an empirical approach (Hayhurst **[59]**). In this approach the CDM law for a multiaxial strain rate is defined as follows:

$$\dot{\varepsilon}_{ij}^{c} = \frac{3}{2} A \left[\frac{\sigma_{eq}}{1-\omega}\right]^{n} \frac{S_{ij}}{\sigma_{eq}} t^{m} \tag{2.11}$$

where A, n and m are the material constants, S_{ij} is the deviatoric stress and σ_{eq} is the von Mises equivalent stress. The material starts off with zero damage, $\omega = 0$, and ω increases with time and failure is assumed to correspond to ω reaching a critical value. The critical value of damage corresponding to failure is commonly assumed to be $\omega = 1$, which corresponds to local material failure point, thereby giving at infinite strain rate. In addition to the creep strain rate definition, a damage evolution equation is required to describe the accumulation of damage with time. This damage rate, equation is typically based on experimental observation from uniaxial and multiaxial creep tests. For example, Hayhurst **[59]** assumed an equation of the following form:

$$\dot{\omega} = \frac{B\sigma_r^{\chi}}{(1-\omega)^{\phi}} t^{m} \tag{2.12}$$

where B, χ, ϕ and m are material constants and σ_r is the multiaxial rupture stress which considers the effect of multiaxial stress states on the damage accumulation. The above equation can also be represented as:

$$\dot{\omega} = \frac{M\sigma_r^{\chi}}{(1+\phi)(1-\omega)^{\phi}} t^{m} \tag{2.13}$$

where M is a material constant. The creep rupture stress employed above is a combination of maximum principal stress, σ_1, and equivalent stress, σ_{eq}, as follows:

$$\sigma_r = \alpha\sigma_1 + (1-\alpha)\sigma_{eq} \tag{2.14}$$

where α is a multiaxial parameter ranging from 0 to 1 (Hayhurst **[60]**, Dyson **[61]** and Gibbons **[62]**).

2.4.2 Material Constants Calculation

The effectiveness of any set of CDM constitutive equations, as described in Section 2.4.1, can be judged by their ability to predict similar creep behaviour to that obtained from experiments. This is usually done by simplifying the equations into uniaxial form, obtaining the necessary material constants and comparing the obtained creep curve with the uniaxial curve from creep tests over a range of stresses. It is also essential to have a clear procedure for acquiring all of the material data **[14, 31]**. For the single parameter CDM laws (Eqs. 2.11-2.14), especially for materials with negligible primary creep ($m = 0$), material constants can be easily calculated without the use of complex optimization techniques (Hyde *et al* **[26]**). Creep constants A and n are calculated from the minimum strain rate data obtained from secondary creep stage over a range of stresses. For a uniaxial stress (σ) condition with $m = 0$ and no damage ($\omega = 0$) Eqn. (2.11) reduces to:

$$\dot{\varepsilon}^c_{min} = A\sigma^n \tag{2.15}$$

where $\dot{\varepsilon}^c_{min}$ represents the minimum or the secondary creep strain rate. Thus:

$$\log(\dot{\varepsilon}^c_{min}) = logA + nlog(\sigma) \tag{2.16}$$

where A and n are calculated from the $\log(\dot{\varepsilon}^c_{min})$ vs $log(\sigma)$ plot of the experimental data from creep tests. This data is often referred to as minimum strain rate data. Similarly, integrating Eqn. (2.12) between the limits, time $t = 0$ to time $t = t_f$, where t_f is the time to failure ($\omega = 1$) gives:

$$t_f = \frac{1}{M\sigma^{\chi}} \tag{2.17}$$

giving:

$$\log(t_f) = -logM - \chi\log(\sigma) \tag{2.18}$$

M and χ are obtained from the $\log(t_f)$ vs $\log(\sigma)$ plots. This data is referred to as the rupture data **[55, 57]**. A final optimization of all material constants can be done using simple curve fitting techniques such as the method of least squares.

The multiaxial parameter α is then obtained by performing a series of finite element (FE) damage calculations of notched bars using the other generated material constants, to generate failure times similar to the creep tests on notched bar specimens. For other materials where primary creep is important, curve fitting procedures involving different non-linear optimization techniques have been developed and used successfully to generate the necessary material properties (Dunne *et al* **[63]**, Hyde *et al* **[31]**). The multi-axial form of the Kachanov material behaviour model consists of a pair of coupled creep/damage equations, i.e.

$$\frac{d\varepsilon^c_{ij}}{dt} = \frac{3}{2}A\left(\frac{\sigma_{eq}}{1-\omega}\right)^n \frac{s_{ij}}{\sigma_{eq}} t^m \tag{2.19}$$

$$\frac{d\omega}{dt} = B\frac{(\sigma_r)^{\chi}}{(1-\omega)^{\phi}} \tag{2.20}$$

Integration of Eqn. (2.20) between the limits ω = 0 (no damage) and ω = 1 (failure), under uniaxial conditions, leads to an expression for the uniaxial failure time as follows:

$$t_f = \left[\frac{m+1}{B(1+\phi)\sigma^{\chi}}\right]^{\frac{1}{m+1}} \tag{2.21}$$

Similarly, the uniaxial creep strain versus time relationship can be obtained, i.e.

$$\varepsilon^c = \frac{A\sigma^{(n-\chi)}}{B(n-\phi-1)}\left[\left(1 - \frac{B(1+\phi)\sigma^{\chi}t^{1+\phi}}{1+m}\right)^{\frac{\phi+1-n}{\phi+1}} - 1\right] \tag{2.22}$$

An alternative creep damage model has been proposed by Liu and Murakami **[64, 65]** in order to avoid the very high damage, and hence strain, rates which occur for the Kachanov model when ω approaches unity. It consists a pair of a coupled creep/damage equations, the multiaxial form of which is:

$$\frac{d\varepsilon_{ij}^c}{dt} = \frac{3}{2}A\sigma_{eq}^{n-1}S_{ij}Exp\left[\frac{2(n+1)}{\pi\sqrt{1+3/n}}\left(\frac{\sigma_1}{\sigma_{eq}}\right)\omega^{3/2}\right] \tag{2.23}$$

$$\frac{d\omega}{dt} = \frac{B(1+\phi)[1-Exp(-q_2)]}{q_2}(\sigma_r)^{\chi}Exp(q_2\omega) \tag{2.24}$$

Integration of Eqn. (23), under uniaxial conditions, leads to:

$$\omega = -\frac{1}{q_2}Ln\left[1 - (1 - e^{-q_2})\frac{t}{t_f}\right] \tag{2.25}$$

where $t_f = \frac{1}{B(1+\phi)\sigma^{\chi}}$

The material constants A, n, B, χ, q_2 and ϕ are obtained from curve fitting to the uniaxial creep curves.

2.4.3 Reference Stress Method

Reference stresses are used to relate the creep behaviour of complex components under loading to the simple uniaxial tensile tests **[66-69]**. The reference stress methods have been widely used to study the creep deformations and rupture times of single and multi-material components (Sun **[30]**, Rayner **[70]**). For example, British Energy's R5 **[17]** creep life assessment procedure which uses such a reference stress approach, has shown to give acceptable conservative estimates for the rupture life of homogeneous material components (Goodall *et al* **[71-74]**).

Soderberg **[75]** was first to attempt to relate the creep strain rates of thick walled tubes under internal pressure to the creep rates from uniaxial tensile tests at a stress related to that particular internal pressure, wall thickness and mean radius. Other authors like Anderson **[76]** and Mackenzie **[77]** also proposed analytical methods for identifying the reference stress. However, Sim **[78]** was first to develop an approximate method for determining the reference stress, according to which:

$$\sigma_{ref} = \frac{P}{P_L}\sigma_Y \qquad (2.26)$$

where P_L is the limit load for the component with yield stress σ_Y. The reference stress is in proportion to the applied load P. This reference stress method has been widely used in the creep analysis of homogeneous and two material

components operating in the creep range, in order to give a better understanding of the fundamental concepts behind the definition (Goodall *et al* **[79]**, Boyle **[80]**).

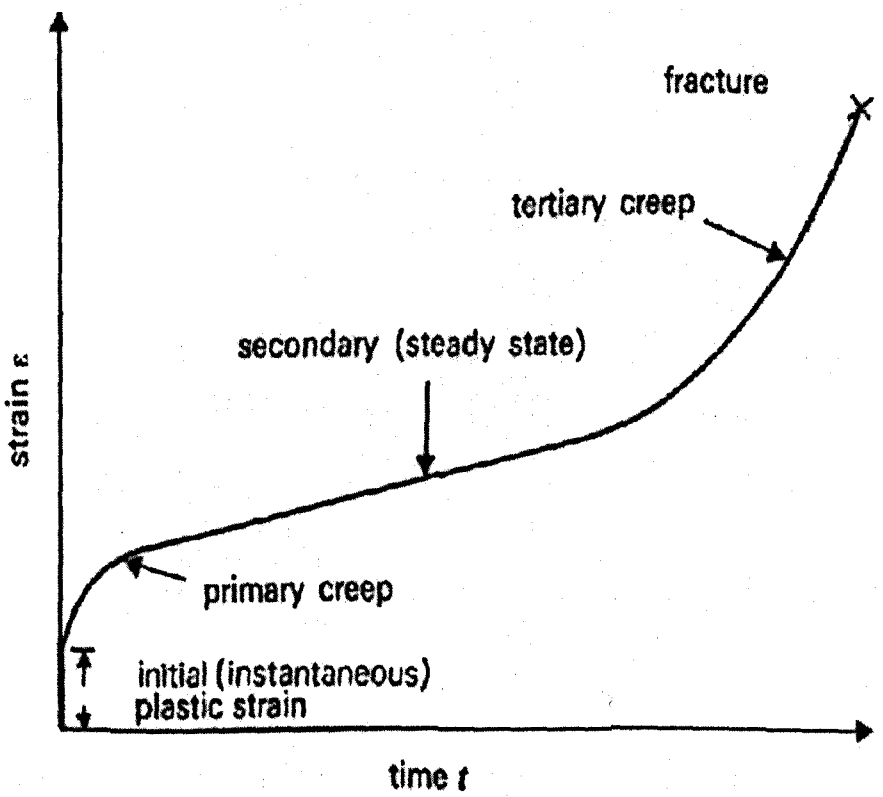

Fig. 2.1 A typical strain versus time curve of uniaxial creep test [1].

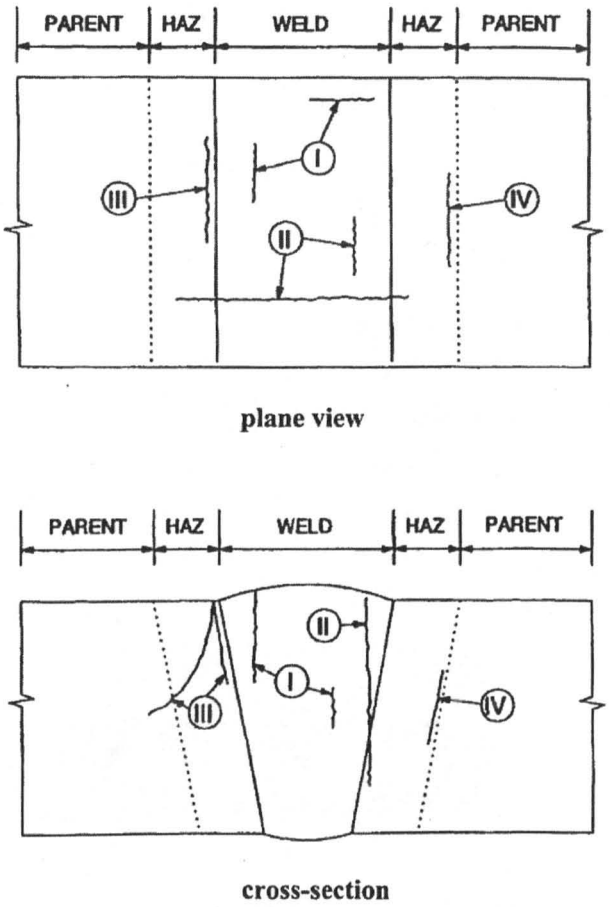

Fig. 2.2 Classification of cracking in weldments **[31]**.

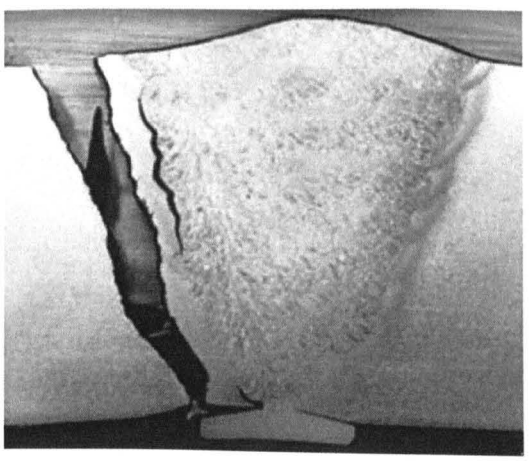

Fig. 2.3 A typical Type IV cracking of a power plant pipe weld **[22]**.

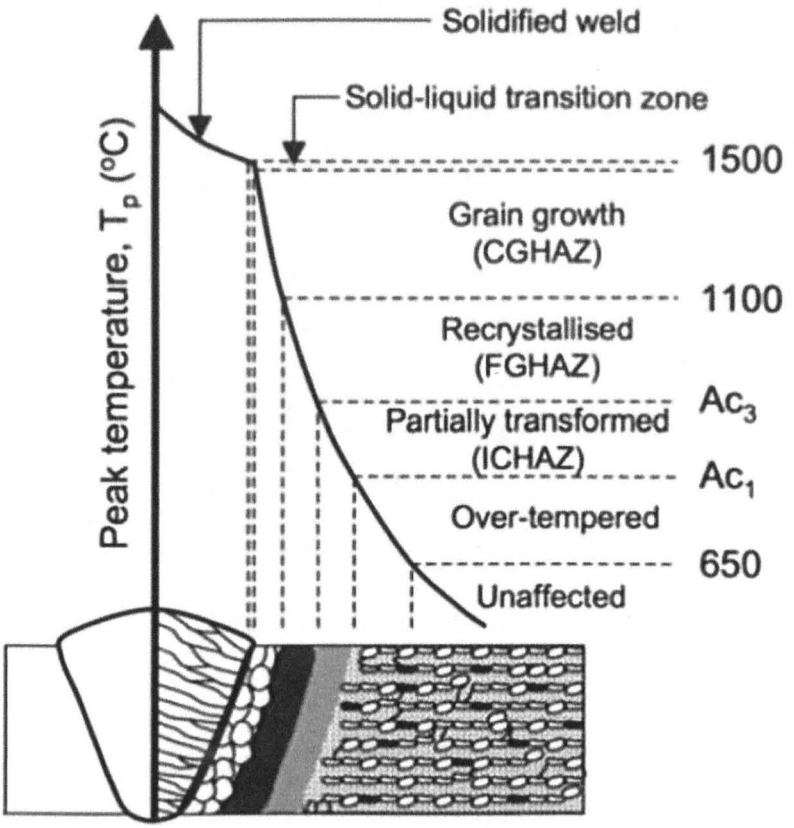

Fig. 2.4 Schematic representation of microstructures development in HAZ as approximate function of peak temperature during welding **[19]**.

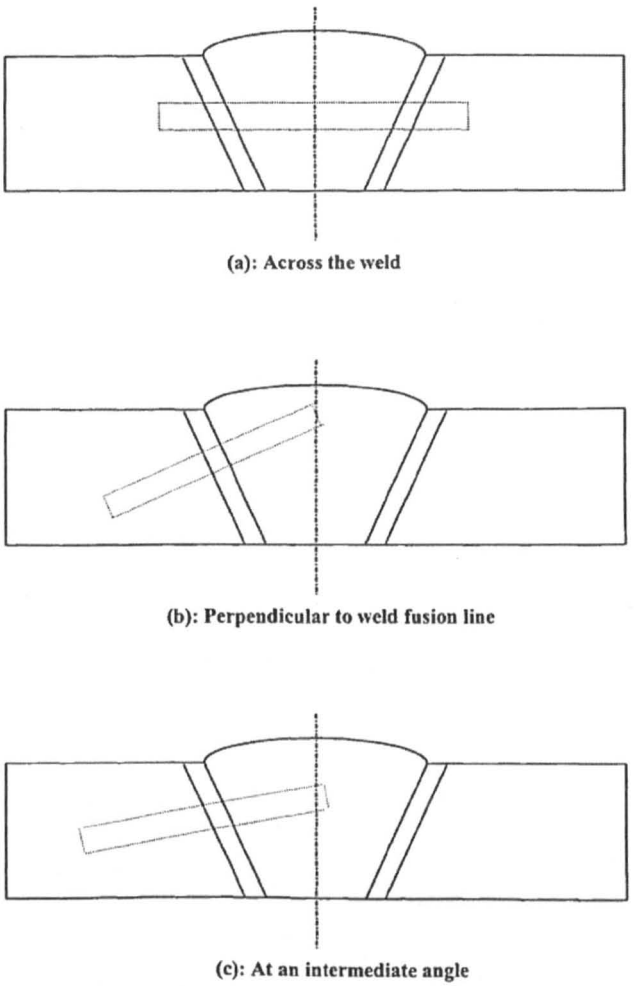

Fig. 2.5 Orientation of cross-weld specimens machined from weldments **[31]**.

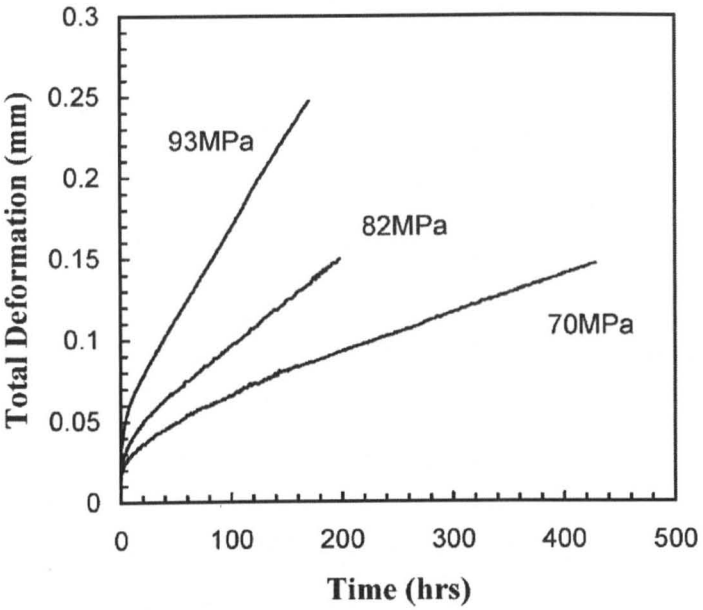

Fig. 2.6 Typical impression creep curves.

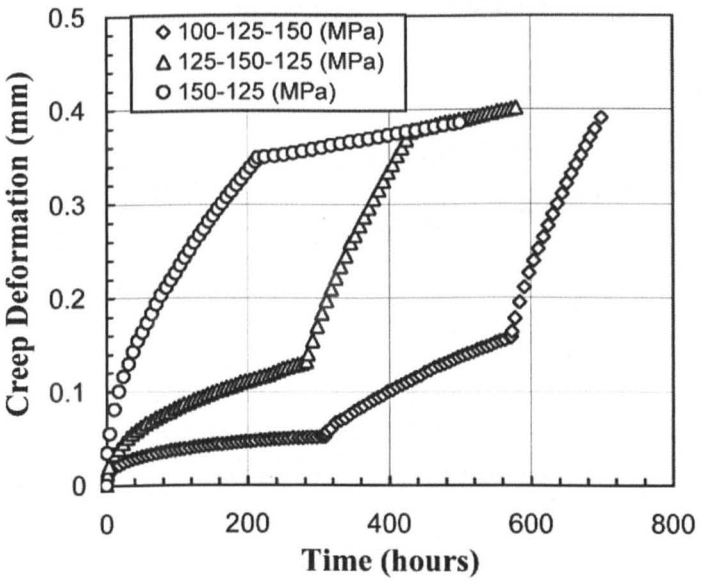

Fig. 2.7 Typical deformation curves for impression creep stepped-load tests **[28]**.

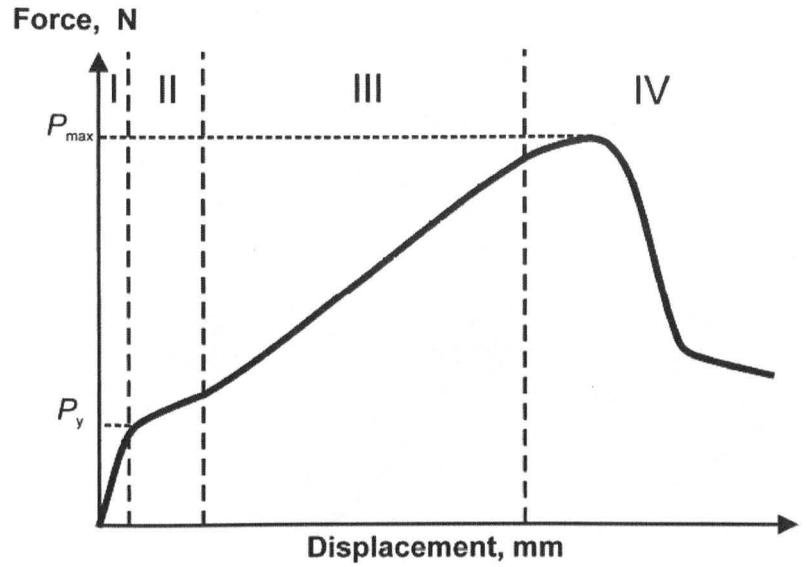

Fig. 2.8 Schematic Force-Displacement curve of room temperature SP test **[43]**.

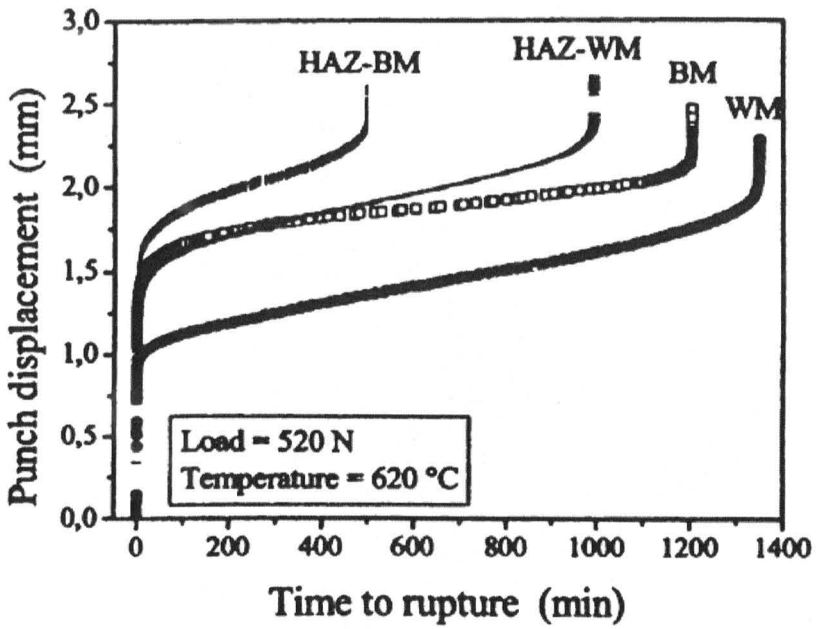

Fig. 2.9 Typical displacement versus time curves for SP creep tests of P91 **[8]**.

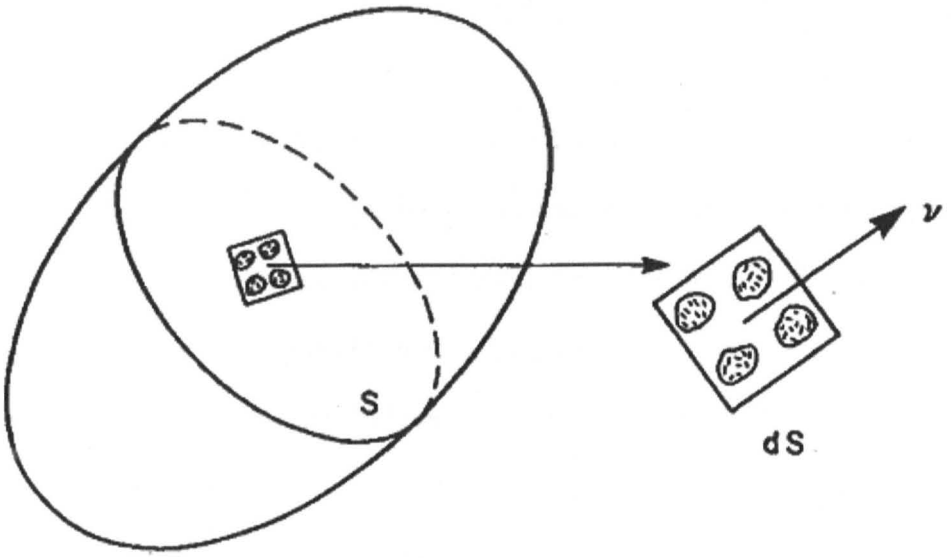

Fig. 2.10 a) Representation of isotropic damage **[55]**.

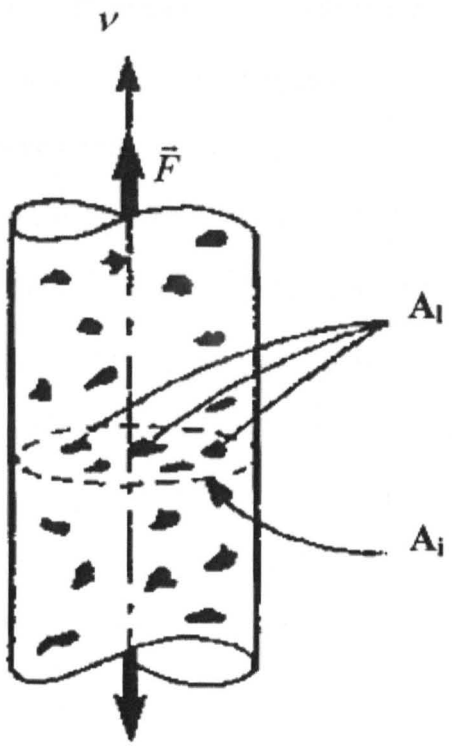

Fig. 2.10 b) Concept of effective stress (Rabotnov, **[57]**).

CHAPTER 3. THE INTERPRETATION OF RESULTS FROM SMALL PUNCH CREEP TESTS

Three specimen types have mainly been used for determining creep properties from small material samples. These are miniature tensile creep specimens [**34**], impression creep specimens [**26**] and small punch test specimens [**39**]; Figs. 3.1(a) to 3.1(c) show a typical conventional uniaxial creep test specimen and a typical set of uniaxial creep and creep rupture test data. Figs. 3.2(a) – 3.2(c) show the small specimens mentioned above. More recently an alternative ring-type small creep test specimen, which enables a relatively large equivalent gauge length to be achieved, has been proposed [**54**]. The processing and interpretation of the results from miniature tensile creep specimens is the same as that used for conventional uniaxial creep tests [**81**]. Also, a mechanics - based procedure has been developed [**26**] for interpretation of the results from impression creep tests. In general, only the primary and secondary creep properties can be determined from impression creep tests; see Fig. 3.1(b) for typical uniaxial creep behaviour curves showing the primary, secondary and tertiary regions. The small punch creep specimen test procedure has also been used to estimate creep properties [**39**] related the secondary and tertiary ranges of creep. However, although a code of practice for performing small punch tests has been produced [**46, 48**] and is becoming generally accepted, there is still a need for a mechanics based approach to explain how the failure time, stress and strain rate from uniaxial tests correspond to the small punch test specimen data.

Finite element modelling consists of three stages: pre-processing, analysis and post-processing. In the pre-processing phase, the user produces a model of the part to be analysed in which the geometry is divided into a number of discrete subregions, or "elements", connected at discrete points called "nodes". The analysis stage of the theoretical modelling uses the dataset which was prepared by the pre-processing as input to the finite element code itself, that conducts and solves a system of linear or nonlinear algebraic equations. Commercial codes may have very large element libraries, with elements appropriate to a wide range of problem types. One of the principal advantages of finite element analysis is that many problem types can be addressed with the same code, merely by specifying the appropriate element types from the library. The post-processing stage is used to generate and visualize of the results from the analysis phase. In the earlier days of finite element analysis, the user would pore through reams of numbers generated by the code, listing displacement and stresses at discrete positions within the model. It is easy to miss important trends and hot spots this way, and modern codes use graphical displays to assist in visualizing the results. A typical post-processor display overlays coloured contours representing stress levels on the model, showing a full-field picture similar to that of photo-elastic experimental results.

This chapter contains the results of approximate analytical and detailed finite element analyses of small punch creep tests. It is shown that the regions of the test data dominated by primary, secondary and tertiary creep are not those which are immediately apparent from the displacement versus time records produced during the small punch tests. On the basis of the interpretation of the

FE results presented, a method is proposed for interpreting the results of experimental small punch creep tests.

3.1. GENERAL DESCRIPTION OF SMALL PUNCH TEST SPECIMEN BEHAVIOUR

3.1.1 Problem Definition

A small punch test setup is shown schematically in Fig. 3.3(a). A typical small punch test specimen has the following dimensions: radius of the receiving orifice (lower die), $a_p = 2\,\text{mm}$, radius of the punch, $R_p = 1.25\,\text{mm}$ and thickness of the specimen $t_0 = 0.5\,\text{mm}$. The form of the displacement versus time output obtained from a small punch test is shown schematically in Fig. 3.3(b). The output (typically) includes an initially high, but rapidly decreasing, displacement rate which reduces to a minimum value, which persists for a relatively long time, before accelerating towards the end of the test, leading to fracture. Figure 3.3(b) is drawn to indicate the relative durations and the extents of the deformations which occur at the various stages of a typical test.

The small punch test is highly complex and involves the interactions between a number of nonlinear processes. These include:

(i) Contact; the contact area between the specimen and the punch increases as the "constant load" creep test progresses (the friction conditions may also be important).

(ii) Non-linear material behaviour; in general the elastic - plastic and the creep strains are non - linearly related to the stress state (The simplest constitutive equation that demonstrates this is the Norton creep equation [1], i.e. $\dot{\varepsilon}^c = B\sigma^n$.

(iii) Large deformation; the specimen starts as a flat plate and ends up being approximately conical in shape with a part - spherical shaped end, as indicated in Fig. 3.3(a).

(iv) Large strains; for most engineering materials, which have been tested using the small punch test method [**84**], the failure strains obtained from uniaxial tests are in excess of 25% (see Fig. 3.1(b)) and for SPT specimens, there is often evidence of localised "necking" at or near the edge of contact between the specimen and the punch [**82**], at which position the strains are significantly greater than the general strain level in the specimen as a whole. Taking into account the highly non - linear behaviours experienced during a test, it is hardly surprising that the interpretation of the test results is difficult.

3.1.2 Approximate Theoretical Models

The most comprehensive theoretical study which is relevant to the SPT setup is that of Chakrabarty [**83**]. However, there are a number of restrictions which limit its direct applicability to the SPT specimen behaviour. These include (i) the requirement that the specimen thickness is small compared to the punch radius and (ii) the analysis is strictly only applicable to a specific material behaviour model (rigid plastic) which is assumed in the analysis. Notwithstanding these, and other limitations, the analysis provides some very useful insights into the creep behaviour of the SPT specimen. In particular, Yang and Wang [**84**] have used the Chakrabarty model to derive equations relating (i) the equivalent strain, ε_{eq}, at the edge of contact between the specimen and the sphere to the overall displacement, Δ, and (ii) the membrane stress, to the displacement, Δ. For a specimen with $a_p = 2\ mm$ and $R_p = 1.25\ mm$, the relationships are:

$$\varepsilon_{eq} = 0.17959\Delta + 0.09357\Delta^2 + 0.0044\Delta^3 \qquad (3.1)$$

$$\frac{P}{\sigma_m} = 1.72476\Delta - 0.05638\Delta^2 - 0.17688\Delta^3 \qquad (3.2)$$

Yang and Wang also derived an equation relating the equivalent strain at the disc centre to the deflection [**82**]. There is a maximum value for P/σ_m[**85, 46**] and this has been related to a_p, R_p and t_0 [**71**], i.e.

$$\mathrm{Max}\left(\frac{P}{\sigma_m}\right) = 3.33 K_s a_p^{-0.2} R_p^{1.2} t_0 \qquad (3.3)$$

3.1.3 Estimate of "general" Strain Levels and Membrane Stresses in a SPT Specimen

Experimental observations show that high strain levels and near failure necking occur in the specimen at a position close to the edge of the contact with the sphere [83]. The severe strain variations can make it difficult to interpret the overall behaviour of the specimen. In this section, an approximate analysis is carried out which allows the "general" strain levels to be estimated.

In order to estimate the "general" strain levels, it is assumed that as deformation occurs, the specimen thickness reduces, but remains the same for all positions within the specimen, as indicated in Fig. 3.4. It is also assumed that the thickness, t, is small compared with R_s, a_P and Δ.

The surface area of the cone with centre-line OO` and cone surface ED is given by:

$$A_{s,cone} = \pi a_p L \tag{3.4}$$

where the differences in area between the assumed conical (FD) and actual spherical (FC) end of the specimen are neglected. In addition,

$$\tan\theta = \frac{a_P}{h} \tag{3.5}$$

Assuming constant volume during deformation gives:

$$\pi a_p \sqrt{h^2 + a_p^2}\, t = \pi a_p^2 t_0 \tag{3.6}$$

Therefore $$\frac{t}{t_0} = \frac{1}{\sqrt{1+\left(\frac{h}{a_p}\right)^2}} = \frac{1}{\sqrt{1+\frac{1}{\tan^2\theta}}} \quad (3.7)$$

The length $ABC` = ED - FD + FC$

$$\approx \frac{a_p}{\sin\theta} - \frac{R_s}{\tan\theta} + R_s\left(\frac{\pi}{2} - \theta\right) \quad (3.8)$$

The " general " strain level

$$\bar{\varepsilon}_m = \ln\left(\frac{\frac{a_p}{\sin\theta} - \frac{R_s}{\tan\theta} + R_s\left(\frac{\pi}{2} - \theta\right)}{a_p}\right) \quad (3.9)$$

$$\bar{\varepsilon}_m = \ln\left(\frac{1}{\sin\theta} - \frac{R_s}{a_p \tan\theta} + \frac{R_s}{a_p}\left(\frac{\pi}{2} - \theta\right)\right) \quad (3.10)$$

Similarly, an expression for the displacement, Δ, in terms of cone angle, θ, can be obtained, i.e.:

$$\Delta \approx \text{FD-O`D} + R_s \quad (3.11)$$

i.e. $$\frac{\Delta}{a_p} \approx \frac{1}{\tan\theta} - \frac{R_s}{a_p}\left(\frac{1}{\sin\theta} - 1\right) \quad (3.12)$$

The variation of t/t_0 with θ (equ. 3.7), t/t_0 with Δ/a_p (equs: 3.7 and 3.12), Δ/a_p with θ (equ. 12), $\bar{\varepsilon}_m$ with θ (equ. 10), and $\bar{\varepsilon}_m$ with Δ/a_p (equs. 3.10 and 3.12) are given in Figs. 3.5 to 3.9.

The meridional, membrane stress, σ_m, at a position defined by radius r (see Fig. 3.4) is given by :

$$\sigma_m = \frac{P}{2\pi r t \cos\theta} \quad (3.13)$$

Using equ. 3.7 gives:

$$\sigma_m = \frac{P}{2\pi r t_0} \frac{\sqrt{1+\frac{1}{\tan^2\theta}}}{\cos\theta} \qquad (3.14)$$

Taking the maximum membrane stress, $\hat{\sigma}_m$, to be that at the edge of contact between the specimen and the sphere, where $r = R_s \cos\theta$ (position BB` in Fig. 3.4), as indicated by experimental observation [4], then:

$$\hat{\sigma}_m = \frac{P}{2\pi R_s t_0} \frac{\sqrt{1+\frac{1}{\tan^2\theta}}}{\cos^2\theta} \qquad (3.15)$$

The predicted variation of $\sigma_m/[P/2\pi R_s t_0]$ with θ and with Δ/a_p are given in Figs. 3.10 and 3.11 respectively.

Equations (eqns. (3.1), (3.2) and (3.3)) are applicable to a specific position in the specimen, whereas equations (3.4) to (3.15) provide a measure of stress and strain that characterizes the 'general' states of stress and strain within the specimen. This is based on a very much simpler analysis to obtain the relationships between the "general" states of stress, strain and deformation that exist in the specimen; a clear statement of the assumptions made in the derivation of the 'simpler' equations is provided. The assumption that causes the most significant difference between the derivations by Chakrabarty and that in the simplified analysis is that in the present derivation the specimen thickness is allowed to vary with deformation but it is assumed to be the same at every position within the conical and spherical zones at any particular time.

The predicted variations of P/σ_m and ε_m with normalised displacement, Δ/a_p, are given in Fig. 3.12(a) and (b); ε_m is the meridional strain in the conical

section at the edge of contact between the specimen and the punch and σ_m is the corresponding meridional membrane stress. It can be seen that the predictions for the membrane stress are in reasonably good agreement (Fig. 3.12(b)). However, although the predictions of membrane strain have similar trends (Fig. 3.12(a)) there is a factor of about 2 x difference for $\Delta/a_p \gtrsim 0.3$. This is explicable by the fact that the present model assumes the thickness to be constant (at any given instant), whereas Chakrabarty's model [**83**] allows the thickness to vary. Hence the Chakrabarty model would be expected to result in higher strains at the "edge of contact" than the present model. Both models consider membrane behaviour only. Hence, neither model is applicable for low Δ/a_p values (i.e. $\Delta/a_p \lesssim 0.3$). An important observation is that in a typical test [e.g. **46**] the constant displacement rate region of the curve does not occur until $\Delta/a_p \gtrsim 0.5$, by which time the general strain levels in the specimen (as indicated by the model described in this section) are between 10 and 15% and the peak strains (as indicated by the Chakrabarty model) are about 30%, see Fig. 3.12(a). These strain levels are way beyond the strain levels normally associated with primary and secondary creep and, usually these would only be expected to occur well into the tertiary region, close to failure.

Of the four types of "non-linear" behaviour described in section 3.1.1, the relationship between contact area (a function of θ) and displacement, Δ, is not likely to be greatly affected by the precise details of the material behaviour model; this is implied by equ. 3.12. Also, the strain distribution (expected near to failure) is not strongly affected by the precise material behaviour for a given

displacement, Δ, as equs. (3.1) and (3.10) indicate. However, the material behaviour model will have a direct effect on the displacement, Δ, versus time for a given load, and on the displacement rate, $\dot{\Delta}$, versus load, for a given deformation value. Hence, the material behaviour model and the failure criterion seem to be the most important parameters which affect the behaviour observed in a small punch test.

Relatively simple material behaviour models, e.g. a Norton secondary creep law [1] and a Kachanov damage mechanics model [e.g. **55**], are capable of describing tertiary creep leading to ductile failure, (see section 3.1.4.1) for the case of a Norton behaviour model and tertiary creep leading to brittle failure, (and section 3.1.4.2) for the case of a damage mechanics model; these two cases are typical of the main types of creep behaviour models currently used to predict the creep behaviour of components [e.g. **35**].

3.1.4.1 Ductile failure of a uniaxial specimen obeying a Norton`s creep law

In the case of ductile failure, a large deformation analysis is required.

Norton`s creep law relates the uniaxial strain rate to the stress via:

$$\dot{\varepsilon} = B\sigma^n \qquad (3.16)$$

For a specimen with an initial cross- section area of A_0, and initial gauge length of L_0, subjected to a constant load P, the gauge length will increase(instantaneous value L) and the cross - section area will

decrease(instantaneous value A). Assuming creep occurs under constant volume conditions, then

$$LA = L_0 A_0 \tag{3.17}$$

Hence $$A\frac{dL}{dt} + L\frac{dA}{dt} = 0 \tag{3.18}$$

The instantaneous stress, σ, is given by

$$\sigma = \frac{P}{A} \tag{3.19}$$

From equ. (3.18) it follows that

$$\frac{dL/dt}{L} = \frac{dA/dt}{A} \tag{3.20}$$

Hence $$\dot{\varepsilon} = -\frac{1}{A}\frac{dA}{dt} \tag{3.21}$$

Substituting equ. (3.19) into equ. (3.16) and using equ. (3.21) gives

$$B\frac{P^n}{A^n} = -\frac{1}{A}\frac{dA}{dt} \tag{3.22}$$

For a ductile material, failure occurs as $A \rightarrow 0$. Therefore, the failure time, t_f, is obtained from equ. (3.22) as:

$$BP^n \int_0^{t_f} dt = -\int_{A_0}^{0} A^{n-1} dA \tag{3.23}$$

and since $\sigma_0 = P/A_0$, then

$$t_f = \frac{1}{nB\sigma_0^n} \tag{3.24}$$

For intermediate times, integration of equ. (3.23) between 0 to t and A_0 to A gives

$$\varepsilon_{eng} = \left(1-\frac{t}{t_f}\right)^{-\frac{1}{n}} - 1 \tag{3.25}$$

Typical ductile creep curves, for two n- values, are shown in Fig. 3.13.

Creep rupture is often presented as $\log(\sigma_0)$ versus $\log(t_f)$; equ. (3.25) implies that this would have a gradient of -1/n (see Fig. 3.14). Figures 3.13 and 3.14 show, schematically, the creep strain and creep rupture behaviours predicted by these equations.

3.1.4.2 Brittle failure of a uniaxial specimen obeying a Norton's creep law and Kachanov damage model

In the case of creep brittle failure, the simplest damage mechanics model is that of Kachanov **[55]**.

The Kachanov, single damage parameter creep law relates strain rate and damage rate to the stress via the equations:

$$\dot{\varepsilon} = B\left(\frac{\sigma}{1-\omega}\right)^n \tag{3.26}$$

where $$\dot{\omega} = M\frac{\sigma^\chi}{(1-\omega)^\phi} \tag{3.27}$$

The damage parameter, ω, varies for *0* (initially) to 1 (at fracture). Hence, from equation (3.27):

$$\int_0^1 (1-\omega)^\phi d\omega = M\sigma_0^\chi \int_0^{t_f} dt \tag{3.28}$$

Therefore, $$t_f = \frac{1}{B(1+\phi)\sigma^\chi} \tag{3.29}$$

At intermediate times, *t* when the damage is $0 \prec \omega \prec 1$,

$$\omega = 1-\left(1-\frac{t}{t_f}\right)^{\frac{1}{\phi+1}} \tag{3.30}$$

Substituting equ. (3.30) into equ. (3.26) and integrating leads to:

$$\varepsilon^c = \frac{A\sigma^{n-\chi}}{B(n-\phi-1)}\left\{\left[1-\frac{t}{t_f}\right]^{\frac{\phi+1-n}{\phi+1}} -1\right\} \qquad (3.31)$$

A typical brittle creep curve is shown in Fig. 3.15. Equ. (3.29) implies that a plot of $\log(\sigma_0)$ versus $\log(t_f)$ would have a gradient of $-1/\chi$, as indicated in Fig. 3.16. Figures 3.15 and 3.16 show, schematically, the creep strain and creep rupture behaviours predicted by these equations.

3.1.5 A Qualitative Explanation for the Shape of an SPT Creep Curve

A schematic diagram (approximately to scale), showing the variation of displacement with time, from a small punch creep test, is shown in Fig. 3.3(b). According to eqn. (3.1) the strain levels related to position 1 (see Fig. 3.3(b)) would typically be about 25% and the "general" strain level would be more than 10% (Fig. 3.12(a)), according to eqn. (3.10). By comparison with typical uniaxial data for P91 (Fig. 3.1(b)) it can be seen that the beginning of secondary creep occurs at strains of about 1 to 3%. Hence, it is likely that primary and secondary creep are over well before the time associated with position 1 (Fig. 3.3(b)) is reached.

By the time that position 2 (Fig. 3.3(b)) is reached the strains at the edge of contact are predicted to be greater than 30% (eqn. (3.1) and Fig. 3.12(a)) and the general strains are about 15% (eqn. (3.10) and Fig. 3.12(a)). By comparison with typical uniaxial data (Fig. 3.1(b)) it can be seen that the strains at position 2 would be well into the tertiary creep region (tertiary creeps

seem to start at about 3 to 4% strain). From these comparisons of uniaxial and small punch creep test data, the question arises "What is happening during the minimum deflection rate portion (positions 1 to 2) of the SPT curves if it is not associated with secondary creep stage"?

A tentative, qualitative explanation of the behaviour (quantitative confirmation is given in section 3.2) is that the early part of the region between 0 and 1 (indicated in Fig. 3.3(b)) is predominantly primary and secondary creep. However, the deformation rate continues to decrease, even though the tertiary creep region is being entered; this is due to the "stiffening effect" caused by the deformation entering the membrane loading phase, compared with the relatively " flexible situation " associated with the plate bending effect which occurs at an earlier stage. The minimum deformation rate portion (positions 1 to 2 in Fig. 3.3(b)) is a balance between the increasing deformation rate that would result from the combined effect of the tertiary creep behaviour and specimen thinning (large deformation) effects and opposing these effects, the reducing deformation rate that would result from the increased stiffening which occurs as a result of the cone angle, θ (Fig. 3.4), becoming smaller for higher deformations. The region between 2 and 3, in Fig. 3.3(b), is the acceleration in deformation rate associated with the final necking and/or the high damage regions for the material. Section 3.2 contains the results of detailed finite element (FE) analyses which are used to attempt to verify the above explanation.

3.2 FINITE ELEMENT MODELLING

Section 3.1.4.1 shows how the inclusion of large deformation and large strains can result in a tertiary - like creep behaviour leading to a clearly defined rupture time, even for a material obeying a simple Norton creep law. Section 3.1.4.2 shows how the further direct inclusion of a tertiary creep component (using a pair of coupled strain - rate/damage equations) in the creep law can lead to similar strain versus time behaviour (see Figs. 3.13 and 3.15) but a different dependence of rupture time on applied stress (see Figs. 3.14 and 3.16); for the Norton law, $t_f \propto \sigma^{-n}$,and for the damage model, $t_f \propto \sigma^{-\chi}$, both of which produce straight lines when $\log(t_f)$ is plotted against $\log(\sigma)$. It can be seen that the ductile model results in the same gradient (equal to n), for $\log(\dot{\varepsilon})$ versus $\log(\sigma)$ at all strain levels, see Fig. 3.17, whereas the gradient varies when a damage model is used, but at each strain level a straight line fits, reasonably well, the $\log(\dot{\varepsilon})$ versus $\log(\sigma)$ data, see Figs 3.18 and 3.19. Ductile and damage mechanics material behaviour models have been used in finite element (FE) analyses, with large deformations, to investigate whether the behaviour observed in small punch creep test components can be explained using the two types of material models.

3.2.1 Finite Element Analysis Details

The geometry chosen for the FE analyses is: radius of the lower die orifice, $a_p = 2$ mm, radius of the punch, $R_p = 1.25$ mm, thickness of the specimen, $t_0 = 0.5$ mm; the mesh and boundary conditions are shown in Fig. 3.20. The

specimen mesh consists of eight noded, isoparametric, quadratic axisymmetric elements [77]. The indenter sphere and support are represented by rigid shell elements.

All of the analyses were performed under elastic - creep conditions. The creep behaviour was represented by a Norton`s law [1] and a single parameter damage model [55] as expressed by equation (16) and equations. (3.26) and (3.27), respectively.

3.2.2 Elastic-Creep Behaviour

3.2.2.1 Norton creep model

Typical predictions of displacement versus time are shown in Fig. 3.21, from which it can be seen that although the material behaviour model describes secondary creep only, the displacement versus time results contain an initial reducing displacement rate portion, an almost constant displacement rate, which lasts for the majority of the time, followed by an accelerating region leading to failure. The effect is similar to that described in section 3.1.4.1 for a simple uniaxial specimen undergoing large deformation.

The variation of ε_m with Δ at the apex (inside, i, middle, m, and outside, o), position A in Fig. 3.3(a), at the edge of contact (i, m and o), position B in Fig. 3.3(a) and in the cone section, position C in Fig. 3.3(a), are shown in Figs. 3.22(a), (b) and (c) for $n = 6$. Also shown in Fig. 3.22 are the predictions based on Chakrabarty`s model. It can be seen that the general trend for the results based on Chakrabarty`s model are in good agreement with the FE predictions,

especially for $\Delta \gtrsim 0.3$. Similarly, the agreement between P/σ_m versus Δ obtained from the FE analysis and both the Chakrabarty model and present model (see section 2.3), is good for $\Delta \gtrsim 0.3$, as indicated in Fig. 3.23. Also, although the peaks occur at different displacement values, the peak value of $\frac{P}{\sigma_m} \cong 1.82$, obtained from the FE analyses, is in good agreement with the published peak value of 1.89 [**46**]. Similar results to those shown in Figs. 3.22 and 3.23 were obtained for other n - values; the results are given in Figs. 3.24 and 3.25.

For each n - value, calculations were performed with different load levels. From these FE analyses the plots of log ($\dot{\Delta}_{min}$) versus log (P) and log (P) versus log (t_f), shown in Figs. 3.26 and 3.27, respectively, were produced. An important observation from Fig. 3.26 is that all the log ($\dot{\Delta}_{min}$) versus log (P) plots have gradients equal to their respective n - values. Also, the gradients in Fig. 3.27 are equal to $-1/n$ for all three n - values. Plots of Δ versus t/t_f (Fig. 3.21) are similar in appearance to those shown in Fig 3.13, showing the effect of the n - value on the ε versus t/t_f plots. Comparison of the results shown in Fig. 3.22(b), 3.24(a) and 3.25(a) and those shown in Figs. 3.23, 3.24(b), and 3.25(b) confirm that the ε_m versus Δ and P/σ_m versus Δ plots are not greatly sensitive to the exponent, n, in the Norton equation (equ. 3.16). Hence, the large deformation, large strain behaviour of a uniaxial specimen, with a Norton creep law, as indicated by equs. (3.24) and (3.25) is mirrored in the much more complex large deformation, large strain behaviour which occurs in the SPT specimen.

From the FE results, displacement rates, $\dot{\Delta}$, were determined for a series of Δ - values; plots of log ($\dot{\Delta}$) versus log (P) at each value of Δ (Fig. 3.28) were similar in appearance to those for log ($\dot{\Delta}_{min}$) versus log (P), shown in Fig. 3.26. The gradients of these plots are shown plotted against Δ in Fig. 3.29. It can be seen that as is the case for $\dot{\Delta}_{min}$, the gradient at each value of Δ is close to the *n* - value used in the calculation.

3.2.2.2 Single damage - parameter creep model

Real materials do not obey Norton's law from initial loading right up to final fracture. A more realistic material behaviour which describes tertiary creep is the Kachanov single damage - parameter model (equs. (3.26) and (3.27)), [55]. Elastic - creep analyses were performed for a damage model with the following material constants: $B = 1.09x10^{-20}$, $n = 8.462$, $\chi = 6.789$, $M = 3.5367x10^{-17}$ and $\phi = 7.3457$. The Δ versus *t* prediction obtained using the Kachanov model is shown in Fig. 3.30. Also, shown in Fig. 3.30 is the corresponding data obtained for a Norton material model with the same *n* - value, from which it can be seen that the predictions (when compared on the bases of t/t_f) are in reasonably good agreement.

The ε_m versus Δ/a_p and P/σ_m versus Δ/a_p obtained with the Kachanov model are compared with those for the Norton behaviour in Fig. 3.31 and 3.32, respectively. There is a remarkable level of agreement obtained between the two sets of results for the Kachanov and Norton models.

The rupture data obtained from the damage calculations are shown in Fig. 3.33 plotted as log (P) versus log (t_f). The gradient of the fit to this data is -1/5.57; unlike those for the Norton model this value does not correspond to either the n - value or the χ - value used in the damage model. The gradients of log ($\dot{\Delta}$) versus log (P) shown in Fig. 3.34 are not constant, varying from approximately " n " for the lower deflections to approximately " χ " for the higher deflections; the gradients, plotted against displacement, in Fig. 3.35, clearly show this behaviour.

3.3 APPLICATION OF THE REFERENCE STRESS METHOD.

3.3.1 Basis of the Reference Stress Method

The reference stress method was developed to allow the creep deformation of a component at a particular load level to be related to the strains obtained from a single uniaxial creep test (see, for example, references **[1]** and **[83]**. For some components it is possible to obtain an analytical solution which relates the displacement rate (at a point of interest in the component) to the load, material properties and geometry, e.g., for a component obeying Norton creep material behaviour,

$$\dot{\Delta} = f(P, B, n, \text{dimensions}) \qquad (3.32)$$

Inspection of analytical solutions show that they are of the form:

$$\dot{\Delta} = f_1(n)\, f_2(\text{dimensions})\, B(\sigma_{nom})^n \qquad (3.33)$$

The basis of the reference stress method is that a value, α, can be chosen such that $f_1(n)/\alpha^n$ is practically independent of n. Hence, equ. (3.33) can be written as

$$\dot{\Delta} = DB(\alpha\sigma_{nom})^n = D\dot{\varepsilon}(\sigma_{ref}) \qquad (3.34)$$

The quantity $\alpha\sigma_{nom}$ is the so - called reference stress, σ_{ref}, and hence $B(\alpha\,\sigma_{nom})^n = B(\sigma_{ref})^n$ is the creep strain rate produced in a uniaxial specimen subjected to a stress of σ_{ref}. The quantity D is a constant ($D = f_1(n)f_2(\text{dim})/\alpha^n$) which has the units of " length " if $\dot{\Delta}$ is a displacement rate. If an analytical solution does not exist for the particular component of interest, a series of finite elements solutions with different n - values can be used to determine the reference stress, σ_{ref}, and references multiplier, D [**26**]. Alternatively, approximate reference stresses and multipliers can be obtained from limit load and linear elastic solutions for the component [e.g. **26**], i.e.,

$$\sigma_{ref} \approx \frac{P}{P_L}\sigma_y \qquad (3.35)$$

and

$$D \approx \frac{\Delta^e}{(\sigma_{ref}/E)} \qquad (3.36)$$

For creep ductile materials the rupture reference stress, $\sigma^R{}_{ref}$, which relates the failure time of a component to a uniaxial stress, is directly related to the

deformation reference stress, given by $\alpha\sigma_{nom}$, in equ. (3.34), or approximately $(P\sigma_y)/P_L$ in equ. (3.35). Ductile creep behaviour has been defined [**88**] as creep in which the final elongation, ε_f, is greater than five times the product of the minimum creep strain rate and the time to rupture, see Fig. 3.1.

The rupture reference stress for a ductile material is given by [**88**]:

$$\sigma_{ref}^{R} = (1 + 0.13(SCF - 1))\sigma_{ref} \qquad (3.37)$$

For materials which do not satisfy the ductility requirement, the rupture reference stress is given by [**88**]:

$$\sigma_{ref}^{R} = \left(1 + \frac{1}{n}(SCF - 1)\right)\sigma_{ref} \qquad (3.38)$$

In equs. (3.37) and (3.38), SCF, is the 'stress concentration factor' for adjustment of the reference stress, it is given by:

$$SCF = \frac{\bar{\sigma}_{E,max}}{\sigma_{ref}} \qquad (3.39)$$

where $\bar{\sigma}_{E,max}$ is the maximum elastically calculated value of the equivalent value of stress in the structure or feature for the same set of loadings that were used to calculate σ_{ref}[**88**]. This evaluation is considered to be acceptable [**88**] for SCF $\leq$ 4.0; if SCF > 4.0 it should be treated as a crack. For the SPT it is difficult to define an appropriate SCF value; suggestions for the choice of an appropriate value for χ, material constant in Kachanov constitutive damage equations, are given in section 3.3.2 below.

3.3.2 Inferring Uniaxial Behaviour From Small Punch Specimen Tests

Rather than being used to predict the deformation rate for a component, Δ, related to the creep strain rate, $\dot{\varepsilon}(\sigma_{ref})$, from a uniaxial creep test, equ. (3.34), can be re - written as:

$$\dot{\varepsilon}(\sigma_{ref}) = \dot{\Delta}/D \qquad (3.40)$$

Equ. (3.40) infers that the uniaxial creep rate at a stress level equal to σ_{ref} can be obtained by measuring(experimentally) the displacement rate of the component (a small punch test specimen in the present case) and dividing it by the reference multiplier, D, which is in effect the equivalent gauge length of a uniaxial specimen. Hence, the use of small specimen tests to predict corresponding uniaxial creep data requires the reference stress, $\sigma_{ref}(= \alpha\sigma_{nom})$, and reference multiplier, D, to be determined. Essentially, this requires the determination of the appropriate α - value. This approach has been used to interpret the data obtained from impression creep tests [**26**]. There is an additional complication which arises when using this technique to interpret the data from SPTs. Because the geometry changes progressively during the tests, the reference stress and reference multiplier may also change during the test as a result of this.

3.3.3 Reference Stress σ_{ref} and Multiplier D Related to the Minimum Displacement Rate, $\dot{\Delta}_{min}$, in a SPT.

The minimum displacement rates, $\dot{\Delta}_{min}$, for a particular material occurs at about the same value of Δ, irrespective of load level. Finite element solutions have been obtained for various n - values. By plotting log $[\dot{\Delta}_{min}/B(\alpha\sigma_{nom})^n]$ versus n for various values of α, the value of α which produces a horizontal line (see Fig. 3.36) enables the α - values related to the reference stress to be identified, while the intercept on the vertical axis, which is log (D), allows the reference multiplier to be determined. The σ_{nom} value can be arbitrarily chosen; in the present case, for convenience, it is taken to be:

$$\sigma_{nom} = \frac{P}{2\pi a_p t_0} \tag{3.41}$$

From Fig. 3.36, it can be seen that the required α value is 3.08 and D = 2.82. Normalising D with respect to a_p, such that $D = \beta a_p$, gives $\beta = 1.41$.

3.3.4 Variation of α and β with Δ/a_p

Applying the same technique as that described in section 3.3.3 to other values of Δ allows the variation of α and β with Δ/a_p to be obtained, see (Figs. 3.37 and 3.38). The justification for choosing constant Δ values as the basis for determining the reference parameters is that, to a first order of approximation,

the overall shape of the SPT specimen is characterised by the displacement, Δ, of the apex.

From the variations of α and β with Δ which are shown in Fig. 3.38, it can be seen that:

(i) the β - value reduces continuously with increasing displacement, i.e., the effective gauge length reduces with increasing displacement;

(ii) there is a minimum value of α which occurs when $\dot{\Delta}$ is a minimum, i.e. $\alpha_{min} = 3.08$.

Rearranging equ. (3.41) and using $\sigma_{ref} = \alpha\sigma_{nom}$ gives:

$$\frac{P}{\sigma_{ref}} = \frac{2\pi a_p t_0}{\alpha} \tag{3.42}$$

Taking $a_p = 2$ mm and $t_0 = 0.5$ mm gives $\frac{P}{\sigma_{ref}} = \frac{6.28}{\alpha}$; using the variation of α with Δ/a_p (Fig. 3.38), the variation of P/σ_{ref} with Δ/a_p is obtained (see Fig. 3.39). The maximum value of P/σ_{ref}, which occur at $\frac{\Delta}{a_p} \approx 0.7$ is 2.04. This is close to the maximum $P/\sigma_m (= 1.89)$ and Δ/a_p value (0.8) predicted on the basis of the Chakrabarty membrane model (equ. 3.2).

It should be noted that although the reference parameters (α and β) were obtained using a Norton creep model, the results are not restricted to use in secondary creep behaviour governed by Norton`s law. The material behaviour

model is simply a convenient vehicle for obtaining the reference parameters [**1, 83**].

3.4 DISCUSSION

In order to relate the Δ v. t and t_f v. P data obtained from SPTs to the corresponding data from uniaxial creep tests, i.e., ε^c v. t and t_f v. σ, it is necessary to define a stress corresponding to a SPTs as a function of P, a_p, R_s and t_0, which is equivalent to a uniaxial creep test, and to determine a method for converting the creep displacement, Δ^c, from a SPT to an equivalent uniaxial creep strain, ε^c, obtained at the corresponding equivalent uniaxial creep test.

3.4.1 The Equivalent Uniaxial Stress

Attempts have been made to determine an appropriate stress to relate the minimum displacement rate, $\dot{\Delta}_{min}$, and failure time, t_f, obtained from small punch tests, to the corresponding uniaxial data **[60]**. Equation (3.3) seems to be the most widely accepted for relating σ_m to P, a_p, t_0 and R_p, which leads to:

$$\sigma_m = \frac{P}{3.33\, K_s {a_p}^{-0.2} {R_p}^{1.2} t_0} \tag{3.43}$$

using the dimensions $a_p = 2$ mm, $R_p = 1.25$ mm and $t_0 = 0.5$ mm results in the relationship:

$$\sigma_m = \frac{0.528}{K_s} P \tag{3.44}$$

The correction factor, K_s, which is a material dependent correction factor, is usually found to be in the range 1 - 1.3.

The deformation reference stress, obtained for $R_p = 1.25$ mm, defined by equ. (3.42), results in:

$$\sigma_{ref} = \frac{\alpha P}{2\pi a_p t_0} \tag{3.45}$$

Using the dimensions $a_p = 2$ mm and $t_0 = 0.5$ mm results in the relationship:

$$\sigma_{ref} = \frac{\alpha P}{6.28} \tag{3.46}$$

The variation of α with Δ (Fig. 3.38) has been used to obtain the variation of σ_{ref}/P with t, shown in Fig. 3.40, from which it can be seen that for the vast majority of the test period, σ_{ref}/P is approximately 0.512 P. If K_s is taken to be 1.0 in equ. (3.44), then $\sigma_m \approx 0.528$ P, which is very close to the value of 0.512 P (obtained for σ_{ref}), over the vast majority of the period. It should be noted that the reference stress method results in a σ_{ref}/P value which is the same as the value which has been proposed to be used to relate the SPT creep behaviour to the corresponding uniaxial test stress. The reference stress approach described in this thesis therefore supports the stress proposed **[4]** for use in interpreting SPT data.

The detailed finite element analyses carried out using a large deformation, "ductile", Norton material model and a "damage - mechanics" material model show that the variation of P/σ_m with Δ for both models are practically the same (see Figs. 3.32(a) and (b)). These P/σ_m versus Δ variations are also very

similar to the approximate, analytical solutions based on Chakrabarty's model and that derived in section 3.1.3 (see Figs. 23, 24(b), 25(b) and 39). These results also support the stress proposed **[84]** for use in interpreting SPT deformation versus time data.

The choice of the appropriate rupture reference stress, σ^R_{ref}, defined by equs. (3.37) and (3.38), depends on whether the material is taken to be ductile or brittle. If the material is ductile the conversion ratio, $\sigma^R_{ref}/\sigma_{ref}$, is a function of the stress concentration factor, SCF, i.e.

$$\frac{\sigma^R_{ref}}{\sigma_{ref}} = [1 + 0.13(SCF\text{-}1)] \qquad (3.47)$$

If the material is brittle, the conversion ratio also requires an estimate of the stress index, n, i.e., the conversion ratio is given by:

$$\frac{\sigma^R_{ref}}{\sigma_{ref}} = [1 + 1/n(SCF - 1)] \qquad (3.48)$$

It is usually possible to estimate the n - value, but for a SPT specimen, the choice of an appropriate SCF is not easy. If K_s (equ. (3.44)) is taken to be 1.0, the value of SCF, in equs. (3.37) and (3.38) can be estimated from equs. (3.44) and (3.37) or equs. (3.44) and (3.38) for ductile and brittle materials, respectively. For both ductile and brittle materials, the SCF, is predicted to be 1.0. This is consistent with the fact that the membrane stress at positions B and C (Fig. 3.4) are the same (see Fig. 3.23, for example) and do not vary across the wall thickness to any significant extent; indicating that the stress concentration factor is approximately 1.0.

The multiaxial stress version of the damage equation (equ. 3.27) is:

$$\dot{\omega} = \frac{M\,\sigma_r^{\chi}}{(1\text{-}\omega)^{\Phi}} \qquad (3.49)$$

where

$$\sigma_r = \alpha\,\sigma_1 + (1\text{-}\alpha)\,\sigma_{eq} \qquad (3.50)$$

and α is the multiaxiality material dependent constant.

Throughout the conical section and hemispherical end section of the SPT specimen, the stress field is essentially biaxial. The value of σ_{eq} can range from $0.866\,\sigma_1$ to σ_1 for $0 \prec \sigma_2 \prec \sigma_1$ (with $\sigma_3 = 0$) and this will vary from position to position. Hence, when incorporated with α in equ. (3.50) and used in equ. (3.49) to obtain the damage rate, the creep deformation rate and failure time will be influenced by the multiaxial creep damage behaviour of the material. This phenomenon has been observed in experimental tests and the inclusion of the K_S parameter in equ. (3.3) may be a reflection of this multiaxiality effect on damage rates. Further work is being carried out on this aspect as part of the SPT data interpretation project.

3.4.2 Converting SPT Displacements to Corresponding Uniaxial Creep Strains

The most commonly used creep constitutive equation is the Norton equation, i.e.

$$\dot{\varepsilon}^c_{min} = B\sigma^n \qquad (3.51)$$

which relates the minimum strain rate (in the secondary creep region, see Fig. 3.41) to the applied stress. Equation (3.51) implies that a straight line, with gradient 'n', would be obtained if $\log(\dot{\varepsilon}^c_{min})$ is plotted against $\log(\sigma)$, see Fig. 3.42.

For the ductile model described in section 3.1.4.1, the strain is related to time via equation (3.25), from which it can be shown that the variation of strain rate with strain is given by:

$$\dot{\varepsilon} = (1 + \grave{\varepsilon})^{n} B\sigma^{n} \qquad (3.52)$$

This equation implies that for a plot of $\log(\dot{\varepsilon})$ versus $\log(\sigma)$ at any specific strain value, $\grave{\varepsilon}$ say, the gradient would be n, i.e. the same gradient as that associated with the minimum strain rates. However, the B value (see equation (3.51)) in equation (3.52) is replaced by $\grave{B} = (1 + \varepsilon)^{n} B$. Figure 3.17 shows some typical results for a 'ductile', Norton equation, for which $B = 1.88\text{x}\,10^{-29}$ and $n = 10.147$.

If the gradients at a series of fixed strain levels (e.g. $\grave{\varepsilon}$ in Fig. 3.41) are plotted against σ (log-log scale), approximately straight-line fits are obtained for materials obeying a number of other creep constitutive equations; see Figs 3.18(a) and (b) for the Liu and Murakami damage model with constants applicable to 316 stainless steel at 600° C and P91 at 650° C. Similar results for a Kachanov damage equation are shown in Figs. 3.19(a) and 3.19(b) from which it can be seen that approximately straight-line fits are obtained again at each strain level. However, it can be seen that, unlike the 'ductile' Norton model (Fig. 3.17), the gradients are not all the same and equal to that for the minimum strain rate.

Typical experimental SPT data (e.g.) is shown in Fig. 3.3(d), from which it can be seen that the minimum displacement rate occurs when the punch displacement is about 1.5 mm or more. The FE results presented in Figs. 3.21

and 3.30 for two material behaviour models also indicate that the minimum displacement rate occurs when the punch displacement is 1.5 mm. When the punch displacement is about 1.5 mm, the general and peak strain levels in a SPT are more than 15% and 30%, respectively; this can be seen from Figs. 3.12(a), 3.22, 3.24(a) and 3.25(a). When compared with the strain levels which exist when the minimum strain rate occurs in a uniaxial creep test, i.e. 1% to 3%, as indicated in Fig. 3.1(b), the strain levels in a SPT test, at the minimum deflection, are extremely high. Nevertheless, when the minimum displacement rate is plotted against the load using log - log scales, near straight line fits occur (see Figs. 3.26, 3.28 and 3.34), reasonably good straight line fits exist, as is the case for the log ($\dot{\varepsilon}_{min}$) versus log (σ) plots obtained from uniaxial creep test data (see Fig. 3.42, for example). Also, the gradient obtained for the large deformation, Norton creep models are equal to the respective stress exponents; this is the case for the displacement rates at fixed displacement levels as well, see Fig. 3.29. The gradients obtained from the results obtained with the FE analyses using the damage material model did not correspond to the n - value, except at the lower displacements (see Fig. 3.35); in general the gradients were between the n and χ values.

The fact that log ($\dot{\Delta}$) versus log(P) plots are straight lines even though the strain levels are too high for secondary creep to be occurring is explained because for a given strain level, in the tertiary range, the log ($\dot{\varepsilon}$) versus log (σ) plots produce approximately straight-line relationships for many materials. Plots of log ($\dot{\varepsilon}$) versus log (σ) for a range of constant strain values, in the tertiary range, are given in Figs. 3.17, 3.18, and 3.19 for three material

behaviour models, i.e. Norton (large deformation), Kachanov and Lui and Murakami **[55, 64, 65]**.

Attempts are usually made to relate the displacement rate, in particular the "minimum displacement rate", to the secondary creep region in a uniaxial creep test. However, it is clear from the detailed FE analyses and the Chakrabarty **[83]** and simple (section 3.1.3) models that the strain levels in the region of the minimum displacement rate are far too high to be related to secondary creep behaviour. Also, the n - values obtained do not necessarily correlate with those of uniaxial creep data. This can be explained by the fact that the β - value continuously decrease (see Fig. 3.38) as the test proceeds, and hence β decreases as Δ increases. Therefore, equ. (3.40) indicates that $\dot{\varepsilon}(\sigma_{ref}) = \dot{\Delta}/\beta a_p$, produces an increasing $\dot{\varepsilon}(\sigma_{ref})$ because β decreases. Therefore, even for a region in which $\dot{\Delta}$ is practically constant $\dot{\varepsilon}(\sigma_{ref})$ increases. This is a mathematical form of the argument which follows from the fact that the general and peak strain levels, when the minimum deformation rate is achieved, are far too high for the material to be still in the secondary region. However, integration of the experimental Δ versus time data, using equ. (3.40) with the instantaneous values of σ_{ref} and β should allow the ε^c versus time data, corresponding to uniaxial data, to be obtained, for the σ_{ref} history experienced by the SPT material. Further work is being carried out on this aspect of the SPT data interpretation project.

3.5 CONCLUSION

1. Reference parameters η and β, which relate to the test conditions (load and specimen dimensions) and test results (deformation versus time and failure time) to corresponding uniaxial stress, uniaxial creep strain versus time, and uniaxial rupture time, have been established for a typical geometry (a_p = 2 mm, R_p = 1.25 mm and t_0 = 0.5 mm). The variations of η and β with Δ are given in Fig. 3.38.
2. For the majority of an SPT duration, see Fig. 3.40, the reference stress is related to the applied load, P, via the relationship $\sigma_{ref} = 0.512\,P$; where P has units of N and σ_{ref} has units of MPa. This is an appropriate stress to relate the SPT load and geometry to a corresponding stress for uniaxial creep and creep rupture data if the material is creep ductile. This is similar to the value recommended in the proposed code of practice [**84**]. For creep brittle materials the conversion factor (0.512) may need to be modified.
3. The strain rate related to the minimum displacement rate can be determined by using equation (3.40) with $D = \beta a_p$ and β is obtained from Fig. 3.38. At the minimum displacement rate position in an SPT, ε' can be estimated from one of the relationships between ε and Δ (e.g. equation (3.1), Fig. 3.9, Fig. 3.22(b), Fig. 3.24(a), etc.) and hence the strain rate obtained using equation (3.40) can be converted to the minimum creep stain rate using equation (3.52), i.e. $\dot{\varepsilon}_{min} = \dot{\varepsilon}(\varepsilon = \varepsilon')/(1+\varepsilon')^n$. If a series of tests are performed with different load levels (hence different σ_{ref} values) and the $\log(\dot{\varepsilon}_{min})$, calculated as indicated above, is plotted against $\log(\sigma_{ref})$, this will correlate with the data obtained from the uniaxial tests, provided the

material is 'ductile'. For a brittle material, the gradient obtained from the SPT data may not be exactly the same as that obtained for minimum uniaxial creep strain rate data.

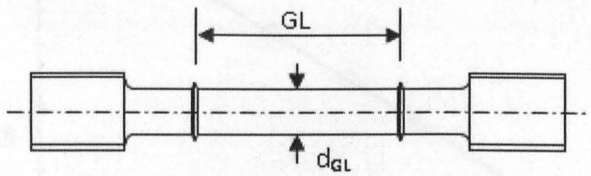
GL
d_{GL}

(a)

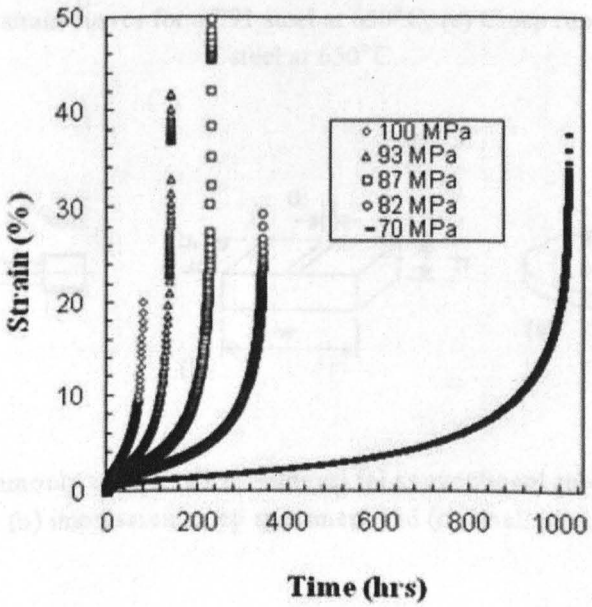
100 MPa
93 MPa
87 MPa
82 MPa
70 MPa
Strain (%)
Time (hrs)
0
10
20
30
40
50
0
200
400
600
800
1000

(b)

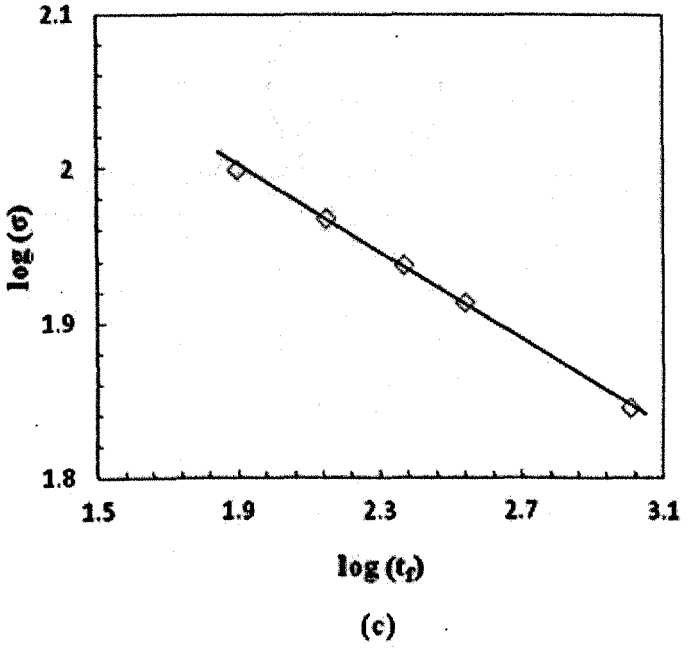

Fig. 3.1 (a)Typical conventional creep test specimen (GL ≈ 50mm, d_{GL} ≈ 10mm); (b) Uniaxial creep strain curves for a P91 steel at 650° C; (c) Creep rupture data for a P91 steel at 650° C.

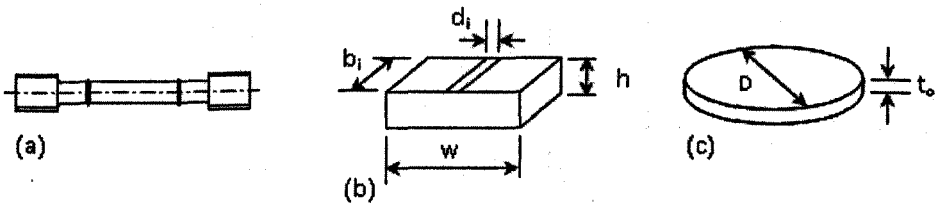

Fig. 3.2 Commonly used small specimens: (a) conventional sub - size uniaxial specimen; (b) impression creep specimen, and (c) small punch specimen.

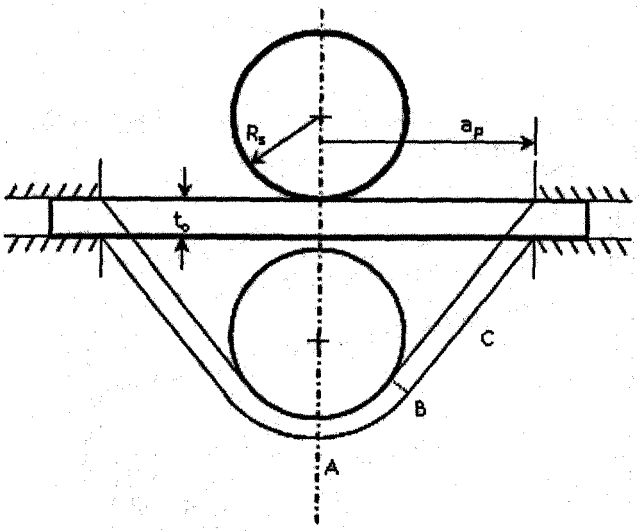

(a)

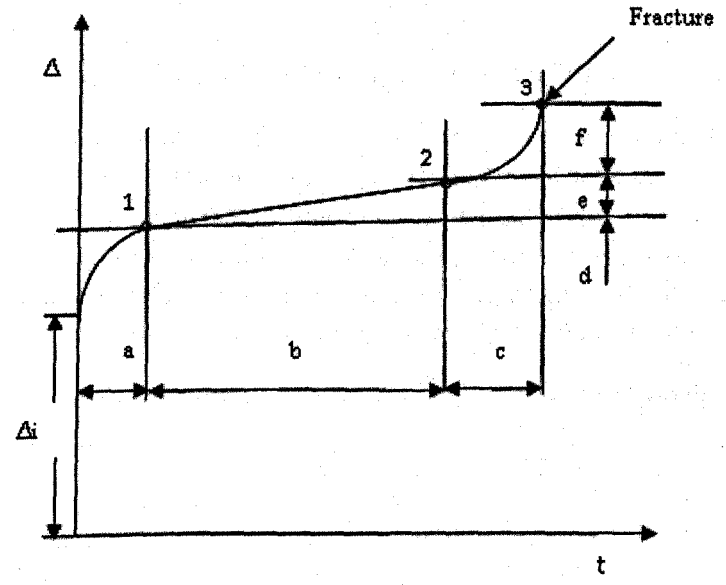

(b)

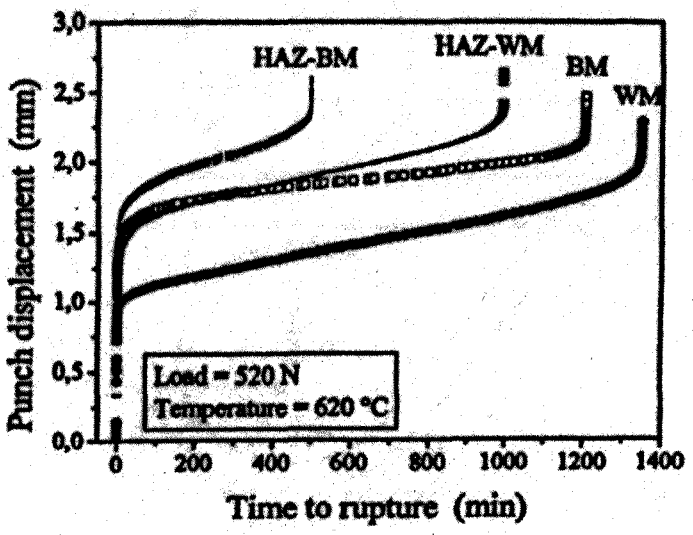

(c)

Fig. 3.3 (a) Schematic diagram of typical SPT setup;

(b) Schematic representation of displacement versus time curve from SPT showing different deformation regions(where Δi is the instantaneous elastic and plastic deformation): a) reducing deformation rate; b) approximately constant deformation rate; c) increasing deformation rate; d) deformation occurring during reducing deformation rate; e) deformation occurring during "constant" deformation rate, and f) deformation occurring during increasing deformation rate;

(c) Typical small punch test curves for different zones of a P91 weldment **[54]**.

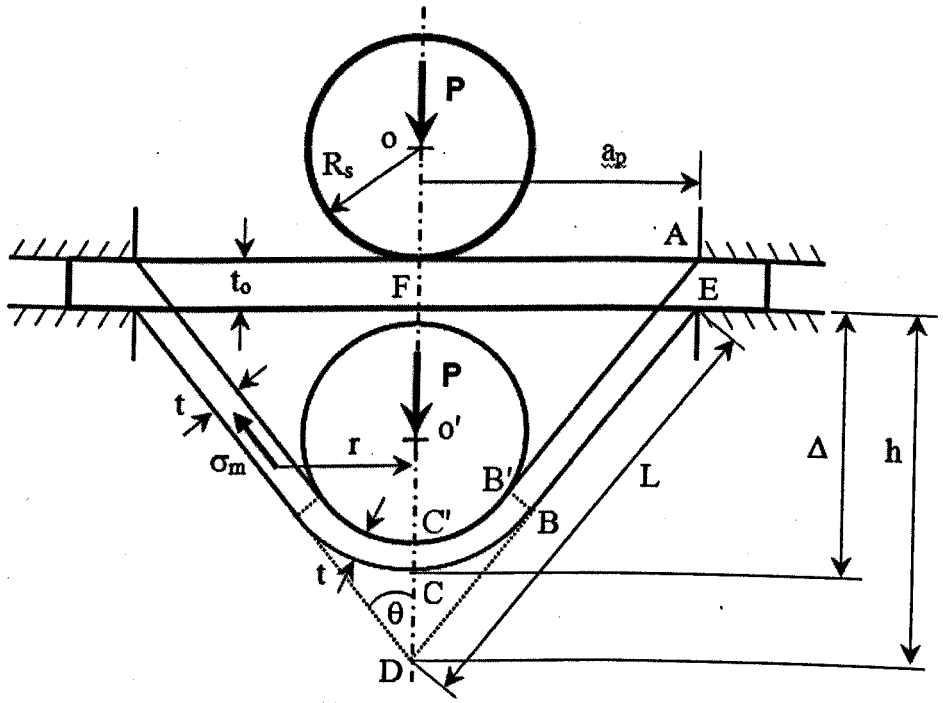

Fig. 3.4 Initial and deformed (assumed constant thickness) shape of the SPT specimen.

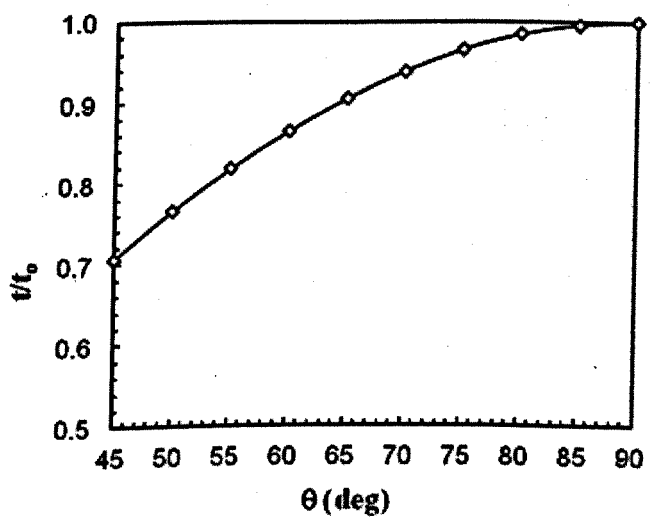

Fig. 3.5 Variation of t/t_o with θ.

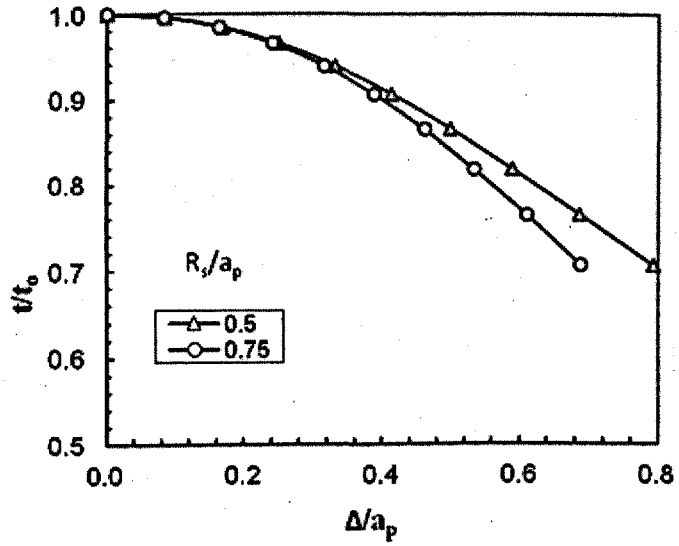

Fig. 3.6 Variation of t/t_o with Δ/a_p.

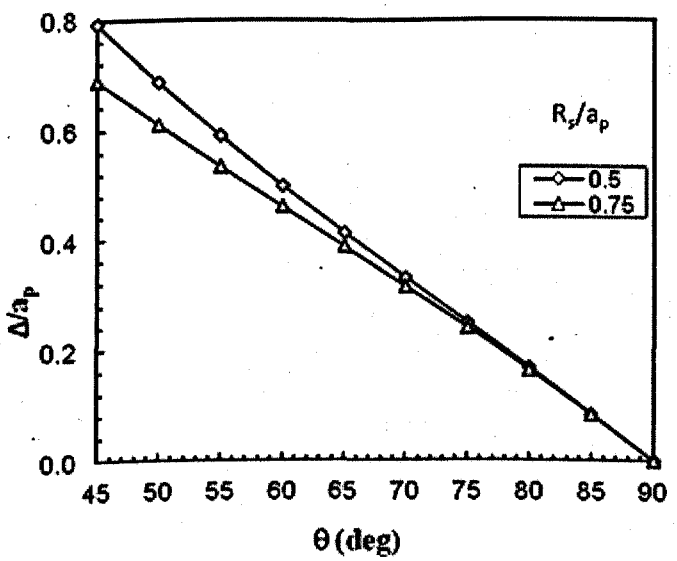

Fig. 3.7 Variation of Δ/a_p with θ.

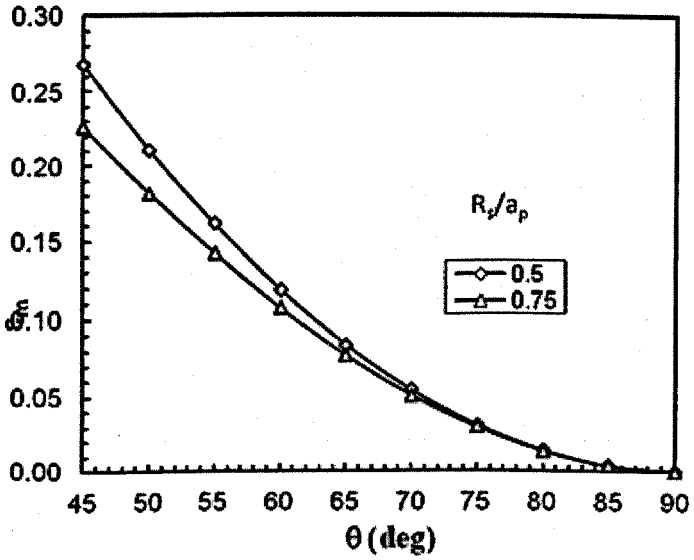

Fig. 3.8 Variation of ε_m with θ.

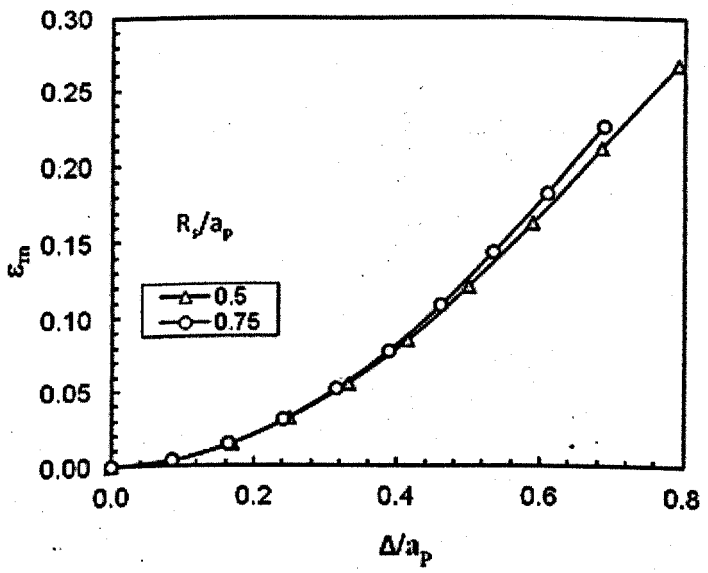

Fig. 3.9 Variation of ε_m with Δ/a_p .

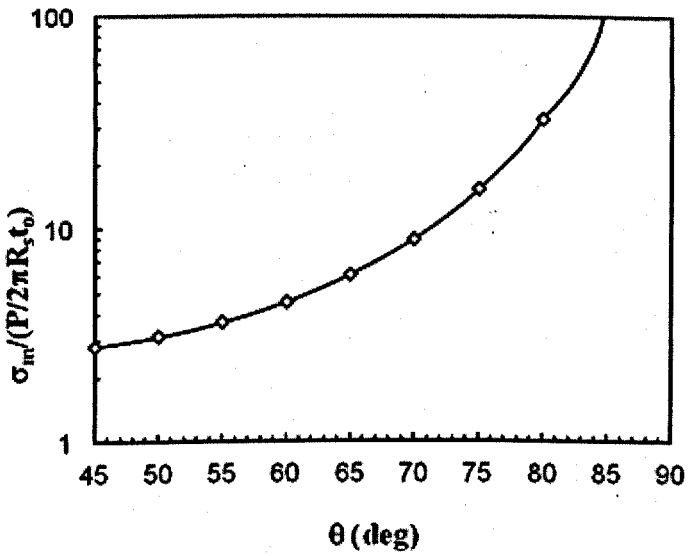

Fig. 3.10 Variation of $\sigma_m/(P/2\pi R_s t_o)$ with θ.

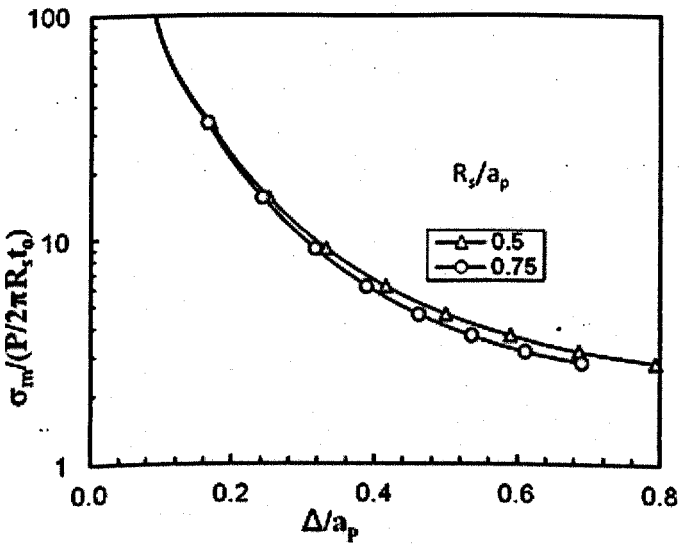

Fig. 3.11 Variation of $\sigma_m/(P/2\pi R_s t_o)$ with Δ/a_p.

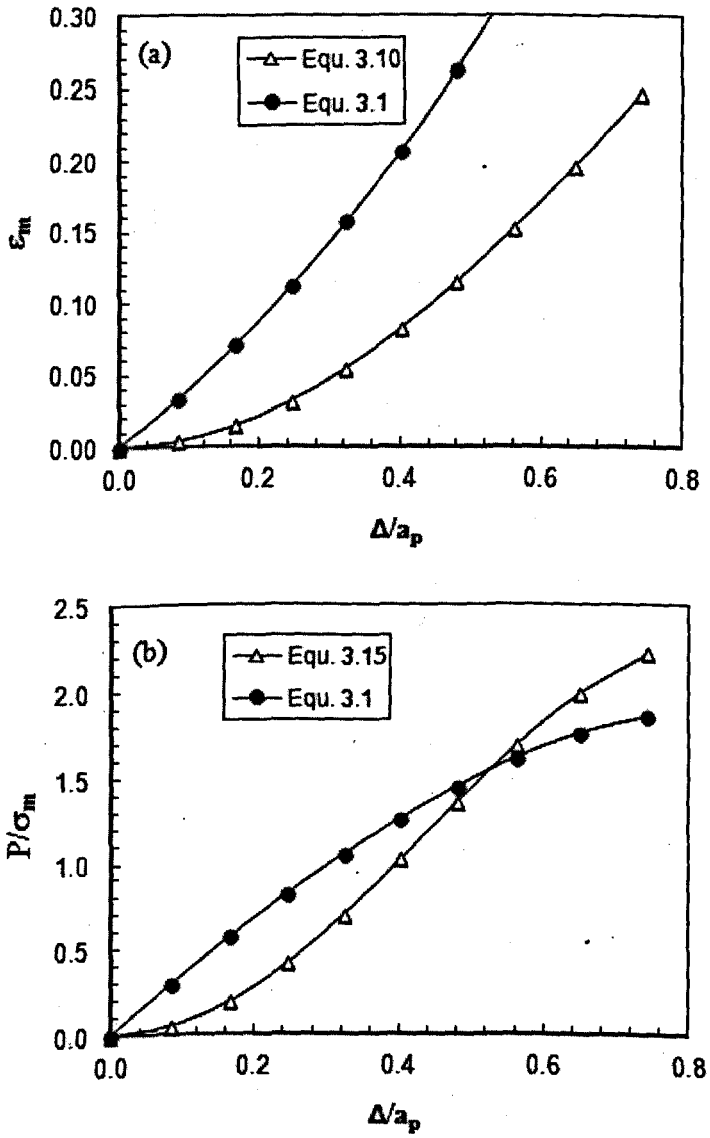

Fig. 3.12 (a) Variation of ε_m with Δ/a_p for a_p = 2mm and R_s = 1.25mm; (b) Variation of P/σ_m with Δ/a_p with a_p = 2mm, R_s = 1.25mm and t_0 = 0.5mm.

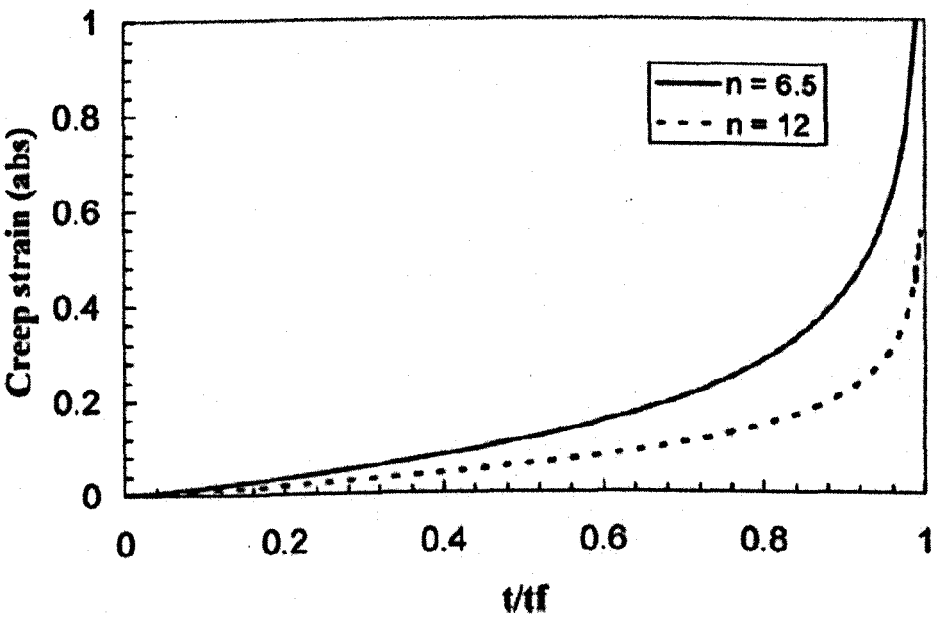

Fig. 3.13 Creep strain data for ductile (Norton's creep law) failure model.

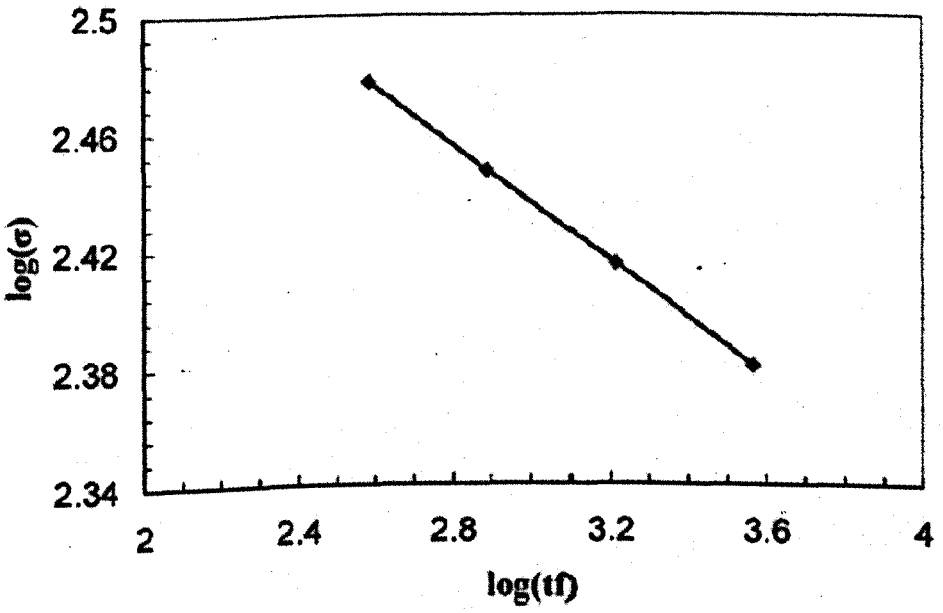

Fig. 3.14 Creep rupture data for a ductile (Norton's creep law) failure model, based on constants for 316 stainless steel at 600° C (gradient = $-1/n$).

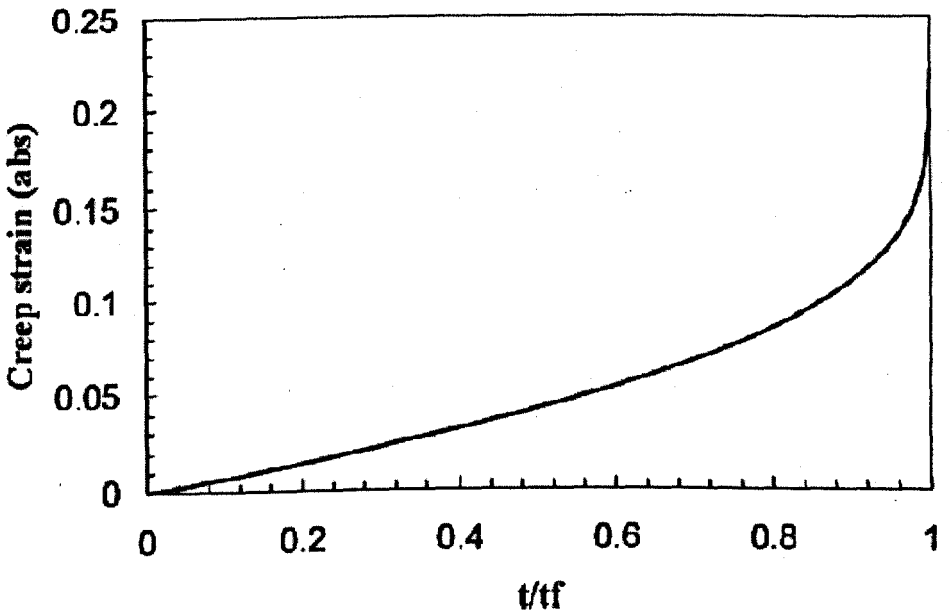

Fig. 3.15 Creep strain data for brittle (Kachanov damage) failure model, using constants for 316 stainless steel at 600° C.

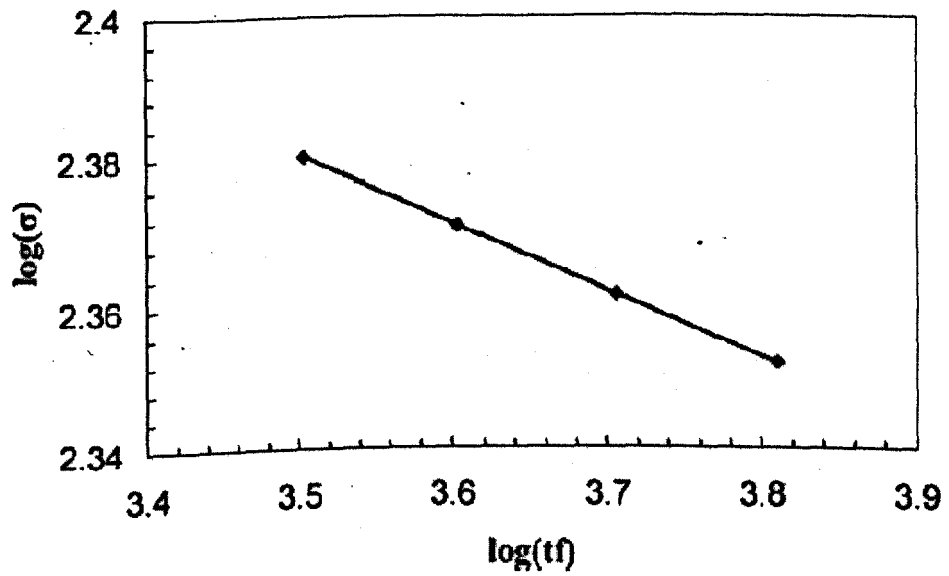

Fig. 3.16 Creep rupture data for a brittle (Kachanov damage) failure model using constants for 316 stainless steel at 600° C (gradient = $-1/n$).

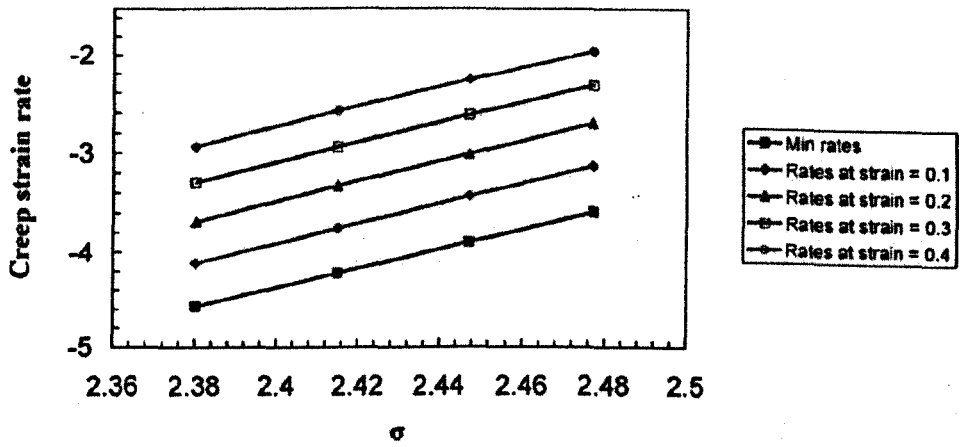

Fig. 3.17 Variations of creep strain rate with σ on a log-log scale for a material obeying a 'ductile' Norton model (for 316 stainless steel at 600° C).

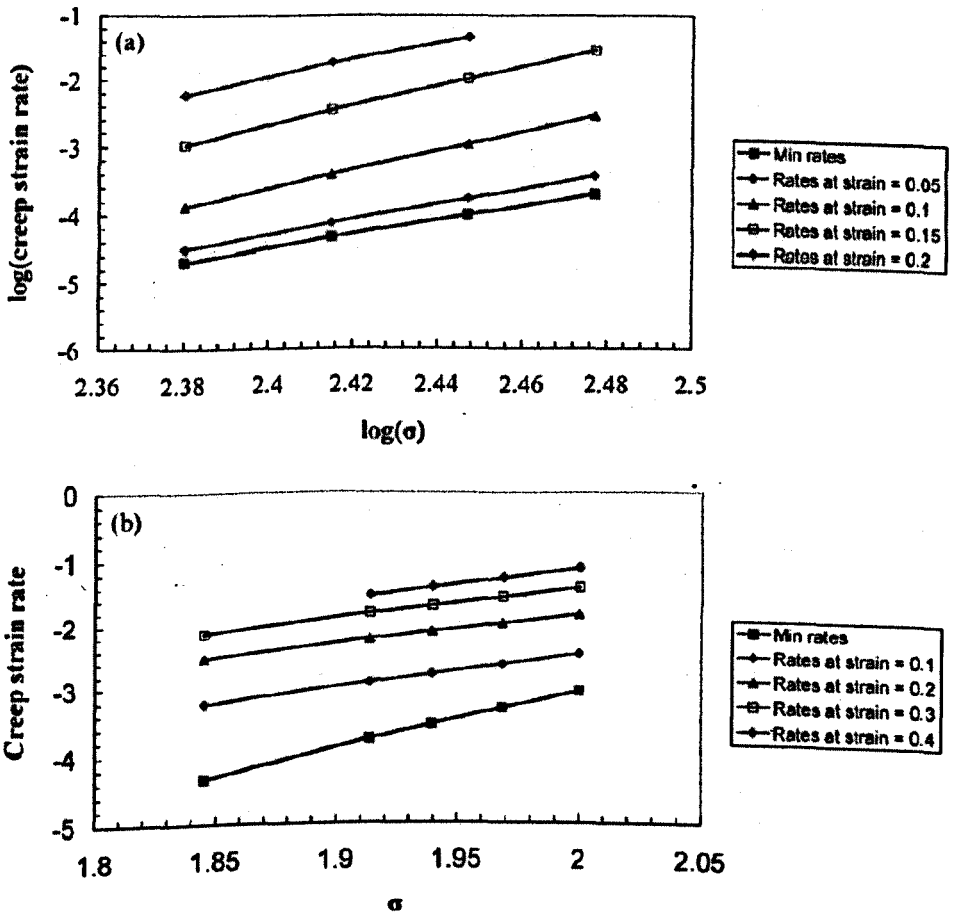

Fig. 3.18 (a) Creep strain rate versus σ on log-log scale using the Liu and Murakami [4] damage model (for 316 stainless steel at 600° C); (b) Creep strain rate versus σ on log-log scale using the Liu and Murakami [46] damage model (for P91 steel at 650° C.

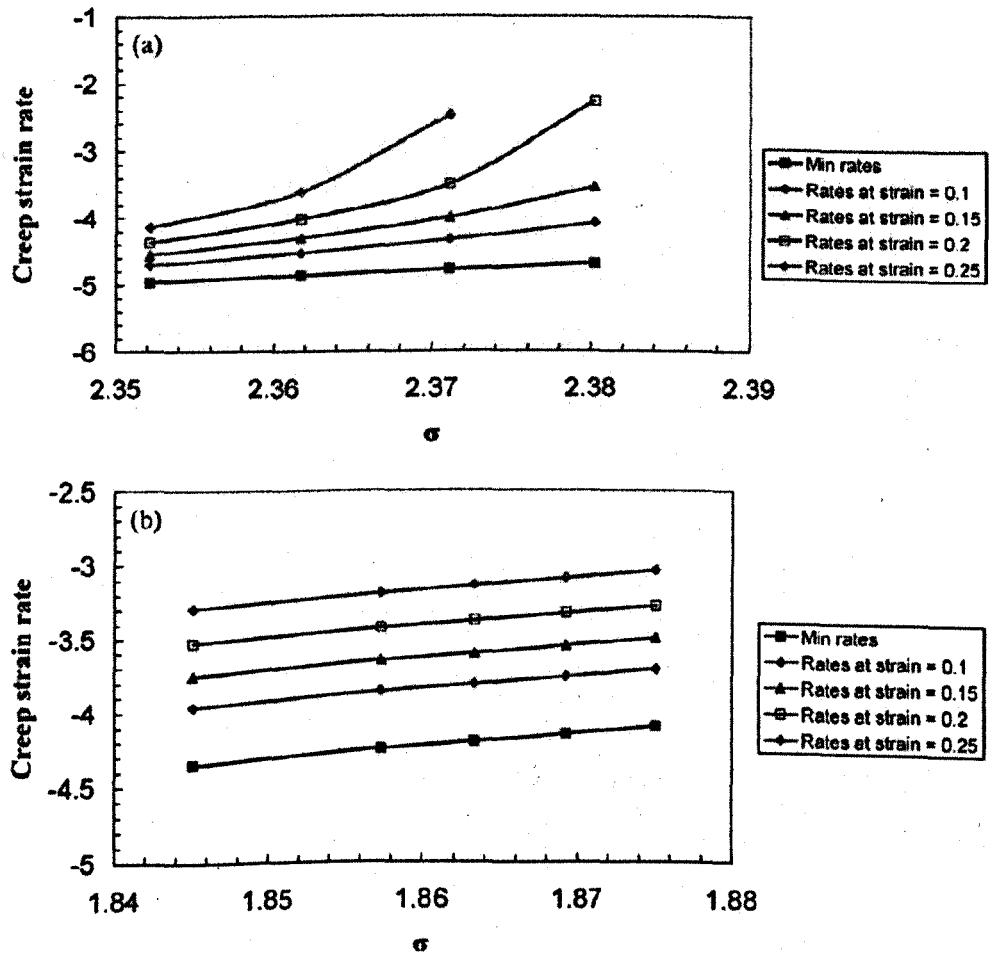

Fig. 3.19 (a) Creep strain rate versus σ on log-log scale using the Kachanov damage model (for 316 stainless steel at 600° C); (b) Creep strain rate versus σ on log-log scale using the Kachanov damage model (for P91 steel at 650° C).

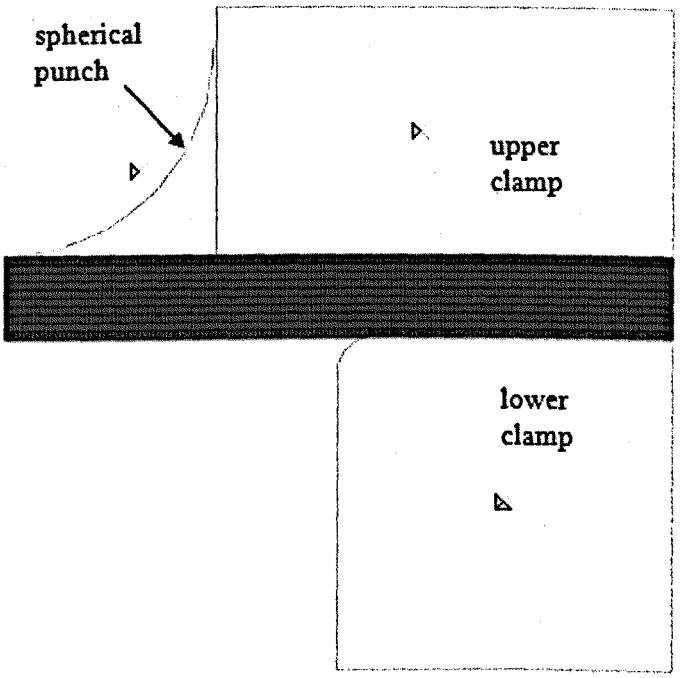

Fig. 3.20 FE model used for the SPT analyses.

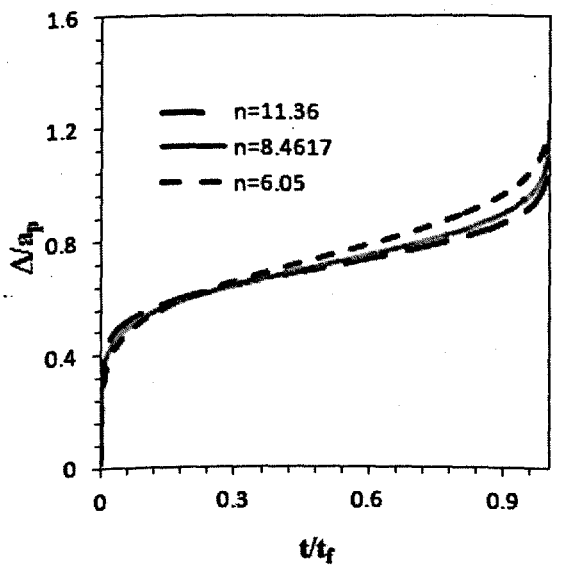

Fig. 3.21 Δ versus t_f for Norton law creep behaviour with $n = 6.05, 8.4617,$ and 11.36.

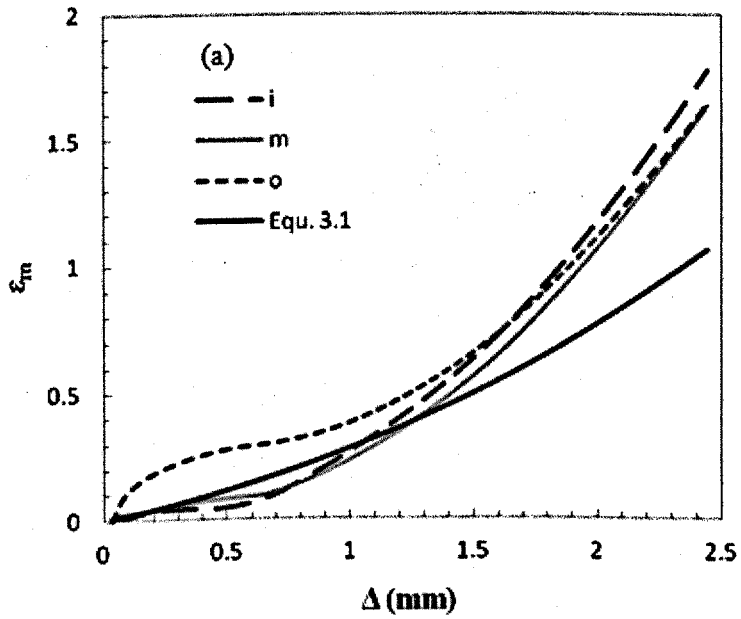
(a)
i
m
o
Equ. 3.1
ε_m
2
1.5
1
0.5
0
0
0.5
1
1.5
2
2.5
Δ (mm)

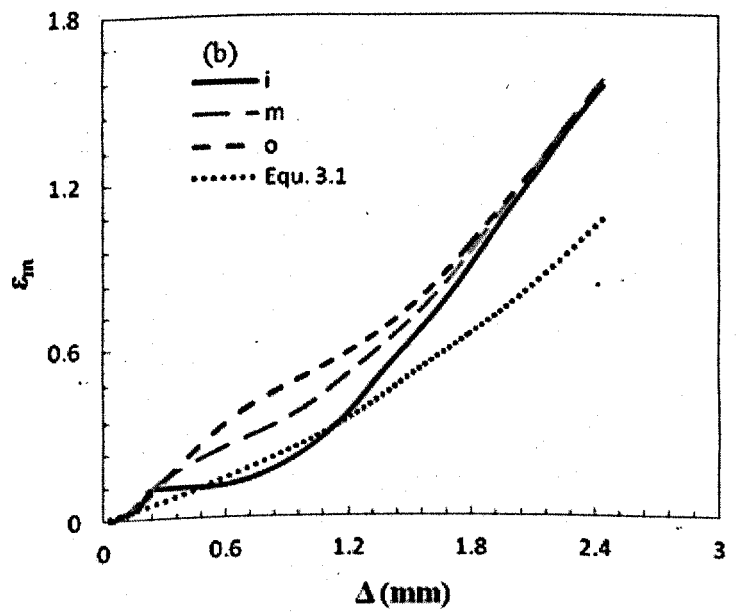
(b)
i
m
o
Equ. 3.1
ε_m
1.8
1.2
0.6
0
0
0.6
1.2
1.8
2.4
3
Δ (mm)

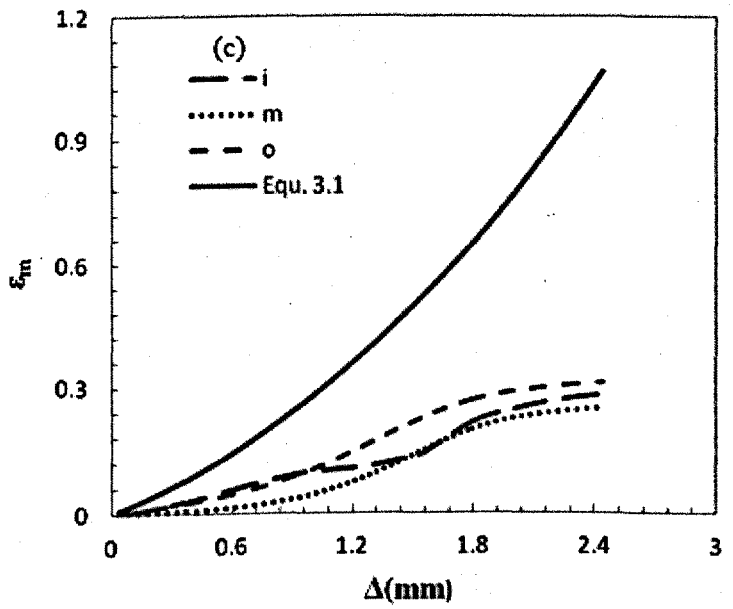

Fig. 3.22 ε_m versus Δ at inside (i), middle (m), and outside (o). (a) Position A; $n = 6.05$, (b) Position B; $n = 6.05$, (c) Position C; $n = 6.05$.

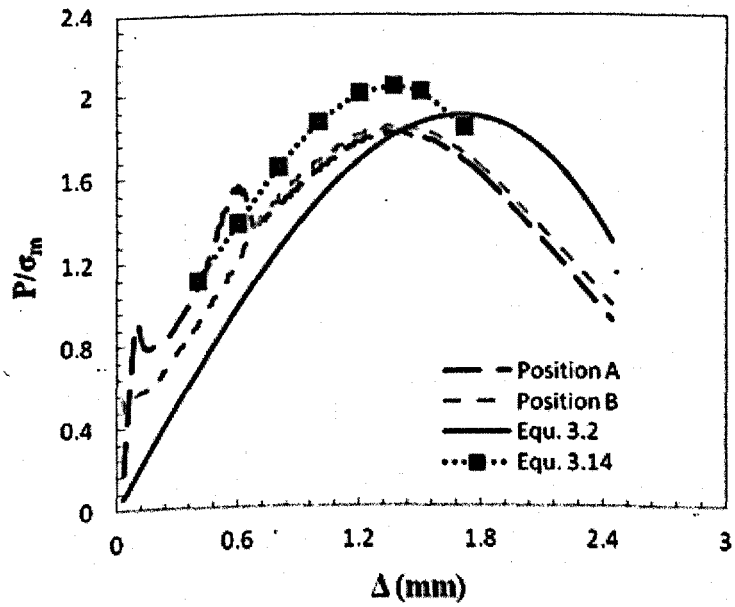

Fig. 3.23 Variations of P/σ_m with Δ (middle, m); $n = 6.05$.

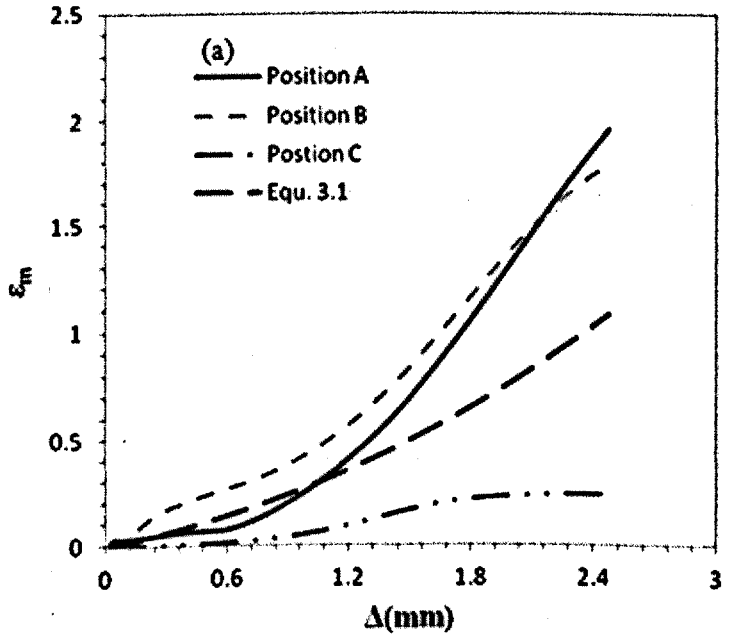

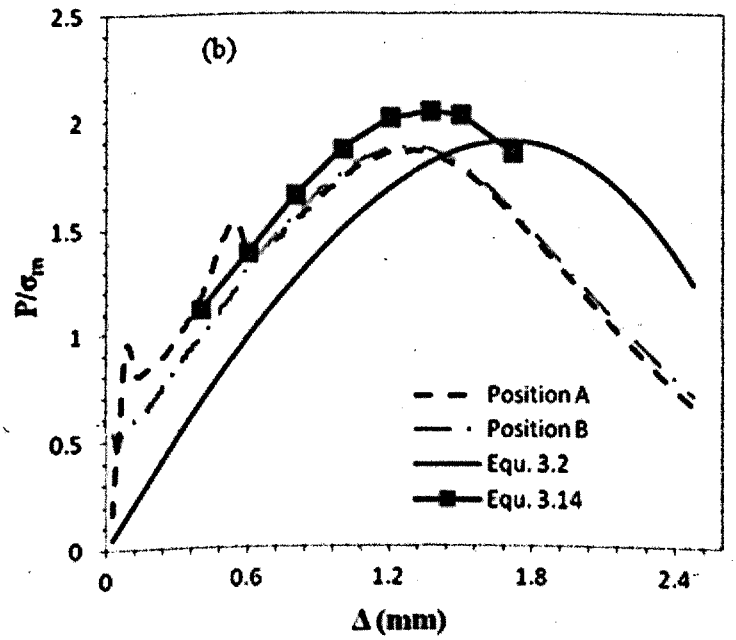

Fig. 3.24 (a) ε_m (middle, m) versus Δ at three positions; $n = 8.4617$. (b) Variations of P/σ_m with Δ; $n = 8.4617$.

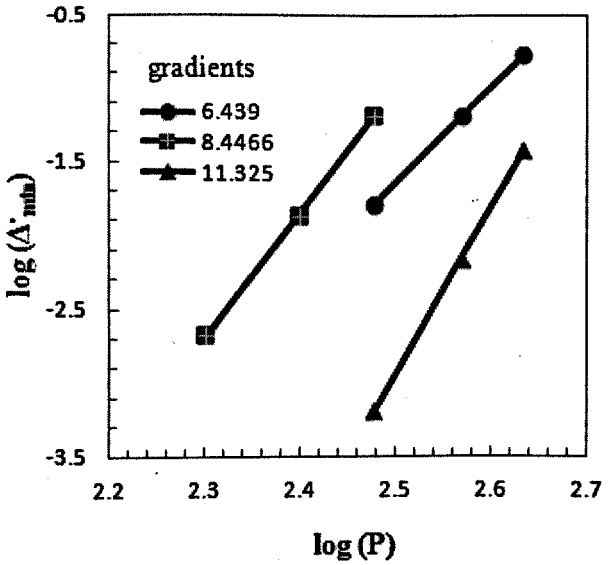

Fig. 3.26 FE predictions of $\log(\Delta_{min})$ versus $\log(P)$ based on Norton's law ($n = 6.05, B = 1.88 \times 10^{-18}; n = 8.4617, B = 1.09 \times 10^{-20}; n = 11.36, B = 5.38 \times 10^{-29}$).

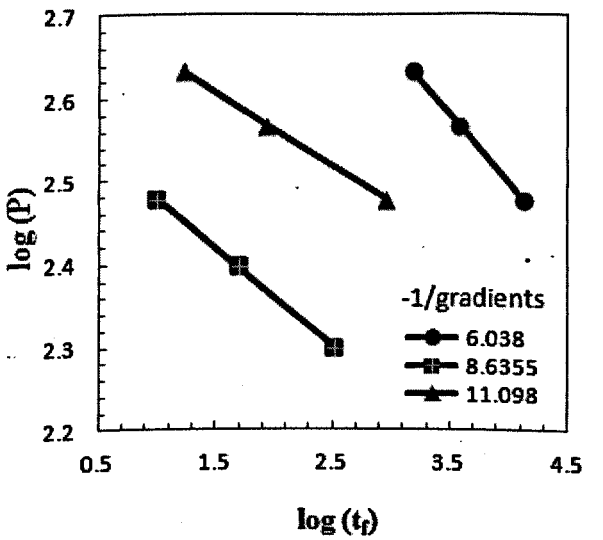

Fig. 3.27 FE predictions of $\log(P)$ versus $\log(t_f)$ based on Norton's law ($n = 6.05; n = 8.4617; n = 11.36$).

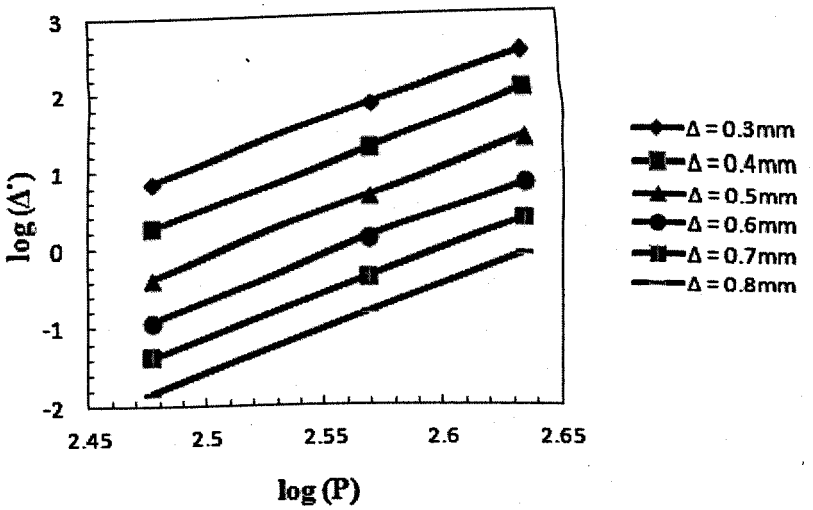

Fig. 3.28 Plot of $\log(\dot{\Delta})$ versus $\log(P)$ for different displacements ($n = 11.36, B = 5.38 \times 10^{-29}$).

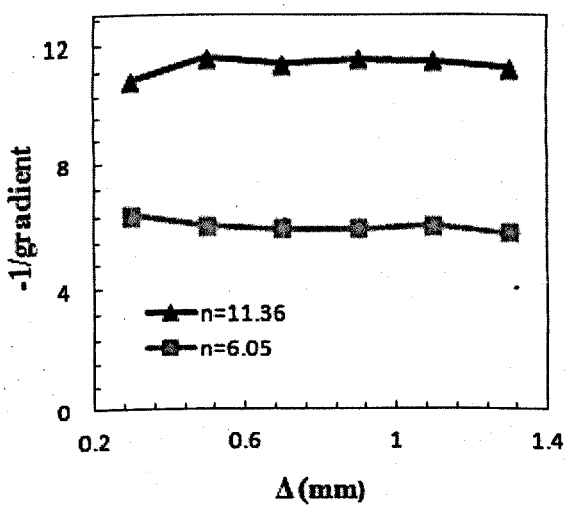

Fig. 3.29 Variation of gradients (of $\log(\dot{\Delta})$ versus $\log(P)$) with Δ.

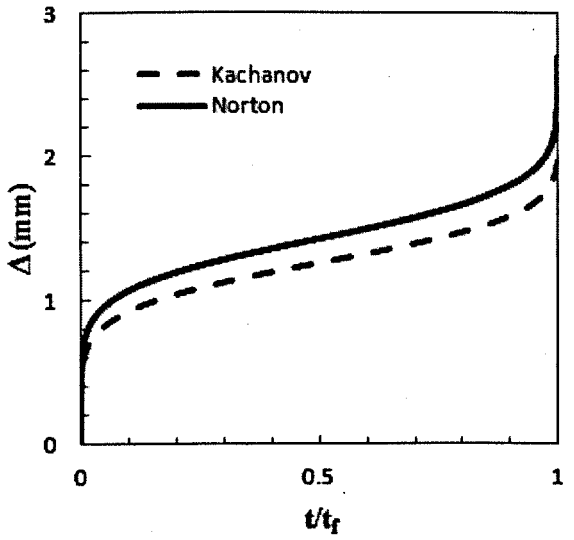

Fig. 3.30 Comparison of Δ versus t/t_f for both the Kachanov damage model and Norton's law.

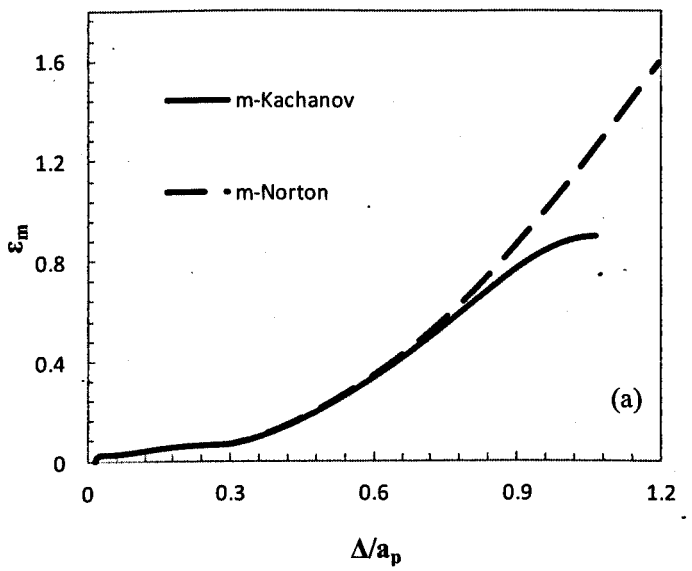

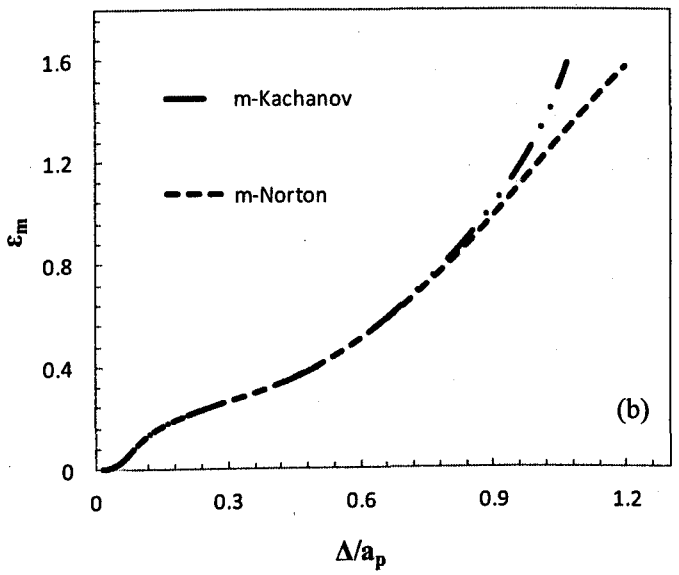

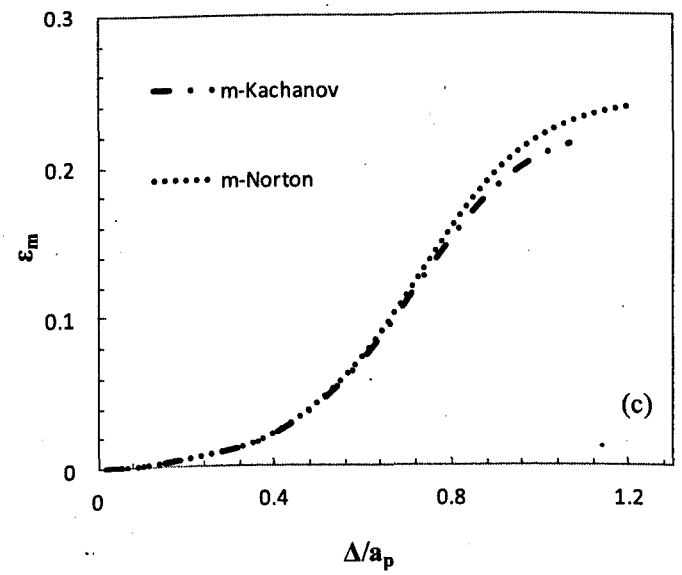

Fig. 3.31 ε_m versus Δ at the middle (m) for both the Kachanov damage model and Norton's law. (a) Position A, (b) Position B, (c) Position C.

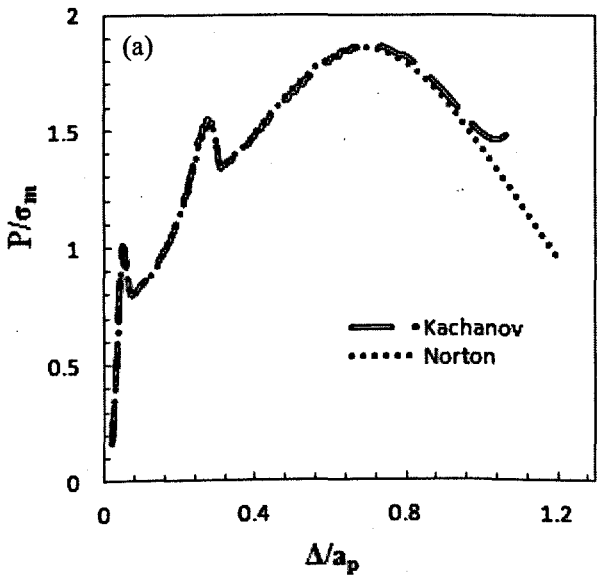

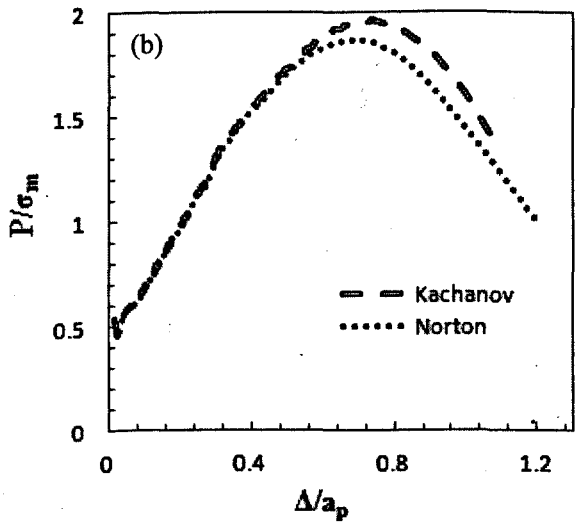

Fig. 3.32 Variation of P/σ_m with Δ/a_p (middle, m) for both the Kachanov and Norton models, (a) Position A, (b) Position B.

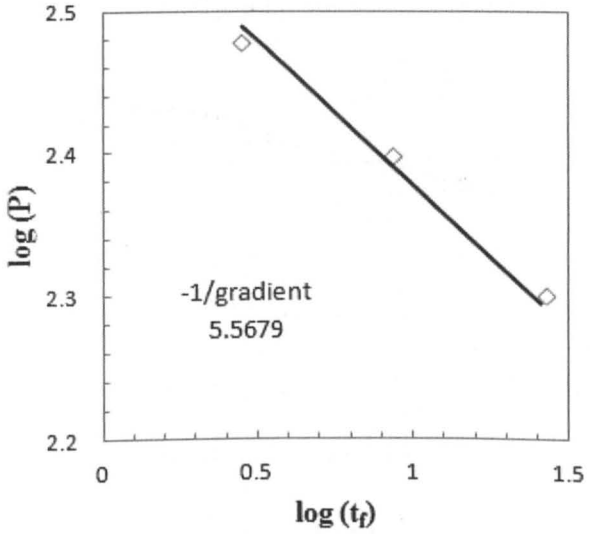

Fig. 3.33 FE predictions of $\log(P)$ versus $\log(t_f)$ based on the Kachanov damage model.

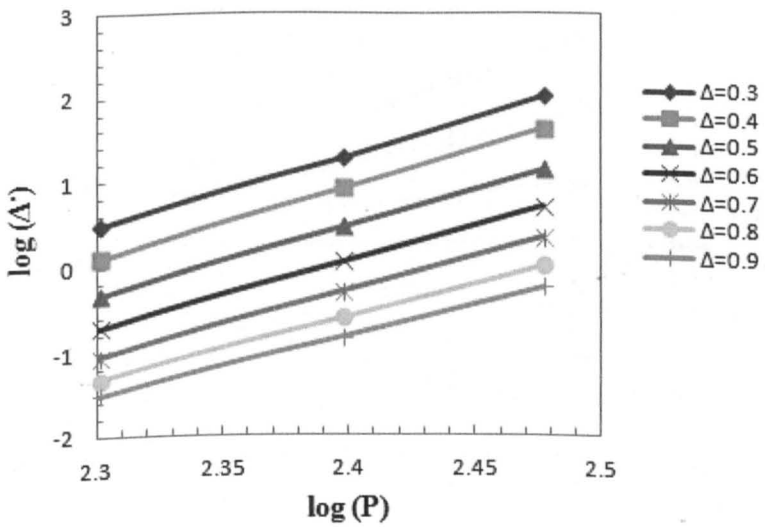

Fig. 3.34 FE predictions of $\log(\dot{\Delta})$ versus $\log(P)$ based on the Kachanov damage model for different Δ values.

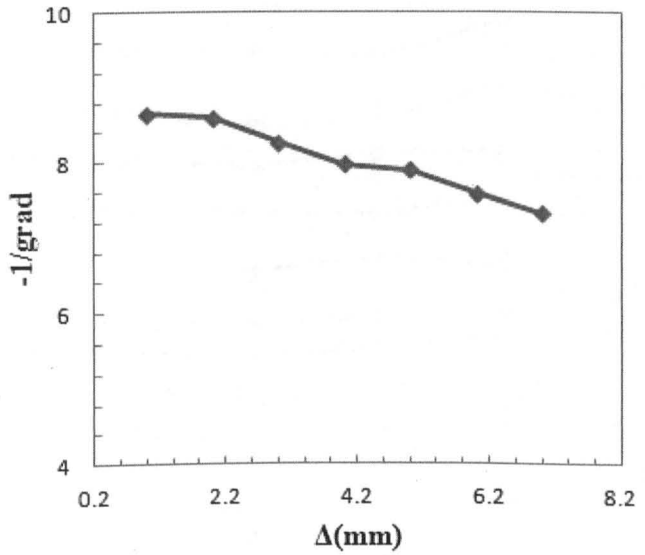

Fig. 3.35 Variation of the gradient for $\log(\dot{\Delta})$ versus $\log(P)$ with Δ for the Kachanov model ($n = 8.4617, \chi = 6.789$).

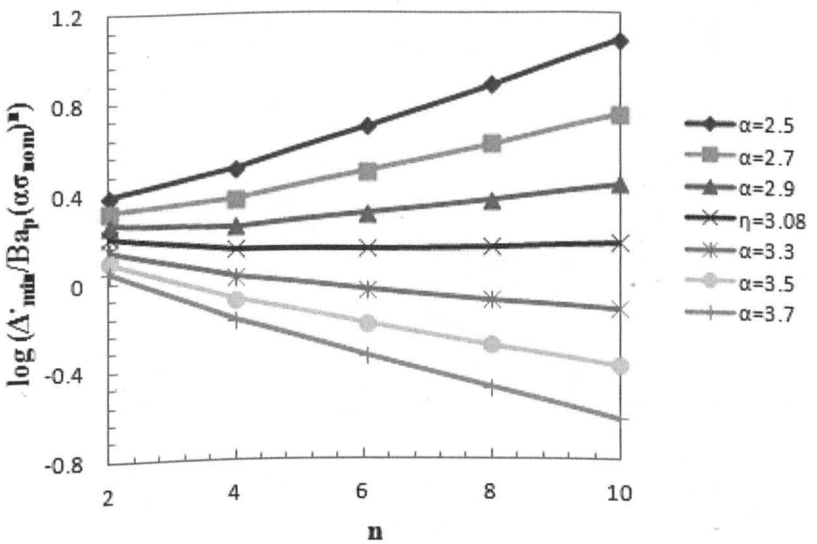

Fig. 3.36 Variations of $\log\left[(\dot{\Delta}_{min})/Ba_p(\alpha\sigma_{nom})^n\right]$ with n for various α values.

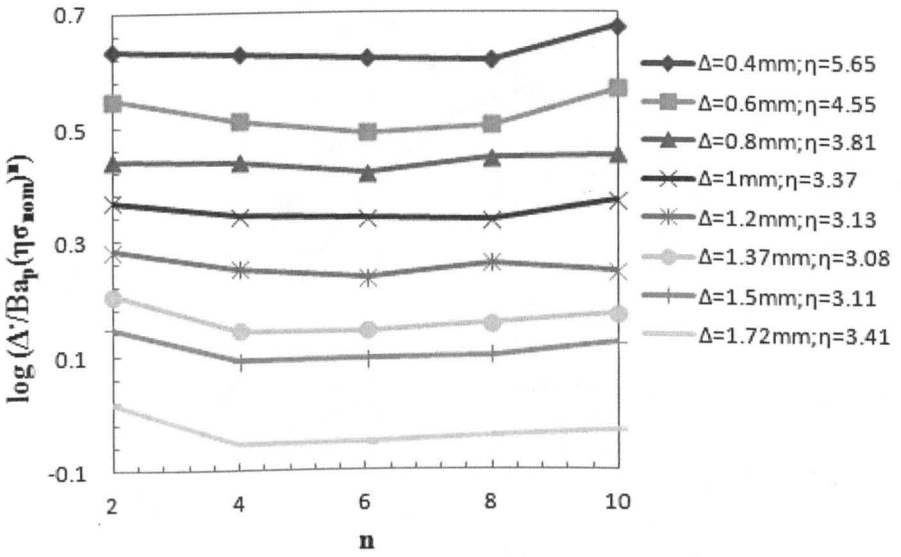

Fig. 3.37 Variations of $\log(\dot{\Delta}/Ba_p(\eta\sigma_{nom})^n)$ with n for various Δ values for the α value that produce approximately horizontal lines (NB for this conditions $\alpha = \eta$).

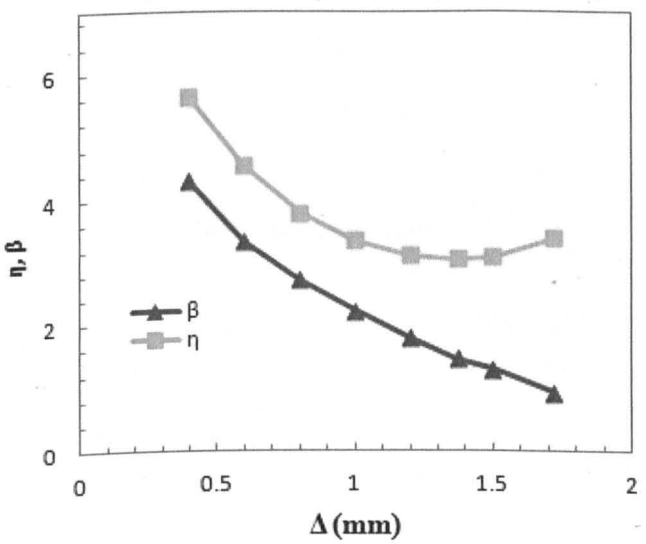

Fig. 3.38 Variations of reference parameters (α and β) with Δ.

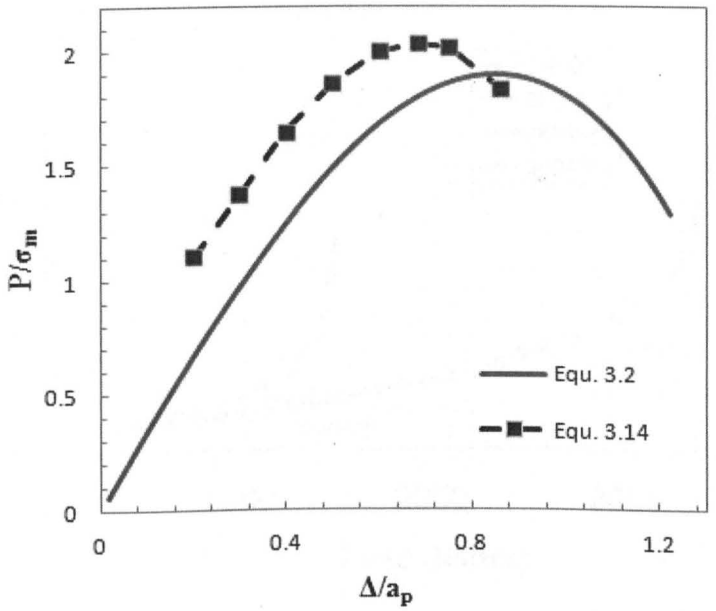

Fig. 3.39 Variation of P/σ_m with Δ/a_p.

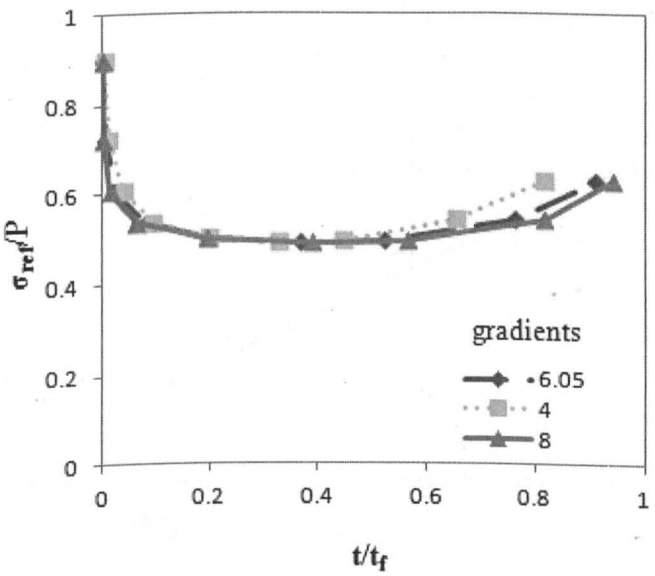

Fig. 3.40 Variation of σ_{ref}/P with t/t_f for different n values.

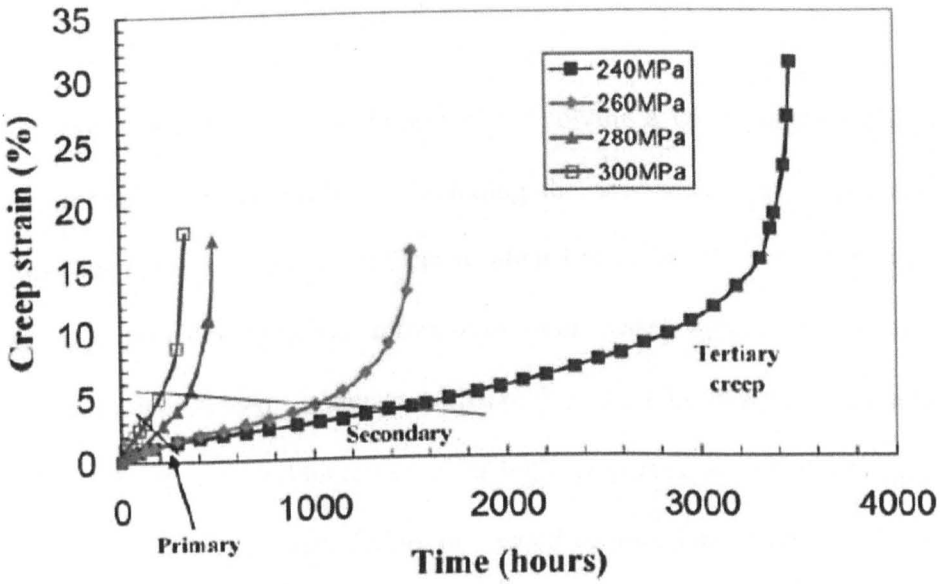

Fig. 3.41 Typical creep curves showing the primary, secondary, and tertiary regions (for 316 stainless steel at 600° C).

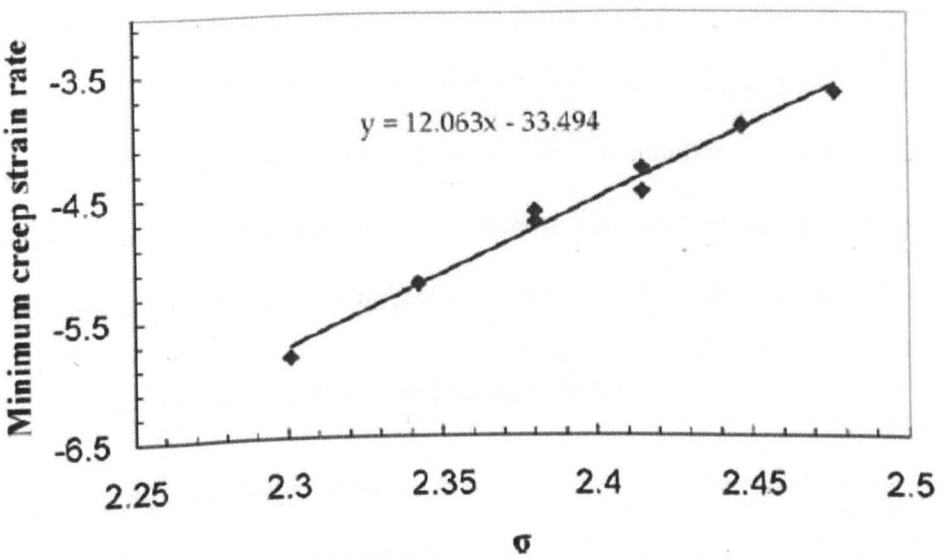

Fig. 3.42 Linear fit to minimum creep strain rate versus σ on a log-log scale for material obeying Norton's creep law (for 316 stainless steel at 600° C).

CHAPTER 4. FINITE ELEMENT ANALYSES

The finite element method is important for solving a wide range of complex engineering tasks and problems including the assessment of creep material properties and the estimation of the residual life of welded constructions. Its use also provides valuable information and better understanding of the phenomenon of "creep" in metals, which occurs in welds under severe working conditions such as constant stress under high temperatures for long periods of time, that lead to premature failure of welded components in power, chemical and many other areas of the industry.

A number of FE analyses of small punch (SP) creep tests were carried out in order to investigate two sets of geometries and their effects on the experimental data. SP creep testing is complicated, the process of which includes contacts, large strains and deformations. Because of that, the coefficient of friction is important for the final results of such tests. A number of finite element analyses under different conditions of friction were studied and the effects on the displacement and rupture properties were examined in this chapter.

4.1 Liu and Murakami Creep Damage Model

The Liu and Murakami damage model was used to describe the material behaviour including tertiary creep because its mesh sensitivity is less than the Kachanov creep damage model. As a result of that, the Liu and Murakami model is more economical and requires less computational time **[89]**. The multi-axial form of the model consists of a pair of coupled creep/damage equations (Eqs. 2.23 - 2.24) which have been described in Chapter 2.

Integration of Eqn. (2.24), under uniaxial conditions, leads to

$$\omega = -\frac{1}{q_2} Ln\left[1-\left(1-e^{-q_2}\right)\frac{t}{t_f}\right] \tag{4.1}$$

where

$$t_f = \frac{1}{B(1+\phi)\sigma^{\chi}} \tag{4.2}$$

The material constants B, χ, q_2 and ϕ are obtained by curve fitting to the uniaxial creep curves, and the triaxial stress state parameter, α, is obtained by creep damage modelling of the notched bar creep rupture tests **[2]**.

4.2 General Methodology of Obtaining Creep Properties

Usually, the data obtained from uniaxial creep and creep rupture curves for P91 steel at 650^0 C are processed in order to calculate the material constants. Material constants A and n are obtained by plotting the uniaxial minimum creep strain rates against the applied stresses (log-log scales) and obtaining the slope, n and the intercept, log (A). The other material constants, χ and M, where $M = B(1+\phi)$, are obtained by plotting the uniaxial failure times against the applied stresses (log-log scales) and obtaining the slope, -1/ χ, and the intercept, log (M) **[2]**. For the Liu and Murakami model, q_2 can be obtained by fitting the uniaxial creep strain curves using Liu/Murakami model, to the experimental uniaxial creep curves at different q_2 values keeping the other material constants the same. The q_2 value that gives the best fitting is then taken as the correct value.

The multiaxial stress parameter, α, for the parent material and the weld metal are usually obtained by determining, experimentally, the time to failure of notched bar specimens. Then, by performing a series of notched bar FE analyses using material properties, obtained from the fits to the uniaxial tests data, for the damage model, Eqns. (1-3), with a range of α values; the α-value which gives the same failure time as the corresponding experimental value, can be determined. Usually, this process is carried out for a number of test loads (resulting in a number of failure times) and the average value of α is taken to be the final α-value. The resulting α-value for P91 steel at $650^0\ C$ is given in Table 1.

Table 1 P91 Material constants for damage constitutive equations at 650 °C (σ in MPa and time in h)

A	n	B	χ	q_2	ϕ	α
1.09e-20	8.4617	3.5367e-17	6.789	3.2	7.3457	0.312

4.3 FE Results for E.ON testing set-up

A set of FE analyses were carried out to compare and examine the results with the testing machine used in the experimental work. Fig. 4.1 shows the main dimensions of the small punch set-up for the E.ON testing equipment, where $R_s = 1mm$ is the radius of the hemi-spherical punch, and $a_p = 2mm$ is the radius of the receiving orifice, $t_0 = 0.5mm$ and $D = 4mm$ are the thickness and radius of the disc sample, respectively. The punch, and the lower and upper die were modelled as axisymetric analytical rigid components. Similarly, the small

punch specimen was chosen to be an axisymetric deformable shell. The reduced integration element type CAX4R is chosen to prevent the shear and volume locking due to severe shear and torsion effects, which tend to occur in a contact simulation **[89]**. The boundary conditions are shown in Fig. 4.1. It should be noticed that a clamping force was used to restrict the specimen and prevent its displacement in the horizontal direction. A set of FE analyses was carried out in order to find suitable clamping force. It was found that the magnitude of the clamping force should be approximately three times bigger than the applied force on the punch for the set-up shown in Fig. 4.1. A sliding of the specimen could occur if the clamping force is less than the ratio mentioned above. On the other hand, the use of very high clamping force is likely to cause creep of the clamped area of the specimen and change of material behaviour. A coefficient of friction, $\mu = 0.3$, was used in the contact conditions between the small punch sample, upper and lower dies. Two coefficients of friction, $\mu = 0.3$ and 0.6, were used for the contact between the punch and the specimen. All of the FE analyses were carried out using the Liu and Murakami damage model which has been described in Section 4.1. Fig. 4.2 a) shows the displacement versus time results of SP creep tests with coefficient of friction, $\mu = 0.3$, between the punch and specimen. It is interesting to notice that the form of the data seems similar to a typical creep curve with three distinguished regions of "primary", "secondary" and "tertiary" creep. However, the theoretical model used in this research describes only secondary and tertiary creep behaviour. Usually, the method used for obtaining small punch creep data is similar to that used for deriving material properties from uniaxial creep tests. Fig. 4.3 shows a typical progress of small punch creep

analysis in three different positions of the specimen (displacements of Δ = 0.8mm, 1mm, and 1.2mm). This figure shows also the deformed shape of the small punch disc and the damage levels in all elements according to the Liu and Murakami theoretical model. There is an area of the disc which is with very high damage even for displacements associated with steady state displacement rates. The small punch creep material properties for a particular geometry may be obtained from plots of minimum displacement rate, $\dot{\Delta}_{min}$, versus load, P, and load, P, versus failure time, t, in log scale (Figs. 4.4 and 4.5).

Another set of data was obtained from small punch creep analyses with coefficient of friction, $\mu = 0.6$, between the punch and the specimen. The boundary conditions and the loads were kept the same as the analyses described above. A comparison of displacement, Δ, versus time, t, plots shows that the higher coefficients of friction lead to an increase of time to failure (Figs. 4.2 a) and b)). The creep data derived from these analyses are shown in Fig. 4.4 and Fig. 4.5.

4.4 FE Results for Tinius Olsen Testing Set-up

A second set-up for small punch creep testing using a Tinius Olsen machine in order to obtain more reliable data and to find out the significance of the variation in the punch radius. FE analyses of the Tinius geometry were carried out and the results were processed and presented in this section. Fig. 4.6 shows the basic dimensions of the set-up. Boundary conditions, load levels and coefficients of friction were kept the same as the ones used for the E.ON set-

up. The type and number of elements and components are exactly the same as those in Section 4.3. The only differences are in the punch radius ($R_s = 1.25mm$) and the introduced radius on the edge of the lower die orifice. Again, the material properties were derived from small punch creep displacement rate and rupture data using the same technique described in the previous section for E.ON design. Figs. 4.9 a) and b) show plots of the log P versus log t_f, and log $\dot{\Delta}_{min}$ versus log P data for coefficient of friction, $\mu = 0.3$, between the punch and specimen. Also, the results for another set of data, with $\mu = 0.6$, are compared in Figs. 4.9 a) and b). All of these results were derived from displacement versus time curves shown in Figs. 4.7 a) and b). It should be noted that a change in coefficient of friction for Tinius small punch testing design leads to even greater difference in time to failure data than the E.ON set-up. The deformed shapes and damage levels of the elements for a typical small punch creep analysis at three different positions (displacements) are shown in Fig. 4.9.

4.5 Discussion and Conclusions

FE analyses of small punch creep tests for two different punch radii and two coefficients of friction were carried out using the commercial software ABAQUS. The Liu and Murakami damage model, which describes secondary and tertiary regions of creep, was used in all of the calculations. Displacement versus time curve shows similarity with the standard creep curve with distinguished "primary", "secondary" and "tertiary" creep although the theoretical model does not include the primary creep. Also, it is found that a

variation in friction between the punch and sample affects the failure time of the small punch creep tests. A comparison of the displacement data (Figs. 4.2 and 4.9) obtained for two punch radii, i.e., $R_s = 1mm$ and $1.25mm$, shows a significant increase in time to failure for the case with $R_s = 1.25mm$. Again, the small punch data for the larger radius of the hemi-spherical punch is more affected by the coefficient of friction than the data for $R_s = 1mm$ (Figs 4.2 b and 4.9 b)) Good linear fitting was achieved for $\log P$ versus $\log t_f$, and $\log \dot{\Delta}_{min}$ versus $\log P$ plots. Despite the difference in failure times between the friction calculations and the hemi-spherical punch radii, all of the data show gradients close to χ value used in the subroutine input. This could indicate that the area of the displacement curve, where the minimum displacement rate occurs and is usually believed to be associated with the secondary creep region, is actually in tertiary creep. Figs. 4.3 and 4.8 show that there is an area of the small punch specimen (for both geometries), where elements with very high damage exist even for displacement of 0.8mm which is related to the minimum displacement rate. It looks like the minimum displacement rate which lasts during the majority of creep time is due to the increasing contact area between the punch and specimen (changing in the load magnitude), and decreasing of the thickness of the disc (stiffening of the sample) at the same time.

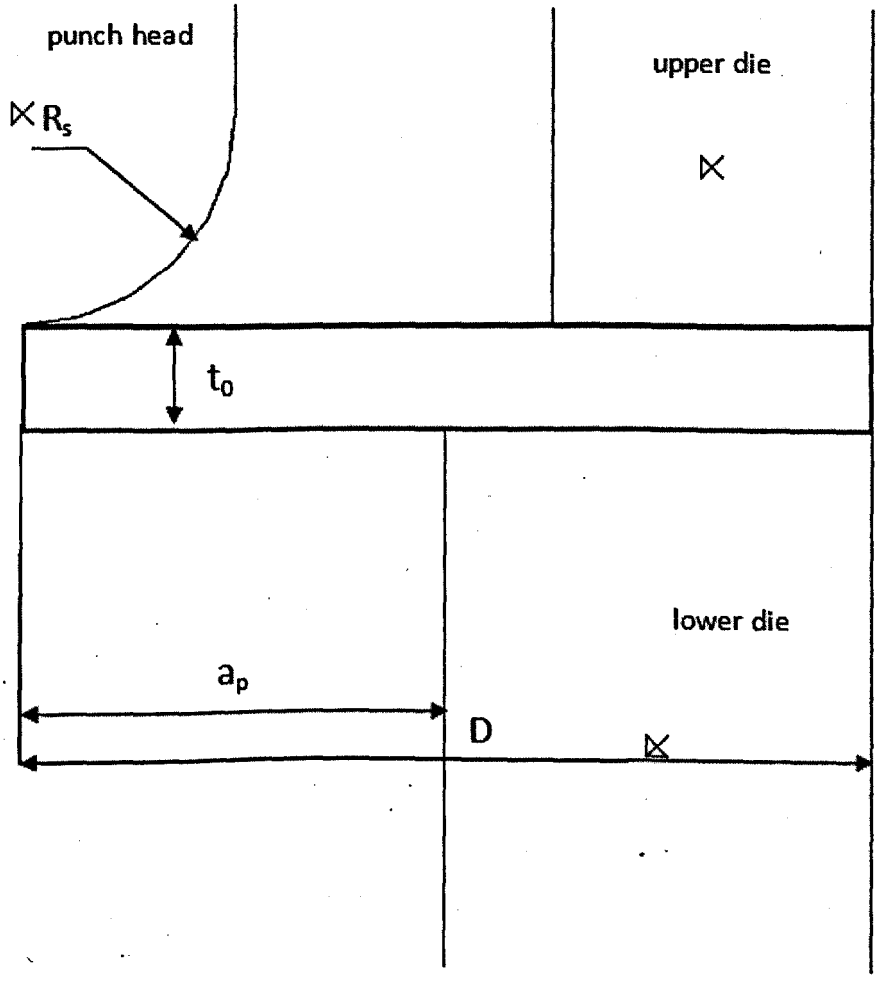

Fig. 4.1 Basic dimensions of the SP set-up for Eon testing rig.

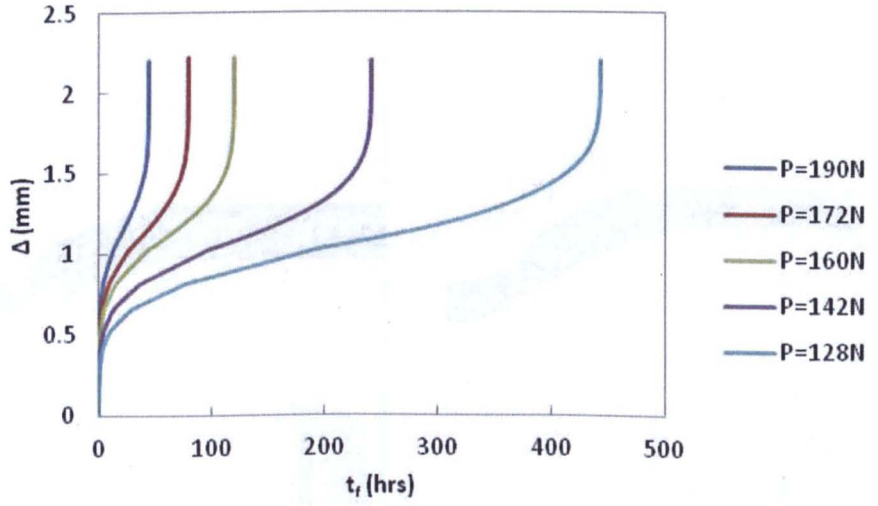

a)

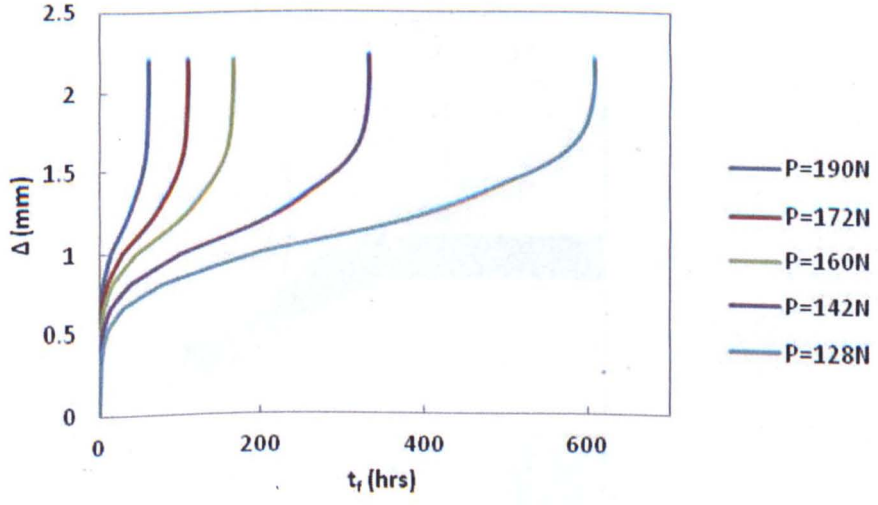

b)

Fig. 4.2 Displacement versus time curves for Eon testing design with coefficients of friction:

a) $\mu = 0.3$ and b) $\mu = 0.6$.

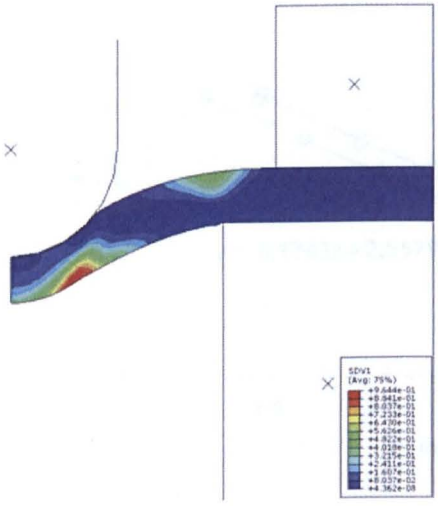

a) Δ=0.8mm

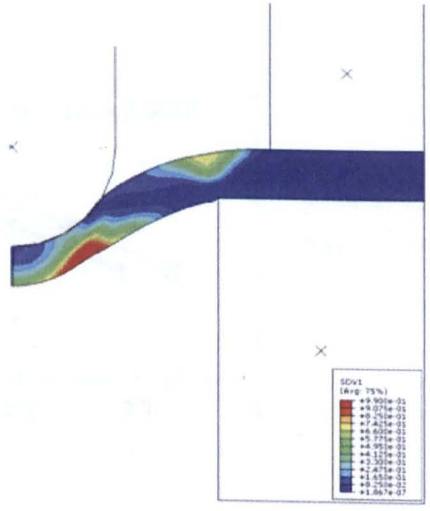

b) Δ=1mm

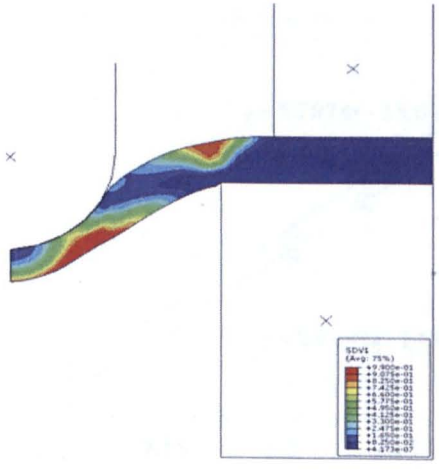

c) Δ=1.2mm

Fig. 4.3 Deformed shapes and damage levels of SP creep analysis at three displacement values (Eon testing set-up).

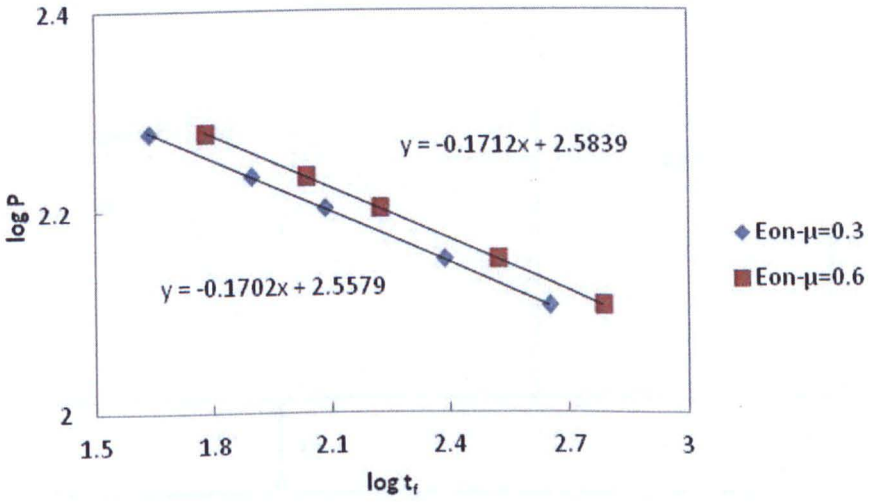

Fig. 4.4 FE results of log P versus log t_f for Eon testing set-up with coefficients of friction, $\mu = 0.3$ and 0.6.

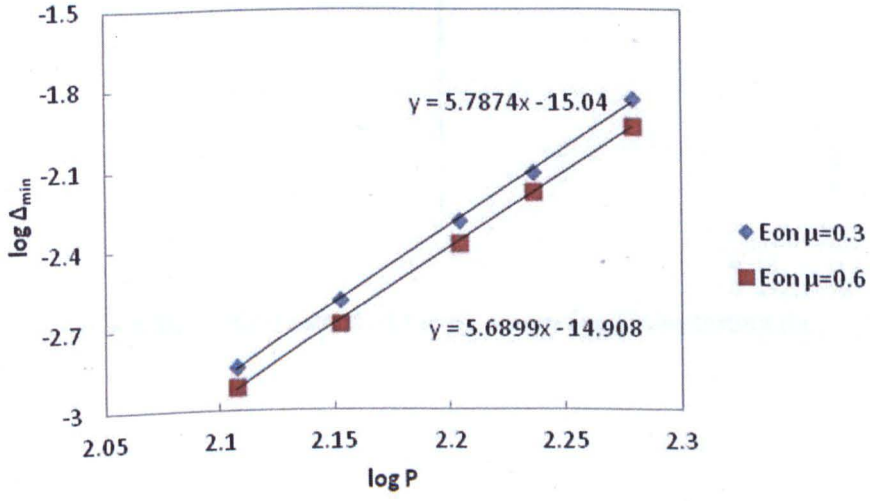

Fig. 4.5 Comparison of log $\dot{\Delta}_{min}$ versus log P data between coefficients of friction, $\mu = 0.3$ and 0.6 obtained for Eon geometry.

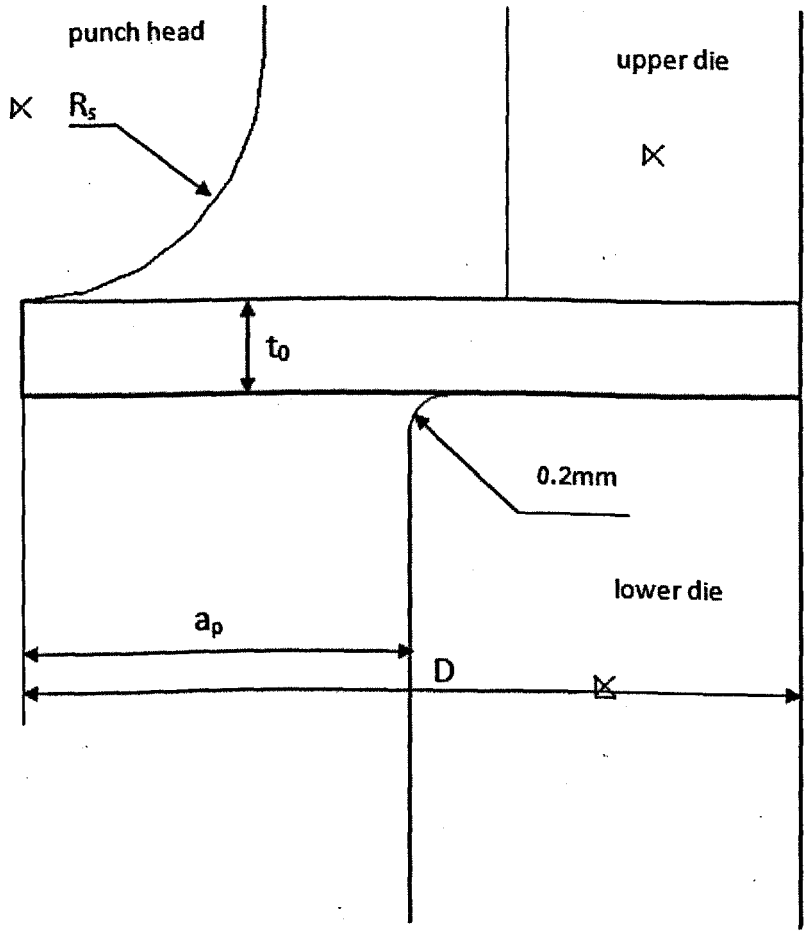

Fig. 4.6 Basic dimensions of the SP set-up for Tinius testing rig.

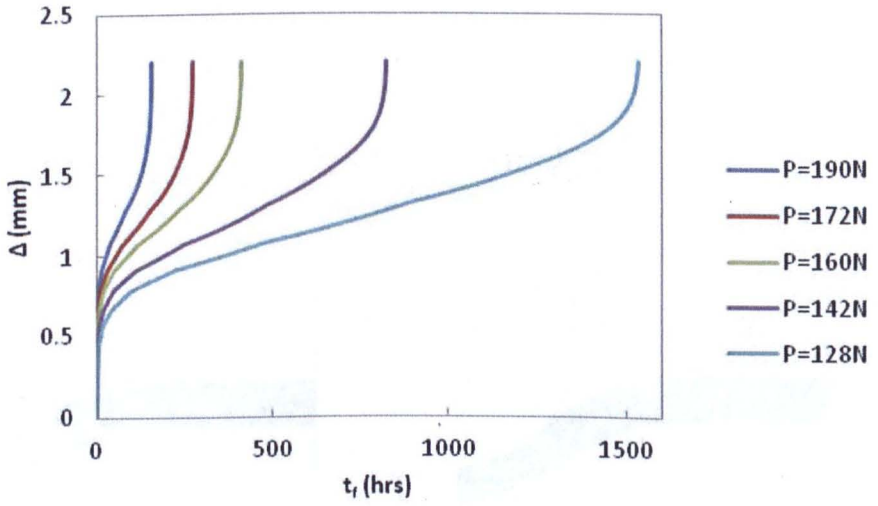

a) FE data derived for Tinius testing set-up with coefficient of friction, $\mu = 0.3$;

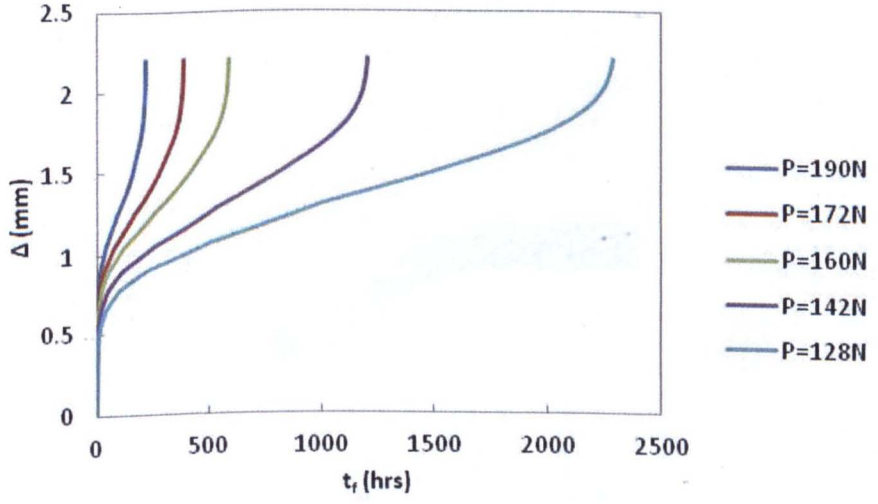

b) Results obtained from FE analyses for Tinius design with coefficient of friction, $\mu = 0.6$;

Fig. 4.7 Comparison between displacement, Δ, versus time to fail, t_f, curves for Tinius geometry with coefficients of friction, $\mu = 0.3$ and 0.6.

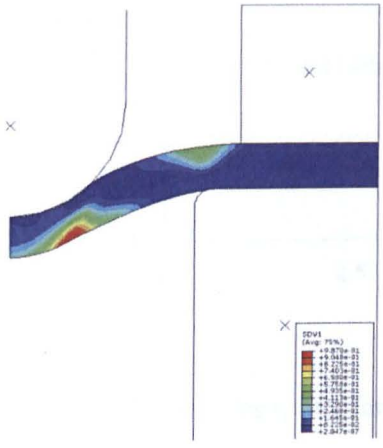

a) Δ=0.8mm

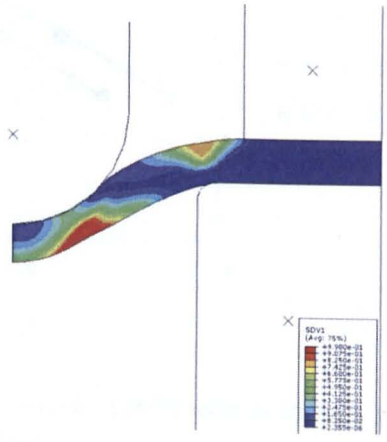

b) Δ=1mm

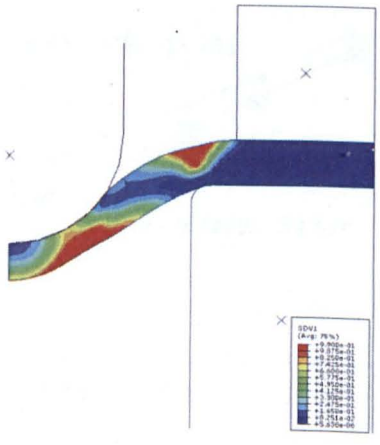

c) Δ=1.2mm

Fig. 4.8 Deformed shapes and damage levels of SP creep analysis at three displacement values (Tinius testing set-up).

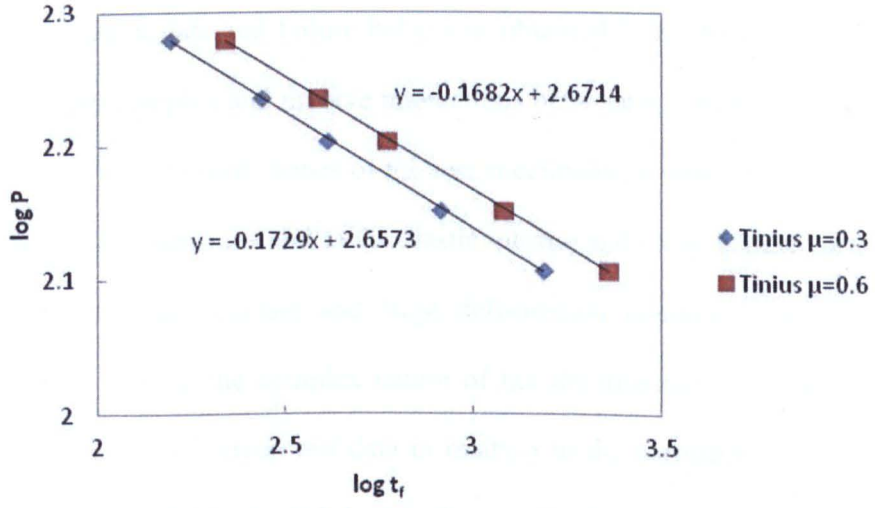

a) log P versus log t_f data for Tinius set-up under coefficients of friction, μ = 0.3 and 0.6;

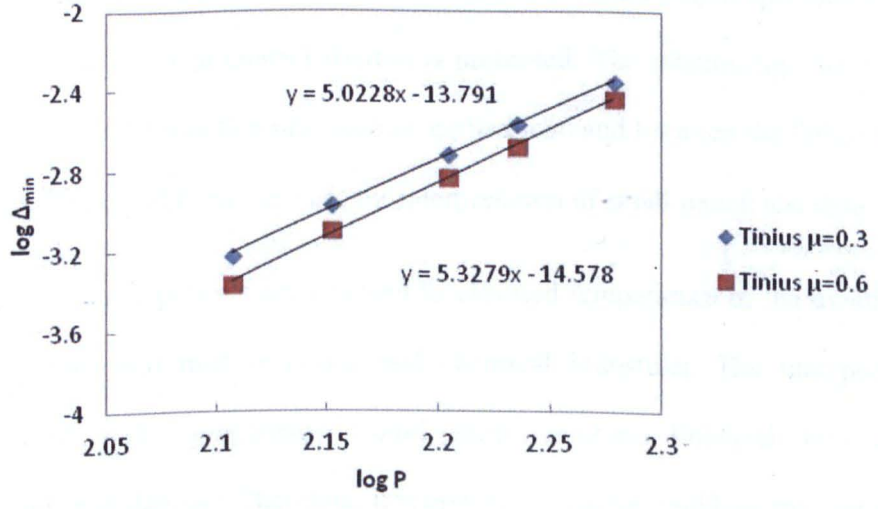

b) log $\dot{\Delta}_{min}$ versus log P data for Tinius design under coefficients of friction, μ = 0.3 and 0.6;

Fig. 4.9 Comparison of material properties obtained from FE analyses with coefficients of friction, μ = 0.3 and 0.6 for Tinius geometry.

CHAPTER 5. PARAMETRIC ANALYSES OF SP CREEP TESTS

The deformation data and failure behaviour obtained from small punch creep tests are very complex and involve interactions between a number of nonlinear processes. The deformed shapes of the test specimens are related to the punch and specimen dimensions and to the elastic, plastic and creep behaviour of the test material, under contact and large deformation conditions, at elevated temperature. Due to the complex nature of the deformation, it is difficult to interpret small punch creep test data in relation to the corresponding uniaxial creep behaviour of the material. In this chapter, results of a parametric analysis obtained from a series of finite element (FE) calculations using the Lui and Murakami creep damage model are presented, for the purpose of investigating the effects of specimen and punch dimensions on the minimum deformation rate, the failure life and on the failure location of small punch specimens. In addition, the effect of contact friction is presented. The relationships between the minimum deformation rate and the applied load and between the failure life and the load could form the basis for interpretation of small punch test data.

Many metal components are exposed to elevated temperature in the aviation, conventional and nuclear power and chemical industries. The unexpected failure of such components would cause injuries, financial loss and environmental damage. Therefore, it is essential to understand how the material deteriorates with time **[1]**, in order to assure that such failures do not occur. This leads to the need for the analysis of the damage of components and the need for methods for estimating residual life **[20]**. Two methods are used commonly, one is to use non-destructive evaluation and the other is to use sampling experiments **[20]**. In one of the weakest zones, such as heat-affected

zone (HAZ) **[34]** in welded joints, the amount of material that exists may be very small. Therefore, obtaining material properties from relatively small volumes of metal has been of primary importance for the safety work of fossil fired power plants. A number of attempts has been reported **[35]** for devising small specimens in order to derive engineering properties from critical regions of in-service components. Small punch testing has been considered as a potentially valuable method for gaining creep rupture properties from those regions. A small puncher, usually a small radius ceramic ball, penetrates under a force F through a very thin disc into a hole (Fig. 5.1), in these tests **[36]**. However, a variety of different small punch (SP) set-ups have been used to determine material properties. The range of these set-ups has been narrowed due to the production of a draft Code of Practice by the CEN (one of three European standardizations organizations recognized by the EC) **[16]**, but there is still a need of further research to clarify consequences of different geometries on test data and mechanical properties. For this reason, finite element (FE) analyses have been carried out and the effects of different radii of the puncher and thicknesses of the sample disc on the deformation and rupture behaviour have been investigated in this Chapter. Moreover, FE analyses of SP creep tests with different coefficients of friction have been considered. The relationships between the minimum deflection rate versus load and the load versus failure life, obtained from FE analyses of SP creep tests using the methodology described in Section 2.4.2, have been studied and the parameters derived from small punch numerical analyses, C, N, N' and C', have been obtained from $log\dot{\Delta}_{min}$ versus $logt_f$ and $logP$ versus $logt_f$ plots.

5.1 TYPICAL SPECIMEN BEHAVIOUR

5.1.1 Problem Definition

The influence of the parameters mentioned above (in Section 3) on the rupture life has been studied, using the Liu and Murakami damage model for a P91 steel at 650^0C. It is difficult to measure the actual coefficient of friction during a SP creep test, which may affect the experimental data and failure mode. For this reason, FE analyses were used to derive the displacement versus time curves from small punch creep tests with different coefficients of friction.

5.1.2 Typical behaviour

The geometry of the punch and the disc is shown in Fig. 5.2. The form of displacement versus time output obtained from a small punch creep test is shown schematically in Fig. 5.3. The output typically includes rapidly decreasing displacement rate due to the increasing of the contact area between the specimen and the spherical punch, which reduces to a minimum value and persists for a relatively long time owing to 'stiffening' effect of the sample, before accelerating towards the end of the test, leading to fracture. An example of the deformations that would occur for a typical small punch creep test is illustrated in Fig. 3.3 (b). Typical test curves for the different material zones of a weld have been shown earlier in Fig. 3.1 (c) in Chapter 3.

5.1.3 Typical Specimen Dimensions

A typical SP test specimen has the following dimensions: $D = 8mm$ $R_s = 1.25mm$, $a_p = 2mm$ and $t_0 = 0.5mm$. In addition, the European Code allows the radius of the hemi-spherical punch to vary between 1.0 and 1.25mm and the diameter of the disc to vary between 8-10mm. However, a certain clamped area of the disc has to be secured. In this work, the radius of the receiving hole, a_p, has been kept constant for all analyses with different specimen and punch dimensions . The specimen and punch dimensions are defined by two ratios, i.e. R_s/a_p and t_0/a_p and FE analyses were carried out with $t_0/a_p = 0.1, 0.175$ and 0.25 and $R_s/a_p = 0.4, 0.5, 0.6$ and 0.7.

5.2 FINITE ELEMENT ANALYSIS

FE analysis was used to obtain the relationship between the load, P, and the minimum displacement rate, $\dot{\Delta}_{min}$, and between the load and failure time, t_f using a simplified, axi-symmetric model. For all the analyses, the material properties for a P91 steel at $650^0\ C$ were used. The finite element software ABAQUS was used to model and calculate the time-dependent performance of the small punch test. The mesh and boundary conditions are shown in Fig. 5.3. The reduced integration element type CAX4R is chosen to prevent the shear and volume locking due to severe shear and torsion effects, which tend to occur in a contact simulation. The punch sphere and supports are represented by rigid shell elements.

36 analyses for R_s/a_p and t_0/a_p were performed with three load levels for each geometry. Also, simulations with a typical geometry but for coefficient of friction $\mu = 0,0.3$ and 0.6 were used to investigate the effect of friction.

5.3. FINITE ELEMENT RESULTS

5.3.1 Illustrative Results and Uniaxial Behaviour

Standard uniaxial tensile creep tests are commonly used for the determination of material properties. Typical specimen dimensions of an uniaxial creep specimen is shown in Fig. 5.4(a). Strain versus time data consisting of primary, secondary and tertiary creep stages for P91 steel at $650^0\ C$ are shown in Fig. 5.4(b). The relationships between the minimum deflection rate versus load and the load versus failure life, obtained from FE analyses of SP creep tests, are presented here.

5.3.2 Relationship between Minimum Deformation Rate and Load

The results for twelve different SP geometries have been obtained from the FE analyses and the relationship between the minimum deflection rate versus load are shown in Fig. 5.5. Fig. 5.5 shows that when log minimum displacement rate is plotted against log load an approximate simple linear relationship can be obtained. The relationship between $\dot{\Delta}_{min}$ and P can be expressed with the following equations:

$$\dot{\Delta}_{min} = CP^N \qquad (5.1)$$

or

$$log\dot{\Delta}_{min} = logC + NlogP \quad (5.2)$$

where $\dot{\Delta}_{min}$ is minimum deformation rate, P is load, C and N are related to the material properties, and depend on the dimensions of the punch and specimen. The straight line fittings are also shown in Fig. 5.5.

5.3.3 Relationship between Failure Life and Load

Another important relationship obtained from SP creep tests is that between time to failure and the load level. Similar to the approach described in section 5.3.2, the linear relationship between $logP$ and $logt_f$ is used, i.e.

$$t_f = C'P^{N'} \quad (5.3)$$

or

$$logP = -\frac{1}{N'}logc' + \frac{1}{N'}logt_f \quad (5.4)$$

Again the data for each geometry for three different load levels have been plotted and linear fitting has been used to obtain the parameters N' and C'. Good straight lines have been achieved with the present method which can be seen from Fig. 5.6. The effect of R_s/a_p and t_0/a_p is examined further in section 5.3.4.

5.3.4 Effects of the Dimension Ratios R_s/a_p and t_0/a_p

The small punch test is complicated because the specimen starts as a flat plate but ends in a conical shape, i.e. large deformations occur as the contact area

between indenter and specimen increases which leads to the change in stress states of the specimen. This behaviour varies with specimen and punch dimensions. Because of the variety of different geometries used in SP tests, the present chapter has the aim to study how the punch radius and sample thickness affect the relationships of the minimum deformation rate versus load and failure time versus load.

Fig. 5.6 shows that for the same loads, t_f increases with increasing radius of the punch. As a consequence, the minimum displacement rate decreases but this variation does not seem to affect significantly the N and C values derived from $log\dot{\Delta}_{min}$ versus $logP$ plot, see Fig. 5.5.

From Fig. 5.6 it can be seen that when the thickness of the specimen disc increases, for the same load, t_f also increases. Figs. 5.5 and 5.6 also show that there is a reduction in the minimum deflection rate due to the significant change in failure time when the thickness of the specimen increases. However, this does not seem to change significantly the N and C values (Figs. 5.7 and 5.8). From the comparison of all of the rupture life results shown in Figs. 5.9 and 5.10 it can be concluded that the gradient N' reduces slightly when the thicknesses of the specimen and radius of the punch are increased. However, the variation of C' is influenced more than N' is, with the changes of dimension ratios R_s/a_p and t_0/a_p, and shows the trend to rise with the increase of the radius of the hemi-spherical punch and the thickness of the sample disc, respectively.

5.3.5 Effect of Friction

The effect of friction could be very important in SP creep tests because of the presence of contact between the hemi-spherical punch head and the disc specimen. This contact area increased significantly during the test. Nine analyses were carried out with the most common geometry ($R_s = 1.25mm$, $a_p = 2mm$ and $t_0 = 0.5mm$) under three loads with three values of coefficient of friction, i.e., $\mu = 0, 0.3$ and 0.6. Fig. 5.11 shows a comparison of all $logP$ versus $logt_f$ results. It is interesting that the analyses with higher friction give significant increase in time to failure (Figs. 5.13 and 5.14), which leads to higher gradient in the linear fitting of $logP$ versus $logt_f$ plots (Fig. 5.11). As a result similar trend is observed for the gradient of $log\dot{\Delta}_{min}$ versus $logt_f$ plot as shown in Fig. 5.12. The main reason for the increase of failure time of the analyses with high coefficient of friction could be that the interaction between the punch and the specimen under those conditions prevents any sliding that could occur at the late stage of the creep test because of the large deformations.

5.4 DISCUSSION AND CONCLUSIONS

The effects of the dimension ratios, R_s/a_p and t_0/a_p, on the parameters C, N, C' and N' and have been studied using the relationships between the minimum deformation rate and load, and between the failure life and load obtained from FE analyses based on the Liu and Murakami damage constitutive equations. It has been found that increase of the punch radius and sample disc thickness leads to an increase in t_f and to a decrease of minimum deformation rate. The increase of the punch radius leads to increase in the

contact area between the punch and the specimen which results in a longer time to fail and leads to decrease of $\dot{\Delta}_{min}$. Increase of the small punch specimen thickness leads to increase of the failure time due to improved general strength of the sample because of the additional material. As a result, the minimum displacement rate decreases and effects the small punch creep data obtained from $log\dot{\Delta}_{min}$ versus $logt_f$ and $logP$ versus $logt_f$ plots. The analyses showed that the areas with highest strain occur off the centre of the specimen because of the complicated multiaxial stress state and a number of non-linear processes. As a result of that a significant decrease of specimen thickness followed by failure has been observed during the small punch creep tests. The influence of friction has been investigated. From the results, it can be concluded that friction has a significant effect on the SP creep test data and more specifically on t_f, which is important for the interpretation of the data derived with the SP creep testing method. The gradients, obtained from $log\dot{\Delta}_{min}$ versus $logt_f$ and $logP$ versus $logt_f$ plots for the FE analyses with friction are similar to those derived from the standard uniaxial creep tests and used in the Liu and Murakami damage model. The increase of coefficient of friction results to shifting of the failure position off the centre of the small punch creep specimen which leads to increase of the failure time.

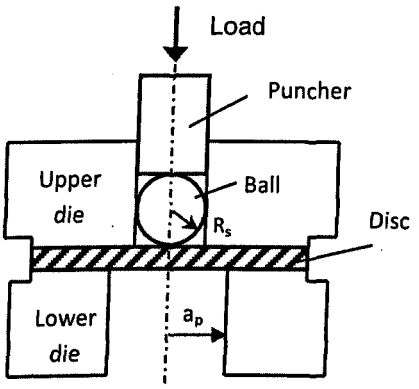

Fig. 5.1 Schematic diagram of small punch test setup.

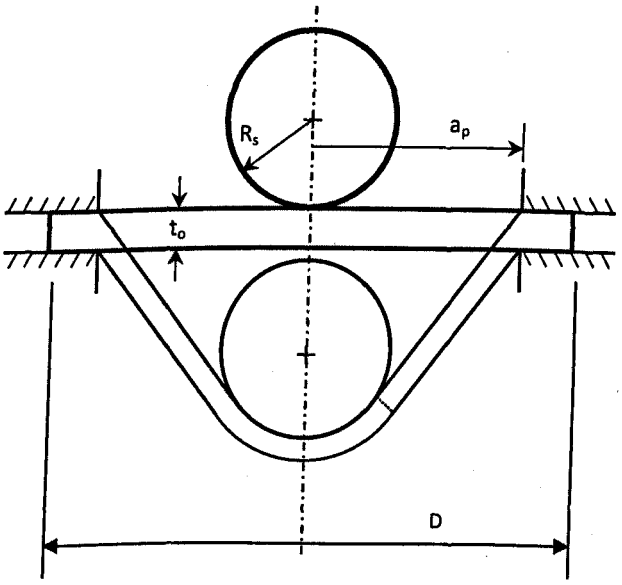

Fig. 5.2 Dimensions and deformed shape.

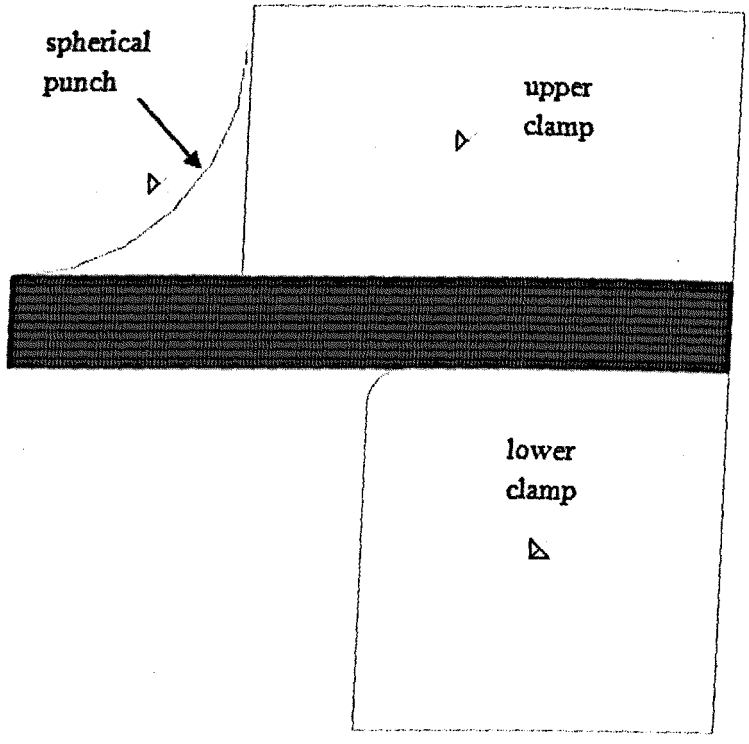

Fig. 5.3 FE model used for the SPT analyses.

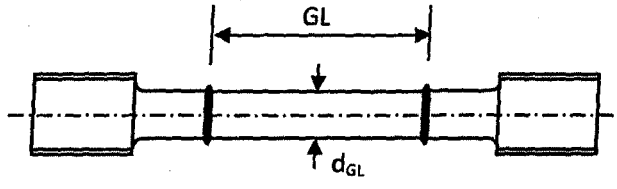

(a)

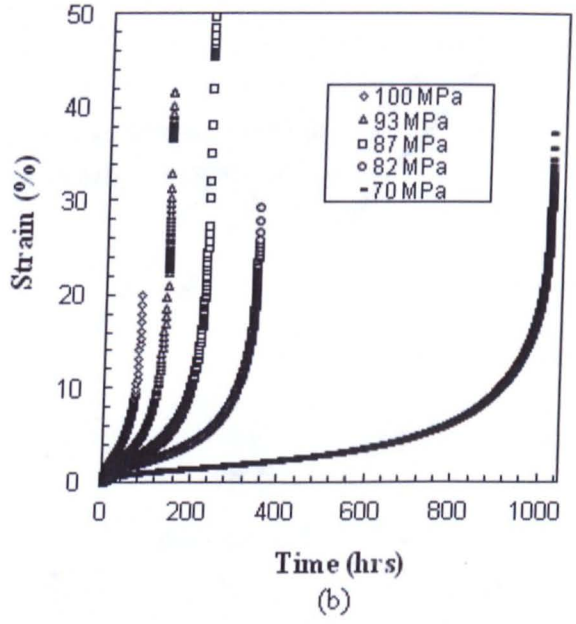

(b)

Fig. 5.4 (a)Typical conventional creep test specimen (GL ≈ 50mm, d_{GL} ≈ 10mm); (b) Uniaxial creep strain curves for a P91 steel at 650° C **[81]**.

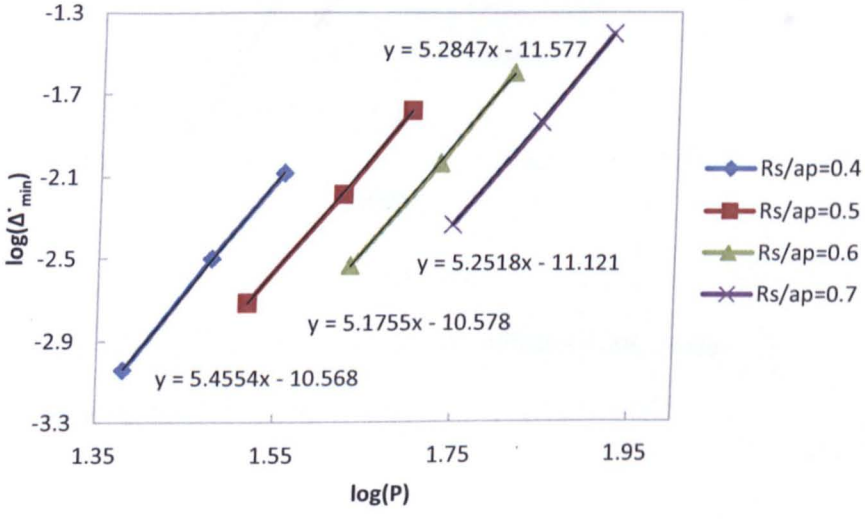

(a) t_0/a_p=0.1

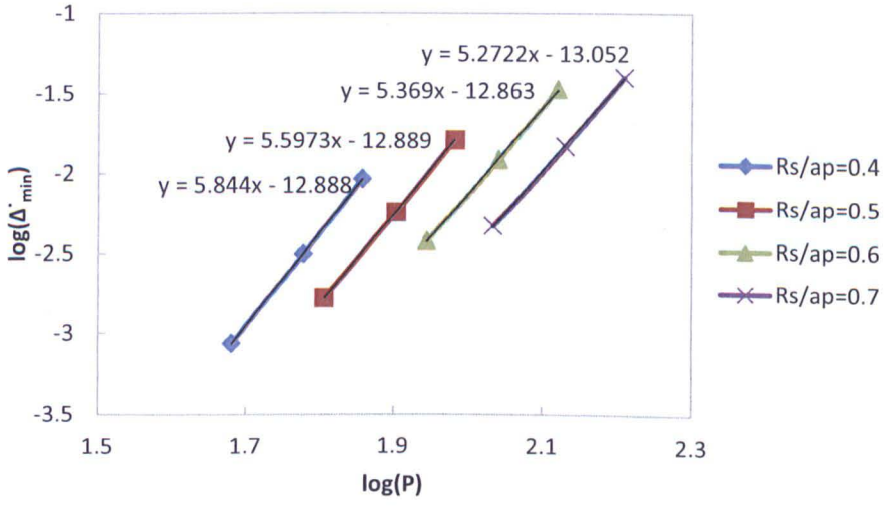

(b) t_0/a_p=0.175

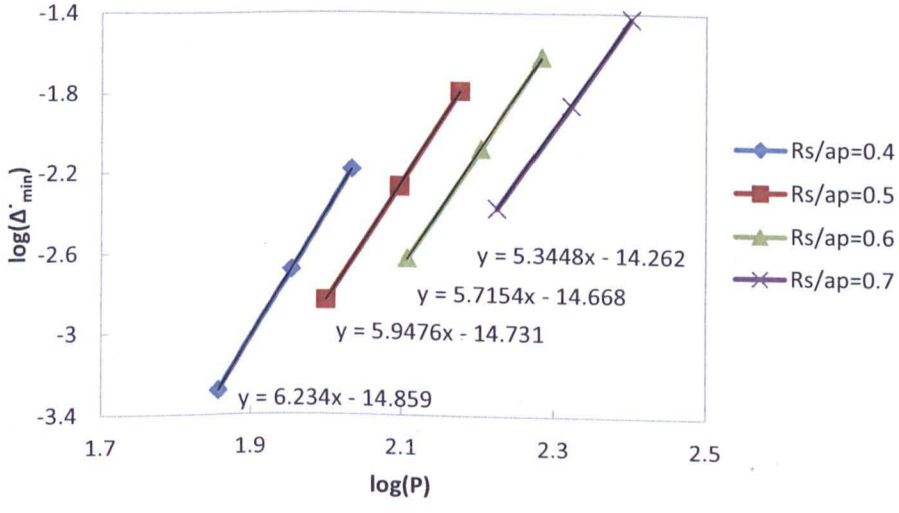

(c) t_0/a_p=0.25

Fig. 5.5 $log\dot{\Delta}_{min}$ versus $logP$ plot for different R_s/a_p ratios:

a) $t_0/a_p = 0.1$; b) $t_0/a_p = 0.175$; and c) $t_0/a_p = 0.25$.

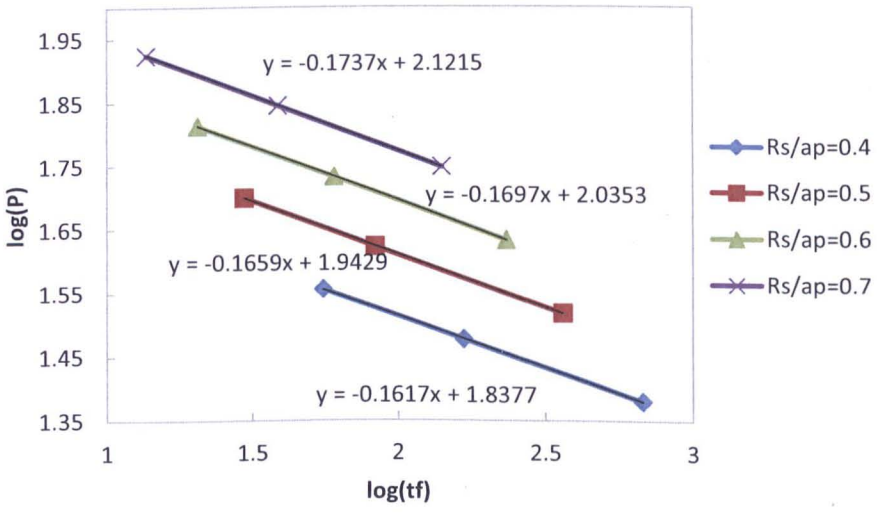

(a) t_0/a_p=0.1

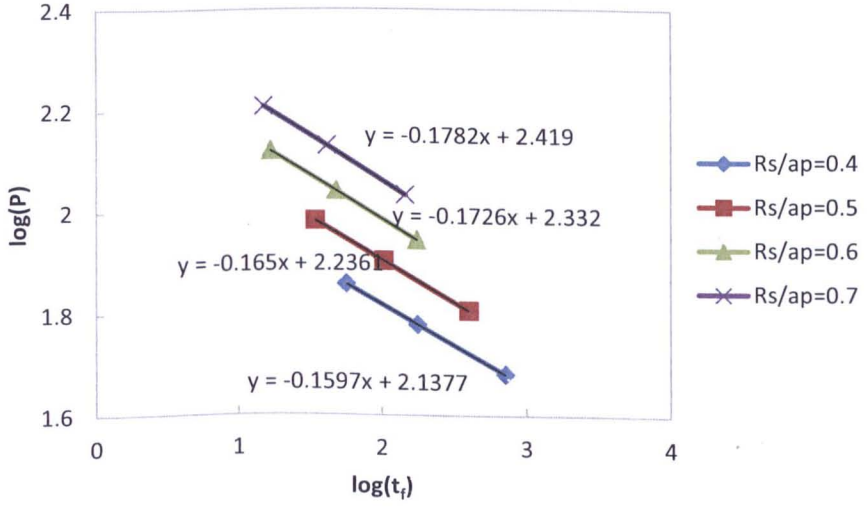

(b) t_0/a_p=0.175

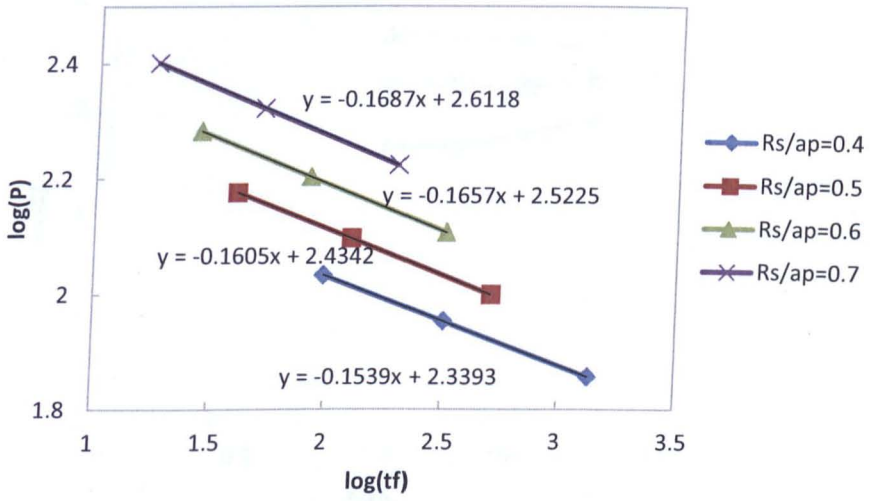

(c) t_0/a_p=0.25

Fig. 5.6 $logP$ versus $logt_f$ plot for different R_s/a_p ratios:

a) $t_0/a_p = 0.1$; b) $t_0/a_p = 0.175$; and c) $t_0/a_p = 0.25$.

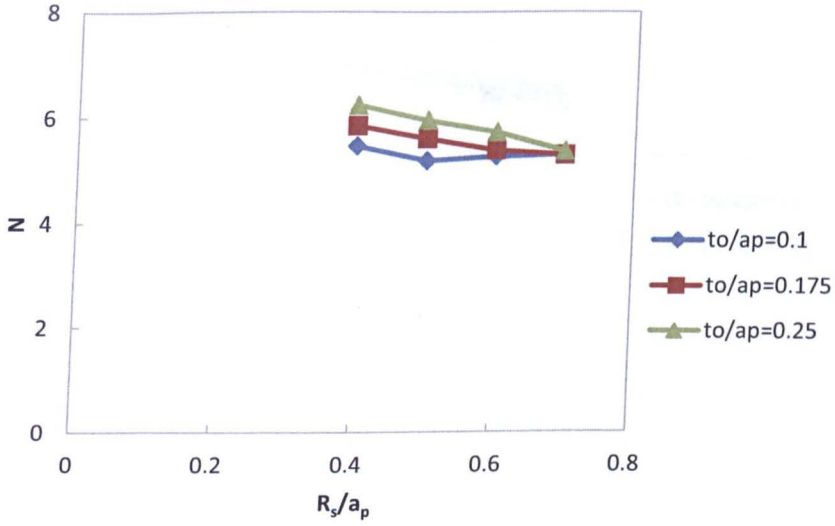

Fig. 5.7 Variation of N with R_s/a_p for different t_0/a_p.

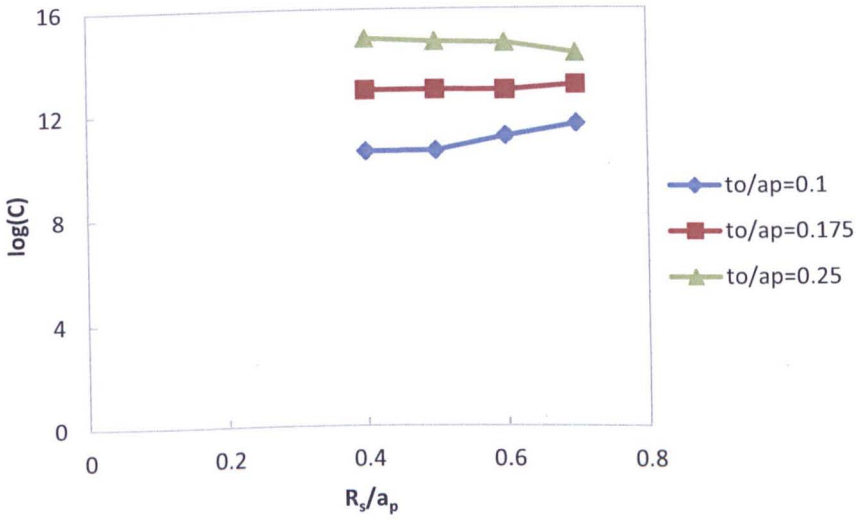

Fig. 5.8 Variation of $logC$ with R_s/a_p for different t_0/a_p.

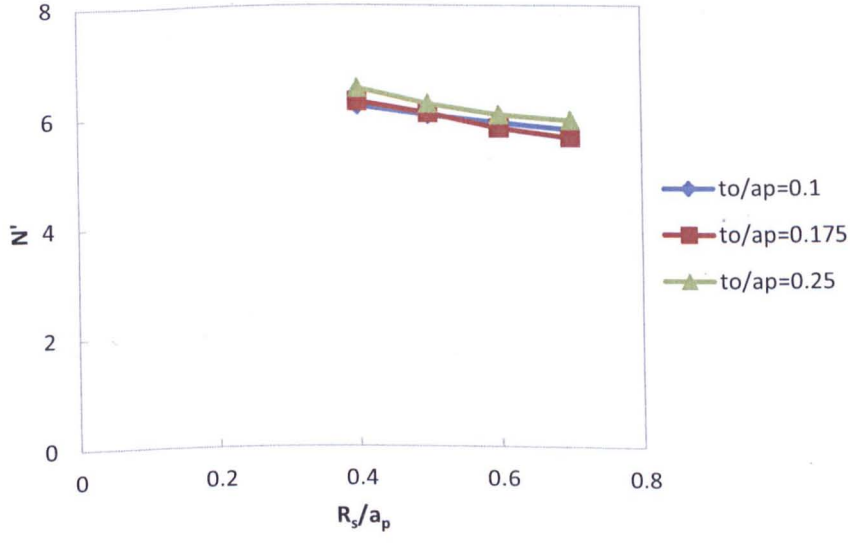

Fig. 5.9 Variation of N' with R_s/a_p for different t_0/a_p.

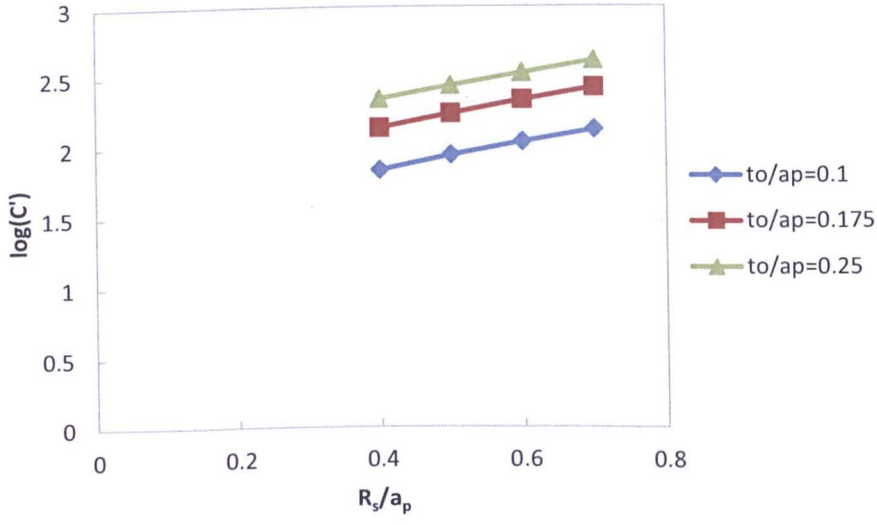

Fig. 5.10 Variation of $logC'$ with R_s/a_p for different t_0/a_p.

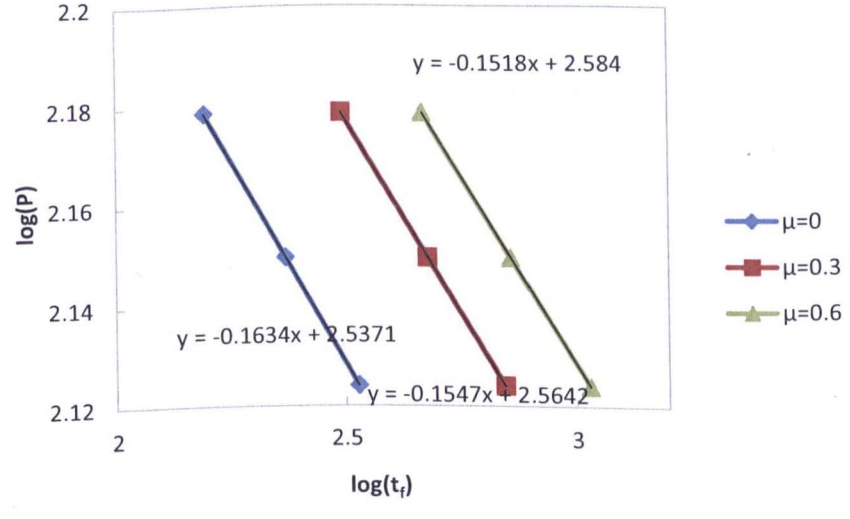

Fig. 5.11 $logP$ versus $logt_f$ for $R_s = 1.25mm,\ a_p = 2mm,\ t_0 = 0.5mm\ \mu = 0; 0.3; 0.6.$

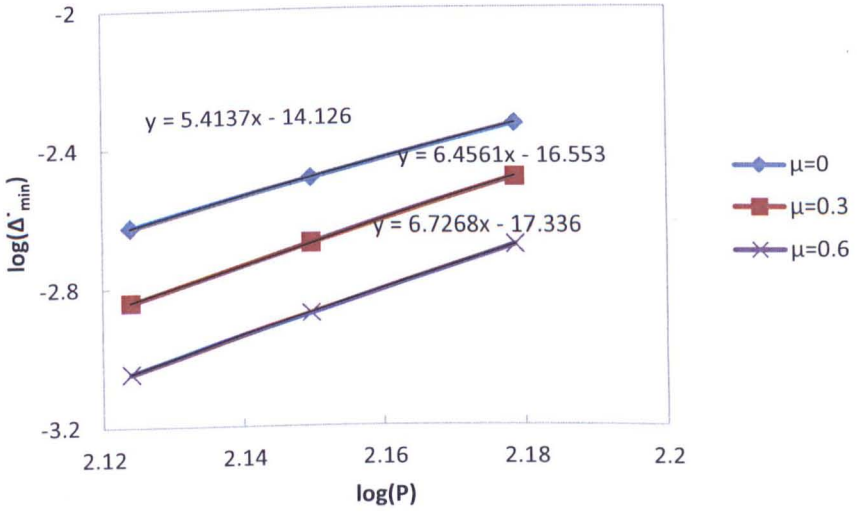

Fig. 5.12 $log\dot{\Delta}_{min}$ versus $logP$ for $R_s = 1.25mm,\ a_p = 2mm,\ t_0 = 0.5mm\ \mu = 0; 0.3; 0.6.$

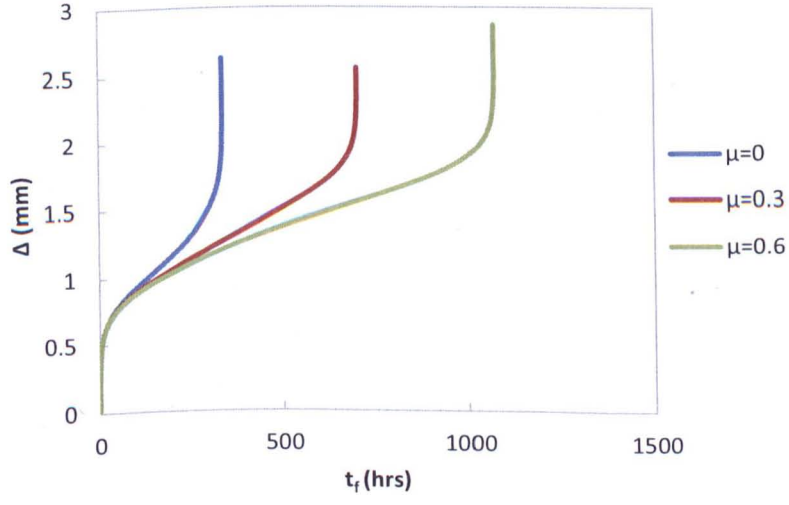

Fig. 5.13 Δ versus t_f for $R_s = 1.25mm,\ a_p = 2mm,\ t_0 = 0.5mm\ \mu = 0; 0.3; 0.6.$

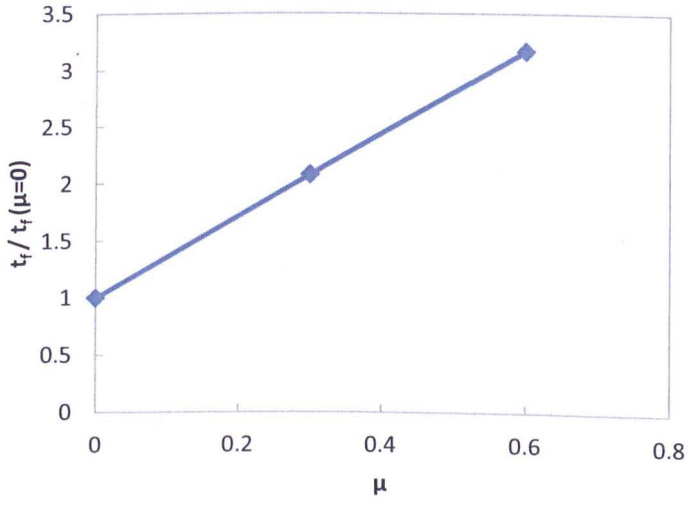

Fig. 5.14 $t_f/t_f(\mu = 0)$ versus μ for $R_s = 1.25mm,\ a_p = 2mm,\ t_0 = 0.5mm.$

CHAPTER 6. EXPERIMENTAL VERIFICATION

The efficiency and exploitation of fossil fired power plants depend on the quality of metals and welds that have been used for their building. The components and welded constructions in these plants operate under extreme conditions, exposed to elevated temperatures, high pressures and loads. In order to ensure safety exploitation, a variety of techniques and methods have been developed such as non-destructive evaluation of welded components, numerical and analytical methods, ect. Development of new creep resistant super-alloys and assessment of creep material properties for in-service welded constructions is of primary importance for the improvement of power plant performance.

However, in order to obtain reliable creep data, testing of actual components is needed. The main creep testing techniques have been described in Chapter 2. The standard creep testing methods usually require significant amount of material for the manufacturing of samples. In order to develop and test new alloys it is more practical to use small volumes of metal. Another problem for the power generating industry is the life assessment and deterioration of welds. It is difficult to extract large amounts of metal from in-service components without the need for repair. Moreover, it has been found that a particular area, known as heat-affected zone, of the welds is more vulnerable to the creep conditions and significant percentage of the cracks occur in that zone due to the complex re-heating and cooling processes during the welding. From everything mentioned above, the need for new creep testing methods which use small quantities of material for the manufacturing of samples becomes clear. Such testing techniques include impression creep testing, small ring creep testing,

miniature tensile creep testing and small punch creep testing. The purpose of this chapter is to describe the small punch creep testing equipment and procedures which were used in the present research. Due to the complex nature of the small punch creep testing, which includes contact between the punch and specimen and large creep strains and complex stress state, a completely theoretical solution of the problem is still not available. Because of that, real experimental data have to be carried out in order to produce material data which can be used for life assessments and for the development of numerical methods and interpretation techniques.

6.1 Experimental Equipment and Procedures

E.ON small punch creep testing machine is shown in Fig. 6.1; this was purchased from E.ON. It consists of the following sub-assemblies: gas jacket assembly, specimen holder assembly and heat sink and support assembly. The gas jacket assembly contains clevis body and spilt heating cylinders. The specimen holder consists of inner and outer tubes, locking bush, spring base and clamping ring. There are two LVDT transducers for observation and recording of the displacements of the indenter and the specimen, respectively, secured on the top and bottom sides of the testing rig. The load is applied with weights on a loading pan which is secured with a loading lock attached to the small punch creep machine.

In order to set-up and perform a small punch creep test, the following procedure was carried out. The specimen holder assembly is dismounted from the clevis body. SPC specimen is placed onto the receiving plattern ensuring that an appropriate anti seize medium is utilised to prevent seizure of the parts

during testing. The clamping ring is placed on the top of the inser tube and assembled. The displacement of the specimen is delivered to the bottom LVDT transducer through a quartz rod. Adjustment of the quartz rod against the bottom of the SPC specimen is achieved by the adjustment of the locking bush against the quartz rod. Pressure is achieved through the attachment of the spring base into the bottom of the inner tube. Care must be taken to ensure that the spring base is screwed passed the base of the inner tube and does not protrude. Care is also to be taken to ensure that there is enough travel of the quartz rod during testing to prevent failure of this component due to the movement of the punch indenter. The bottom LVDT transducer is adjusted to enable clearance for the quartz rod during assembly of the specimen holder assembly to the clevis body. The inner tube is attached to the clevis body and the gas jacket is assembled on the top of specimen holder assembly. The top LVDT transducer, the heat sink and the support assembly, with the correct indenter, should be fitted onto the small punch creep rig frame. It is important to establish good alignment of the indenter to the central orifice of the specimen holder assembly.

- Insert the alignment cap halves into the top of the outer tube.
- Adjust the punch indenter through the heat sink and support assembly and insert it into the alignment cap.
- Withdraw and remove alignment cap halves carefully from the small punch creep rig set-up ensuring that the punch indenter location is not disturbed.
- Insert fall arrest spacer around the indenter section to sit in the recess in outer tube top.

- Insert split heating cylinders around the specimen holder assembly to enable gas tight seal required by the test parameters.
- Secure band clamps to split heat cylinders to ensure the required gas seal to the assembly.
- Close up the furnace ensuring that insulating-wool is utilised to pack the outer extremities.
- Ensure that cooling to the systems is turned on and a constant flow of water is flowing through the system.
- Set the top transducer bracket and the transducer to their in start positions and ensure that the data logger is set running.
- Turn on the argon gas to ensure that oxidation to the specimen will not occur during testing.
- The test parameters require that all air be purged and a constant pressure be maintained from argon during the test. Once the argon pressure has stabilised, turn on the furnace and run up to the required temperature for the test parameters.
- A constant monitor of all systems during the initial testing should be conducted at this juncture.
- Apply the desired weights on the loading pan and conduct the test.

6.2 Testing Results and Discussion

Five small punch creep tests were carried out with five different load levels and at a temperature of 650° *C*. The duration of the heat up of the furnace and the setting of a stable temperature was approximately 4 hours. The temperature was monitored and kept constant (±2°C) with three thermocouples: at the top, middle and bottom of the furnace. The testing samples were manufactured

from P91 (Bar 257) steel with diameter of 8 mm and thickness of 0.5mm. All of the tests were fulfilled under in-air environment because the oxidation level of the particular alloy at the chosen temperature is negligible and relatively close to the actual working conditions of most power plants [2]. Fig. 6.2 shows the displacement versus time curves of the small punch creep tests. Two of the tests were stopped before the full penetration of the indenter through the specimens. Photos of the test carried out under the lowest load level are shown in Fig. 6.3. It should be noticed that even when the displacement rate is still in the "steady state" region there are visible cracks. Images of another SP specimen from an interrupted creep test at displacement of 0.8 mm can be seen in Fig. 6.4. The results of the minimum displacement rate data versus load and load versus failure time in log scales are shown in Figs. 6.5 a) and b) respectively. This figure also depicts a comparison between FE results of SP creep predictions for the Eon geometry for two different coefficients of friction ($\mu = 0.3$ and 0.6) and actual experimental results. The differences in the gradients and failure times between the results obtained from FE analyses and the results from the real creep tests are clear. The reasons for that difference could be mainly due to the large strains, the material behaviour after plastic deformations and the triaxial stress state of the specimen that occur during small punch creep test. However, FE results show that when the friction between the punch and SP specimen is high, the results change significantly and shift closer to the data from the real SP creep tests.

6.3 Conclusions

A number of SP creep tests for P91 (Bar 257) steel were successfully carried out at 650° *C*. The data from the interrupted tests show the presence of cracks

from P91 (Bar 257) steel with diameter of 8 mm and thickness of 0.5mm. All of the tests were fulfilled under in-air environment because the oxidation level of the particular alloy at the chosen temperature is negligible and relatively close to the actual working conditions of most power plants [2]. Fig. 6.2 shows the displacement versus time curves of the small punch creep tests. Two of the tests were stopped before the full penetration of the indenter through the specimens. Photos of the test carried out under the lowest load level are shown in Fig. 6.3. It should be noticed that even when the displacement rate is still in the "steady state" region there are visible cracks. Images of another SP specimen from an interrupted creep test at displacement of 0.8 mm can be seen in Fig. 6.4. The results of the minimum displacement rate data versus load and load versus failure time in log scales are shown in Figs. 6.5 a) and b) respectively. This figure also depicts a comparison between FE results of SP creep predictions for the Eon geometry for two different coefficients of friction ($\mu = 0.3$ and 0.6) and actual experimental results. The differences in the gradients and failure times between the results obtained from FE analyses and the results from the real creep tests are clear. The reasons for that difference could be mainly due to the large strains, the material behaviour after plastic deformations and the triaxial stress state of the specimen that occur during small punch creep test. However, FE results show that when the friction between the punch and SP specimen is high, the results change significantly and shift closer to the data from the real SP creep tests.

6.3 Conclusions

A number of SP creep tests for P91 (Bar 257) steel were successfully carried out at 650° *C*. The data from the interrupted tests show the presence of cracks

in the outer side of the SP specimens, even for displacement levels usually associated with the "steady state" creep region (constant displacement rates). Similar material behaviour was observed during the FE creep analyses (Figs. 4.3 and 4.8). The position with the highest damage in the small punch creep analyses is in good agreement with the position of the cracks that occur at the interrupted experimental tests. This leads to the conclusion that the "secondary" creep area could be very short and occur in the early stage of the SP creep tests (primary or transition look alike stage of the small punch tests). It should be noted that the design of SP testing rig may make the alignment of the indenter difficult. The risk of engaging and misaligned the indenter while removing the alignment half caps and applying the weights on the loading pan is high. Moreover, the procedure of adjusting the indenter in the orifice of the outer tube from the specimen holding assembly has to be performed on every new test set-up. As expected, the FE analyses data showed a significant effect of the coefficient of friction on the small punch creep test behaviour, which is logical, due to the increasing contact area between the indenter and the specimen during the creep test.

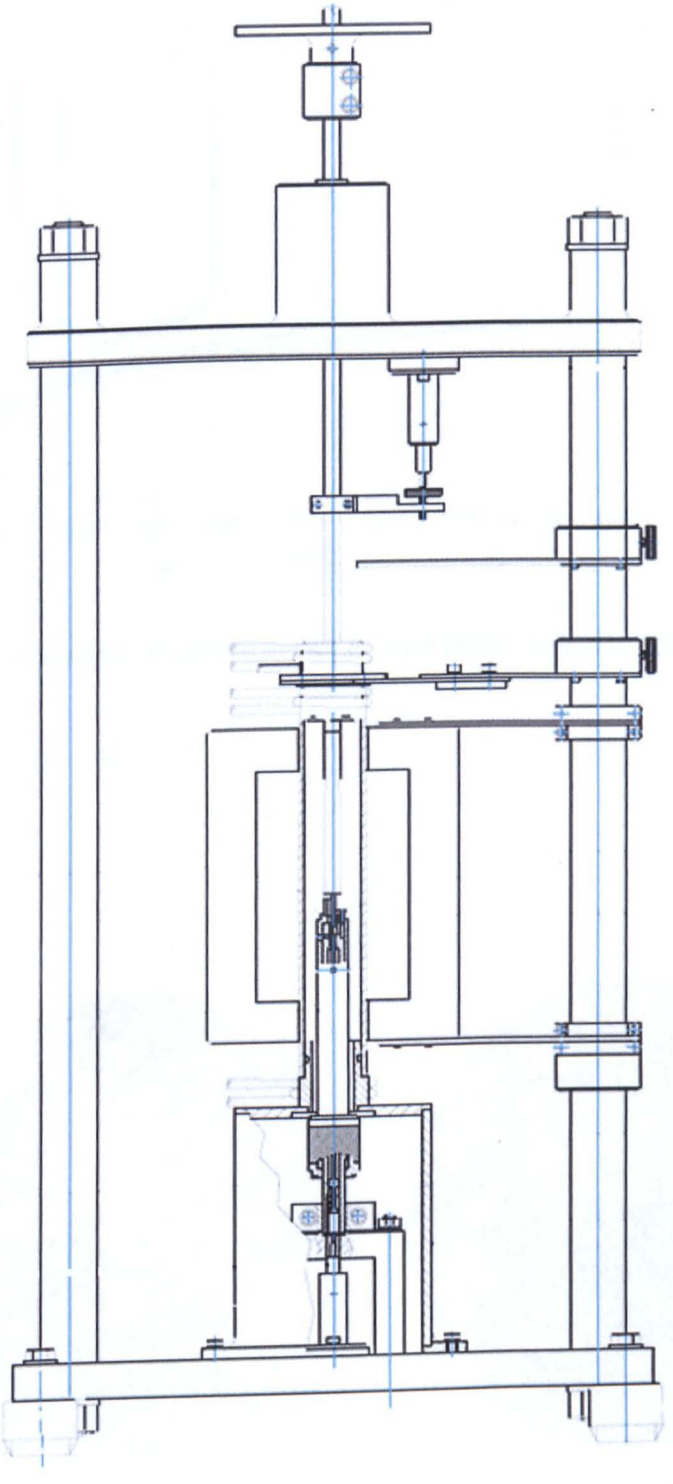

Fig.6.1 Schematic drawing of the Eon small punch testing machine.

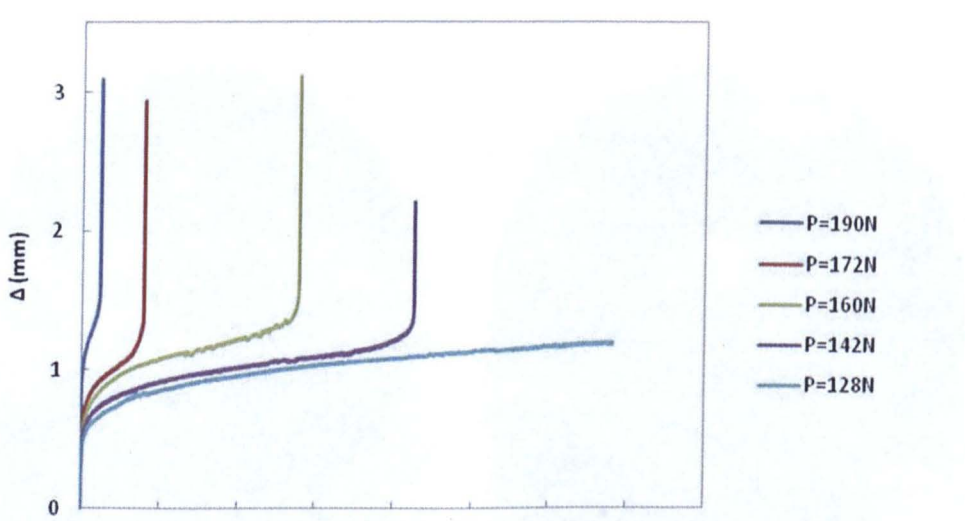

Fig. 6.2 Displacement versus time curves of small punch creep tests under five load levels.

Fig. 6.3 Images of SP creep specimen tested at load level P = 128N.

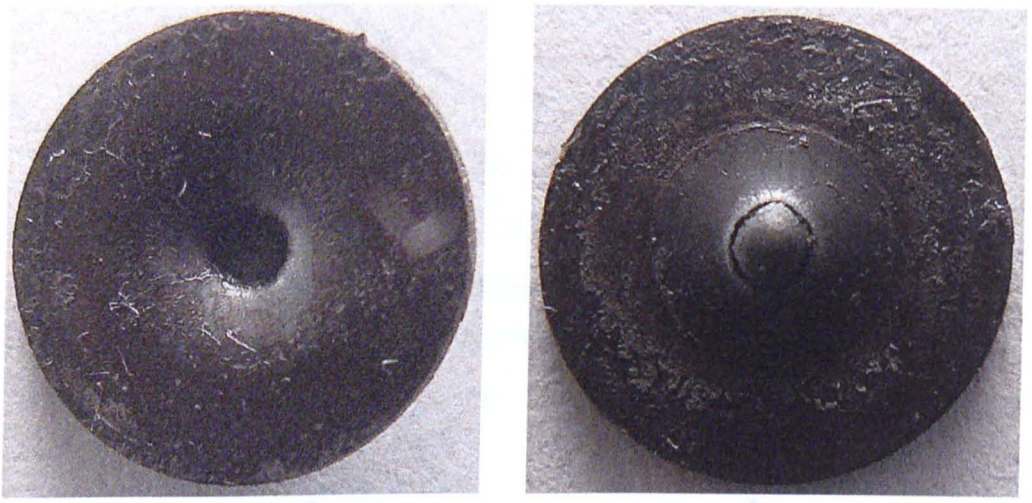

Fig. 6.4 Photos of an interrupted SP creep test at displacement, $\Delta = 0.8$ mm.

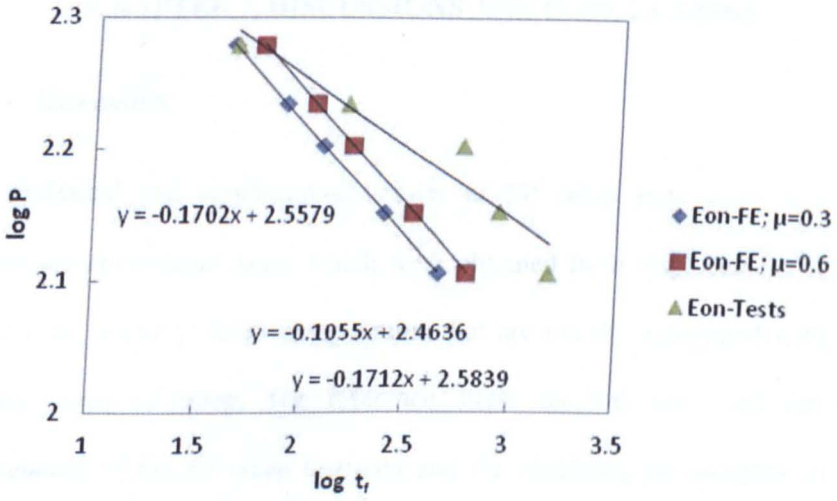

a)

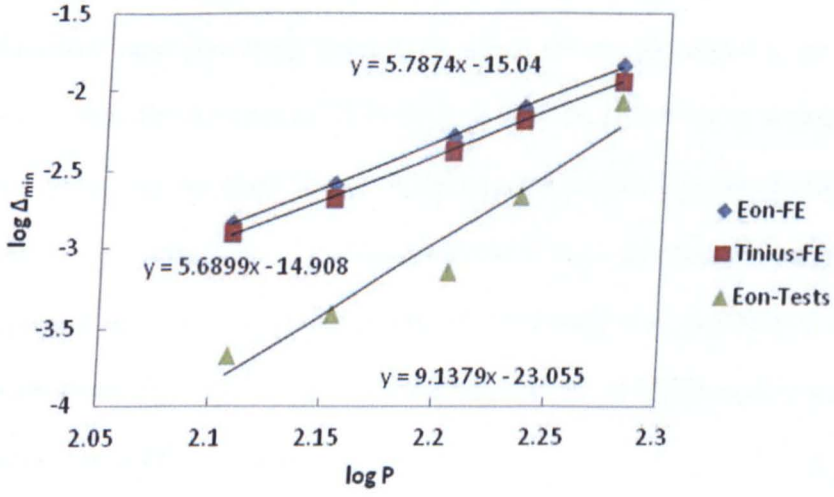

b)

Fig.6.5 Comparison of a) log P versus log t_f and b) log $\dot{\Delta}_{min}$ versus log P between Eon FE analyses data and experimental tests.

CHAPTER 7. DISCUSSIONS AND CONCLUSIONS

7.1 Discussion

The analytical and experimental results of SP creep tests show that the minimum displacement rates, which were obtained from displacement versus failure time, occur at large creep strains that are usually associated with the "tertiary" area of creep. The reference stress method was used for the interpretation of the SP creep test data and for clarifying the complex stress state of the SP creep specimen. A methodology for relating the creep strain rate of uniaxial tensile creep tests to the displacement rate of SP creep tests for "ductile" material using reference stress parameters is suggested in the present study. The results derived from this methodology show that the minimum displacement rates give creep strain levels which are usually related to the final stage of creep. The interrupted SP creep tests reveal a high level of damage on the specimen even for displacement levels that are usually associated with the minimum displacement rate. A conclusion could be made that the minimum displacement rate, which persists for most of the testing time, is actually due to balance between the large strains and the change of the geometry leading to the stiffening effect of the specimen.

SP creep testing data is geometry dependent. In order to save time and resources, a set of theoretical predictions of small punch creep tests using the Liu and Murakami model were conducted and useful inside information for those tests were gained. A number of FE analyses were carried out under a variety of geometries. It can be seen that the radius of the punch has a significant effect on the failure time of the tests. Another factor which is

important and affects significantly the SP creep results is the coefficient of friction. It changes the failure time and the material properties which is logical due to the increasing contact between the punch and the specimen under the severe creep conditions and material deterioration at elevated temperature. This makes the machining process and the final surface quality of the SP samples a very delicate and crucial task. Moreover, the displacement versus time to fail curves depict that the coefficient of friction affects more the failure time in the FE analyses with larger radius of the punch. The numerical analyses based on the finite element method bring some clarity for the complex stress state of the small punch creep specimen and its change during the creep testing. FE analyses provided important information about the effect of the non-linear material behaviour and the evolution of the critical area where the large strains and high damage occur even for a relatively early stage of the small punch creep tests (minimum displacement rates usually associated with the minimum creep strain rate from uniaxial tests). FE results show that larger radii of the punch and high coefficient of friction change the location with the highest strains in the small punch specimen which leads to increase of the failure time of small punch creep tests and different creep data.

In conclusion, it appears that small punch testing technique, due to its complex nature and various technical problems, is not suitable for obtaining creep material properties straightforwardly. In addition, other solutions should be also sought for the problem of deriving creep properties from small quantities of available metal such as the heat-affected zone in welds. Miniature creep testing designs which could use even less material for the manufacturing of samples and provide more reliable predictions should be developed.

7.2 Conclusions

- Methodology based on the reference stress method has been proposed for the interpretation and relation of the small punch creep data to the corresponding uniaxial creep data for ductile materials.
- A set of FE analyses using Liu and Murakami damage model has been carried out successfully.
- The effect of small punch radius and specimen thickness on the creep data has been investigated.
- A set of FE analyses with different coefficients of friction between the small punch specimen and indenter has been carried out.
- Experimental small punch tests have been conducted for P91 steel.

7.3 Future work

- More detailed investigation of the effect of coefficient of friction on the small punch creep tests.
- Studying the effect of misalignment of the small punch indenter on the creep test data.
- Improving of the experimental procedures in order to avoid misalignment of the small punch indenter.
- Further analysis of multi-axial stresses around the contact region.
- Further experimental tests with different small punch geometries.
- Investigating the behaviour of brittle materials by the means of small punch creep testing.

REFERENCES

1. Penny R. K., and Marriott D. L. Design for Creep. Chapman & Hall (2nd Edition), 1995.

2. Viswanathan, R. (1989) Damage Mechanisms and Life Assessmentof High-Temperature Components. ASM International, Metals Park, Ohio.

3. B. Wilshire, R. W. Evans, Acquisition and analysis of creep data, Journal of Strain Analysis, 1994.

4. Goto, T. (1984) Study on residual creep life estimation using non-destructive material properties tests. 2nd international conference on Creep and Fracture of Engineering Materials and Structures, 1135–1146.

5. British Standard BS 4A 4-13, Specification for test pieces for tensile and creep testing, BSI, London, UK. BS EN 10291:20, Metallic materials uniaxial testing in tension, BSI, London, UK.

6. T.H. Hyde, W. Sun, High temperature behaviour of materials and components under creep conditions, Applied Mechanics and Materials, 2004, 25-36.

7. Coussement, C., De Witte, M., De Backer, T. and Vereslst, L., Internal pressure creep testing on welded components of modified 9% Cr and 12% Cr steels, VGB Conf. on Materials and Welding Technology in Power Plants, Essen, Germany (1994).

8. H. Altenbach, Topical problems and applications of creep theory, International Applied Mechanics, 2003, 3906-0631.

9. T. H. Hyde, W. Sun and J. A. Williams, Creep analysis of pressurized circumferential pipe weldments – a review, Strain Analysis, 2003, S07601.

10. Norton F. H., The creep of steel at high temperatures, 1929.

11. Mc Vetty P. G., Creep of metals at elevated temperatures – the hyperbolic sine relation *between stress and creep rate*, Trans. ASME, 1943.

12. Dorn, J. E., Some fundamental experiments on high temperature creep, *J. Mech. Phys. Solids, 1955.*

13. Garofalo, F., Fundamentals of Creep and Creep Rupture in Metals, New York, 1965.

14. Bailey, R. W., The utilization of creep test data in engineering design, Proc. I. Mech. E., 1935.

15. Graham, A. and Walles, K. F. A., Relations between long and short time properties of a commercial alloy, J. Iron Steel Inst., 1955.

16. *CEN CWA 15627 Workshop Agreement: Small punch test method for* metallic materials (Part A). December 2006, European Committee for Standardisation.

17. *R5 Assessment procedure for the high temperature response of* structures. British Energy, Issue 3, 2003.

18. Webster, G. A. and Ainsworth, R. A. (1994) High TemperatureComponent Life Assessment. Chapman & Hall, London, Springer.

19. J. A. Francis, W. Mazur and H. K. D. H. Bhadeshia, Type IV cracking in ferritic power plant steels Material Science and Technology, 2006, 1387.

20. Brett S. J. (2007). Service Experience with a retrofit modified 9Cr *(Grade 91) steel header, EPRI - 5th Int. Conf. on Advances* in Materials Technology for Fossil Power Plants, 2007, Marco Island, Florida.

21. Y. Otoguro, M. Matsubara , I. Itoh, T. Nakazawa, Creep rupture strength of heat affected zone for 9Cr ferritic heat resisting steels, Nuclear Engineering and Design, 1999, 196 51-61.

22. Sun, W., Hyde, T. H, Becker, A. A. and Williams, J. A., Comparison of the creep and damage failure prediction of the new, service-aged and repaired thick-walled circumferential CrMoV pipe welds using material properties at 640° C, Int. J. Pres. Ves. & Piping Vol. 77 (2000), p. 389.

23. S. T. TU, J. M. Gong, X. Ling, The mechanical behaviour of laboratory cross-weld specimen and its relation with the practical cases at elevated temperature, ACTA METALLURGICA SINICA, 1999, 82-88.

24. PARKER, J. D. [1995], Creep behaviour of low alloy steel weldments, Int. J. Pres.

25. TU, S.-T., WU, R. and SANDSTROM, R. [1994], Design against creep failure for weldments in 1/2Cr1l2Mo1l4V pipe, Int. J. Pres. Ves. & Piping 58, pp. 345-354.

26. Hyde T. H., Sun W. and Becker A. A. (1996) Analysis of the impression creep test method using a rectangular indenter for determining the creep properties in welds, Int. J. Mech. Sci., 38, 1089-1102.

27. Sun, W., Hyde, T. H., and Brett, S. J. Application of impression creep data in life assessment of power plant materials at high temperatures. Proc. IMechE, Part L: J. Materials: Design and Applications, 2008, 222(3), 175–182. DOI: 10.1243/14644207JMDA183

28. T. H. Hyde, W. Sun, Multi – step load impression creep tests for a ½Cr ½Mo ½V steel at 565° C, Journal of Strain Analysis, 2001,37, 99–103.

29. WILLIAMS, J. A. [1982-1], A simple approach to the effect of specimen size on the creep rupture of cross weld samples, 1. Eng. Mat. & Tech., Vol. 104, pp. 36-40, Transactions of the ASME.

30. Sun W., Creep of service – aged welds, 1996, University of Nottingham.

31. T. H. Hyde, A. Tang, Creep analysis and life assessment using cross-weld specimens, International Materials Reviews, 1998, 221.

32. STORESUND, J. and TU, S.-T. [1995], Geometrical effect on creep in cross weld specimens, Int. 1. Pres. Ves. & Piping 62, pp. 179-193.

33. ETIENNE, C. F. and HEERINGS, 1. H. [1993], Evaluation of the influence of welding on creep resistance (strength reduction factor and lifetime reduction factor), IIW doc. IX-1725-93, presented at meeting IIW Cie IX Working Croup Creep, Copenhagen.

34. Askins M. C. and Marchant K. D. (1987). Estimating the remanent life of boiler pressure parts, EPRI Contract RP2253-1, Part 2, Miniature specimen creep testing in tension, CEGB Report., TPRD/3099/R86, CEGB, UK.

35. Hyde, T. H., Sun, W., Becker, A. A. and Williams, J. A. (2004) Creep behaviour and failure assessment of new and fully repaired P91 pipe welds at 923 K. Proc. Instn Mech. Engrs. Vol. 218, Part L: J. of Materials: Design & Applications, 211-222.

36. Hyde T. H., Sun W. and Williams J. A. (2007) The requirements for and the use of miniature test specimens to provide mechanical and creep properties of materials: - a review. International Materials Reviews 52 (4), 213-255.

37. Manahan, M. P., Argon, A. S. and Harling, O. K. (1981) The development of a miniaturized disk bend test for the determination of post-irradiation mechanical properties. J. Nucl. Mater. 103 & 104, 1545–1550.

38. Parker, J. D. and James, J. D. (1993) Disc-bend creep deformation behaviour of 1/2Cr1/2Mo1/4V low alloy steel. 5th International Conference on Creep and Fracture of Engineering Materials and Structures, 651–660.

39. Parker, J. D. and James, J. D. (1994) Creep behaviour of miniature disc specimens of low alloy steel. Developments in a progressing technology. ASME PVP 279, 167–172.

40. Parker J. D. and James J. D. (1994) Creep behaviour of miniature disc specimens of low alloy steel, ASME, PVP 279, Developments in a Progressing Technology, 167-172.

41. Tettamanti, S. and Crudeli, R. (1998) Small punch creep test: A promising methodology for high temperature plant components life evaluation. BALTICA IV Plant Mainten. Manag. Life Perform. 2, 501–509.

42. Dobeš F., Milička K., Ule B. et al.: Miniturized disk-bend creep test of heat-resistant steels at elevated temperatures, Engineering Mechanics, 5 (1998), 3, 157–160.

43. Ule B., Šuštar T., Dobeš F. et al.: Small punch test method assessment for the determination of the residual creep life of service exposed components: outcomes from an interlaboratory exercise, Nuclear Engineering and Design, 192 (1999), 1–11.

44. Ule B., Šuštar T., Rodič T., Dobeš F.: Small punch test method assessment for the determination of the residual creep life of service exposed components, Technology, Law and Insurance, 4 (1999), 283–293.

45. Sturm R., Jenjo M., Ule B. and Solar, M. Small-punch testing of smart weld materials, Proc. of the 2nd Int. Conf. on Structural Integrity of High Temperature Welds, November 2003, IOM^3 Communications, London, pp. 269-278.

46. CEN CWA 15627. Workshop Agreement: Small punch test method for metallic materials (Part A), December 2006 (European Committee for Standartization).

47. Hurst, R., Bicego V. and Foulds J. R. (2007) Small punch testing for creep – Progress in Europe. 8th International Conference on Creep and Fatigue at Elevated Temperatures, Paper No. PVP2007-26693.

48. Milička, K. and Dobeš, A. (2006) Small punch testing of P91 steel. Int. J. Pressure Vessels Piping 83, 625–634.

49. Blagoeva, D. T. and Hurst, R. C. (2007) Small-punch creep testing of P91 welded joints. 3rd International Conference on Integrity of High Temperature Welds, 463–472.

50. J. Shan, Z. Qian, X. Ling, Influence of oxidation of small punch creep test, Key Engineering Materials, 2007, 353-358.461.

51. Y. W. Ma, S. Shim, K. B. Yoon, Assessment of power law creep constants of Gr91 steel using small punch creep tests, Fatigue and Fracture of Engineering Materials and Structures, 2009, 32 951-960.

52. Purmensky, J. and Matocha, K. Latest developments in SPT, June 2007 (VITKOVICE Research & Development Ltd, Czech Republic).

53. Jianjun Chen, Young Wha Ma, Kee Bong Yoon, Finite element study for determination of material's creep parameters from small punch test, Journal of Mechanical Science and Technology, 2010, 24 1195-1201.

54. Hyde, T. H. and Sun, W. (2009) A novel, high sensitivity, small specimen creep test. J. of Strain Analysis 44.

55. Kachanov, L.M., On creep rupture time, 1958, Proc. Acad. Sci. USSR Div. Eng. Sci. 8, 26–31.

56. KRAUS, H. [1980], Creep Analysis, John Wiley, New York.

57. Rabotnov, Y. N., Creep Problems in Structural Members, 1969.

58. Aleš Nagode , Ladislav Kosec , Boris Ule, Uni-axial and multi-axial creep behaviour of P91-type steel under constant load, Engineering Failure Analysis, 2010, 1350-6307.

59. HAYHURST, D. R., DIMME, P. R. and MORRISON, C. J. [1984], Development of continuum damage in the creep rupture of notched bars, Phil. Trans R. Soc. London, A 311, pp. 103-129.

60. Hayhurst D. R. Creep rupture under multi-axial states of stress. J. Mech. Phys. Solids 20, pp. 381-390 (1972).

61. B. F. Dyson, Creep and future of metals: mechanisms and mechanics, Applied Physics Review, 1988, 23 605-613.

62. B. F. Dyson, T. B. Gibbons, Tertiary creep in nickel-based super alloys: analysis of experimental data and theoretical synergies. Acta Metall. 1987; 35:2355-69.

63. Dunne FPE, Othman AM, Hall FR, Hayhurst DR, Representation of uniaxial creep curves using continuum damage mechanics, Int. J. Mech. Sci., 1990, 32:945-57.

64. Murakami, S., Ohno, N., A continuum theory of creep and creep damage, 1980, In: Ponter, A.R.S., Hayhurst, D.R. (Eds.), Proceedings of the Third IUTAM Symposium on Creep in Structures. Springer, Berlin, pp. 422–443.

65. Murakami, S., Liu, Y., Mizuno, M., Computational methods for creep fracture analysis by damage mechanics, 2000, Comput. Method. Appl. M. 183, 15–33.

66. J. Fairbairn, A reference stress approach to creep bending of straight tubes, Journal Mechanical Engineering Science, 1974.

67. M. Kamaya, H. Machida, Reference stress method for evaluation of failure assessment curve of cracked pipes in nuclear power plants, International Journal of Pressure Vessels and Piping, 2009, 87 66-73.

68. H. Fessler, T.H. Hyde, J. J. Webster, Stationary creep predictions from model tests using reference stresses, Journal of Strain Analysis, 1977.

69. H. F. Chen, Z. Z. Cen, B. Y. Xu, S. G. Zhan, A numerical method for reference stress in the evaluation of structure integrity, International Journal of Pressure Vessels and Piping, 1997, 71 47-53.

70. Rayner G., Creep of welded branched pipes, 2004, University of Nottingham.

71. Goodall I. W., Cockroft R. D. H. And Chubb E. J., AN approximate description of the creep rupture of structures, 1975, Int. J. Mech. Sci., 17, 351-360.

72. I. W. Goodall, R. P. Skelton, The importance of multiaxial stress in creep deformation and rupture, Fatigue Fract Engng Mater Struct, 2004, 27 267–272.

73. Hua-Tang Yao, Fu-Zhen Xuan, Zhengdong Wang, Shan-Tung Tu, A review of creep analysis and design under multi-axial stress states, Nuclear Engineering and Design, 2007, 237 196-1986.

74. O. Kwon, C.W. Thomas, D. Knowles, Multiaxial stress rupture behaviour and stress-state sensitivity of creep damage distribution in

Durehete 1055 and 2.25Cr1Mo steel, International Journal of Pressure Vessels and Piping, 2004, 81 535-542.

75. Soderberg, C.R. (1941) Interpretation of creep tests on tubes. Trans. ASME, 63, 737-748.

76. ANDERSON, R. G., GARDENER, L. R. T. and HODGKINS, W. R. [1963], Deformation of uniformly loaded beams obeying complex creep laws, 1. Mech. Engng. Sci., Vol. 5, pp. 238-244.

77. MacKenzie A. C. (1968). On the use of a single uniaxial test to estimate deformation rates in some structures undergoing creep, Int. J. Mech. Sci. 10, 441-453.

78. SIM, R. G. [1968], Creep of Structures, PhD Thesis, University of Cambridge.

79. Goodall I. W., The development of high temperature design methods based on reference stress and bounding theorems, 1979, ASME, J. Eng. Mat Tech., 101, 349-355.

80. BOYLE, 1. T. [1983], The reference stress and its role in high temperature design, in Engineering Approach to High Temperature Design, Vol. 2 of Recent Advances in Creep and Fracture of Engineering Materials and Structures, Series Edited by B. Wilshire and D. R. 1. Owen, Pineridge Press, Swansea.

81. T.H. Hyde, A.A. Becker1, W. Sun, A. Yaghi, A.Thomas, P. Seliger, Finite element creep failure analyses of P91 large tensile cross-weld specimens tested at 625° C, 5th International Conference on Mechanics and Materials in Design, Porto-Portugal, 2006.

82. Purmensky J. and Matocha K. Latest developments in SPT. VITKOVICE Research & Development Ltd., Czech Republic, June 2007.

83. Chakrabarty J. (1970). A theory of stretch forming over hemispherical punch heads. Int. J. Mech. Sci. 12, 315-325.

84. Yang Z. and Wang Z-W. (2003). Relationship between strain and central deflection in small punch creep specimens. Int. J. Press. Vess. & Piping 80, 397-404.

85. Li, Y. Z. (2007) Determination of *Norton creep* law and rupture time dependence from small punch test. Proc. of 3rd Int. Conf. on Integrity of High Temp. Welds, April 2007, IoM Communications, London, pp. 433-449.

86. Hyde T.H., Sun W., Williams J.A.: Creep analysis of pressurized circumferential pipe weldments – a review, Journal of Strain Analysis, 38 (2003), 1, 1–29

87. T.H. Hyde, A.A. Becker, W. Sun, J.A. Williamsb, Finite-element creep damage analyses of P91 pipes, 2006, Int. J. Pres. Ves. Pip. 83, 853–863

88. ABAQUS User Manual, version 6.3. Hibbitt, Karlsson & Sorensen, Inc, 2002.

89. Liu Y., Murakami S., Damage Localization of Conventional Creep Damage Models and Proposition of a New Model for Creep Damage Analysis, 1998, JSME, 41.